

EFFECTS OF GEOMETRICAL FACTORS ON FRACTURE TOUGHNESS USING  
SEMI-CIRCULAR BENDING TYPE SPECIMENS

A THESIS SUBMITTED TO  
THE GRADUATE SCHOOL OF NATURAL AND APPLIED SCIENCES  
OF  
MIDDLE EAST TECHNICAL UNIVERSITY

BY

KIVANÇ HET

IN PARTIAL FULFILLMENT OF THE REQUIREMENTS  
FOR  
THE DEGREE OF MASTER OF SCIENCE  
IN  
MINING ENGINEERING

FEBRUARY 2008

Approval of the thesis:

**EFFECTS OF GEOMETRICAL FACTORS ON FRACTURE TOUGHNESS  
USING SCB TYPE SPECIMENS**

submitted by **KIVANÇ HET** in partial fulfillment of the requirements for the degree of **Master of Science in Mining Engineering Department, Middle East Technical University** by,

Prof. Dr. Canan Özgen \_\_\_\_\_  
Dean, Graduate School of **Natural and Applied Sciences**

Prof. Dr. Celal Karpuz \_\_\_\_\_  
Head of Department, **Mining Engineering**

Assoc. Prof. Dr. Levent Tutluoğlu \_\_\_\_\_  
Supervisor, **Mining Engineering Dept., METU**

**Examining Committee Members:**

Prof. Dr. Tevfik Güyagüler \_\_\_\_\_  
Mining Engineering Dept., METU

Assoc. Prof. Dr. Levent Tutluoğlu \_\_\_\_\_  
Mining Engineering Dept., METU

Prof. Dr. Celal Karpuz \_\_\_\_\_  
Mining Engineering Dept., METU

Prof. Dr. Bahtiyar Ünver \_\_\_\_\_  
Mining Engineering Dept., HU

Assist. Prof. Dr. Mehmet Ali Hindistan \_\_\_\_\_  
Mining Engineering Dept., HU

Date: \_\_\_\_\_

**I hereby declare that all information in this document has been obtained and presented in accordance with academic rules and ethical conduct. I also declare that, as required by these rules and conduct, I have fully cited and referenced all material and results that are not original to this work.**

Name, Last Name : Kıvanç HET

Signature : 

## **ABSTRACT**

### EFFECTS OF GEOMETRICAL FACTORS ON FRACTURE TOUGHNESS USING SEMI-CIRCULAR BENDING TYPE SPECIMENS

Het, Kivanç

M.Sc., Department of Mining Engineering

Supervisor: Assoc. Prof. Dr. Levent TUTLUOĞLU

February 2008, 158 pages

Semi-circular specimens (SCB) under three point-bending which are commonly used for fracture testing of rocks were used here for fracture mechanics tests. A total of 65 specimens were tested by using Ankara andesite rock.

Investigations including the effects of initial notch thickness, different loading span ratios (S/R), flattened loading end, and little dimensional variations when preparing the specimens were carried out.

Stress intensity factors for specimens with different geometries were computed individually by using a 3D finite element program ABAQUS.

Specimens with a preliminary notch thickness varying from 0.84 to 3.66 mm were tested under three point bending.

For a second group of specimens loading span was changed and fracture toughness variation was studied. Another change in the specimen geometry was made by machining a flat loading end at the upper load application point. Fracture toughness values were computed using the stress intensity values computed from numerical modeling and failure loads from the experiments.

It was found that up to 2 mm fracture toughness was not affected by variations in the thickness of preliminary notches. Fracture toughness was not affected by changing the loading span. For specimens with flat loading ends, fracture toughness was about 16% lower than the value found from regular SCB type specimens loaded at a point at the top by a steel roller.

As a result of about 46 experiments average fracture toughness of Ankara Gölbaşı andesite was found as  $1.36 \text{ MPa} \sqrt{m}$ .

Keywords: Rock Fracture Toughness, Stress Intensity Factor, Semi-Circular Bending Type Specimens

# ÖZ

## YARIM DAİRESEL EĞİLME NUMUNELERİNİ KULLANARAK GEOMETRİK FAKTÖRLERİN ÇATLAK TOKLUĞU ÜZERİNDEKİ ETKİLERİNİN İNCELENMESİ

Het, Kıvanç

Yüksek Lisans, Maden Mühendisliği Bölümü

Tez Yöneticisi: Doç. Dr. Levent TUTLUOĞLU

Şubat 2008, 158 sayfa

Bu çalışmada çatlak mekanığı testlerinde çoklukla kullanılan yarımdairesel eğilme örnekleri kullanılarak çatlak mekanığı analizleri yapılmıştır. Deneylerde Ankara andezit taşı kullanılmış ve toplamda 65 adet deney örneği hazırlanarak deneyler yapılmıştır.

Analizlerde çentik aralıkalığı, farklı destek mesafesi oranı (S/R), yükleme bölgesi düzleştirmesi ve deney örnekleri hazırlanırken oluşan küçük geometrik farklılıkların deneyler üzerindeki etkileri incelenmiştir.

Gerilme şiddeti değerleri her bir numune için ayrı ayrı olmak üzere 3 boyutlu sonlu eleman programı ABAQUS kullanılarak bulunmuştur.

İlk incelemede çentik aralığı kalınlığı değişiminin çatlak tokluğu üzerindeki etkisi incelenmiştir. Deney örneklerine 0.84 mm den 3.66 mm'ye varan değişik kalınlıklarda çentik aralıkları açılmıştır.

İkinci inceleme olarak deney örneklerinin destek mesafeleri değiştirilerek, bu değişimin çatlak tokluğu üzerindeki etkisi incelenmiştir.

Diğer bir incelemede ise örnek geometrisinde değişiklik yapılarak örnek üstü yükleme bölgesinin düzleştirilmiş ve bu değişimin çatlak tokluğu üzerindeki etkisi incelenmiştir.

Çatlak tokluğu değerleri, nümerik modelleme sonucu elde edilen gerilme şiddeti faktörleri ve deneylerden elde edilen kırılma yükleri kullanarak hesaplanmıştır.

Deney sonuçlarına göre, çatlak tokluğu değerleri başlangıç çentik aralık kalınlığı 2 mm'ye kadar olan örneklerde çentik aralık kalınlığı değişimlerinden etkilenmemiştir. Aynı zamanda çatlak tokluğu değeri destek mesafesi değişimlerinden de etkilenmemiştir. Öte yandan örnek üstü yükleme bölgesinin düzleştirilmesiyle yapılan testler sonucunda, çatlak tokluğu değeri çelik silindir ile yapılan noktadan yükleme analiz sonuçlarına göre 16% daha düşük çıkmıştır

Sonuç olarak, yapılan 46 deney sonucuna göre Ankara andezitin ortalama çatlak tokluğu değeri  $1.36 \text{ MPa} \sqrt{m}$  olarak bulunmuştur.

Anahtar Kelimeler: Çatlak Tokluğu, Gerilme Şiddeti Faktörü, Yarım Dairesel Eğilme Örnekleri

*To My Family...*

## **ACKNOWLEDGMENT**

Firstly I would like to thank my supervisor Assoc. Prof. Dr. Levent Tutluoğlu for his important advices and guidance through my thesis.

I want to acknowledge to the examining committee members, Prof. Dr. Tevfik Güyagüler, Prof. Dr. Bahtiyar Ünver, Prof. Dr. Celal Karpuz and Assist. Prof. Dr. Mehmet Ali Hindistan for being interested in and reading this thesis.

I would like to thank my parents Şenay Het and Timur Het for their morale support and patience during my all education life. I also would like to thank all my family, whom I did not write their names here.

I like to give special thanks to manager of the Aegean Lignite Establishment Mr. Hakkı Duran for his support during my thesis.

I want to thank my friend Burkay Tez his assistance during the experimental studies and also his grateful friendship.

I would like to express sincere appreciation to research assistances of METU Mining Engineering department, Çiğdem Alkılıçgil, Arman Koçal, Ceyda Atlı and B. Barış Çakmak for their support and help during in my experimental studies and computer analysis.

I want to thank Tahsin İşiksal, Hakan Uysal, İsmail Kaya for their help during the experimental studies.

# TABLE OF CONTENTS

PLAGIARISM.....	iii
ABSTRACT .....	iv
ÖZ .....	vi
DEDICATION.....	viii
ACKNOWLEDGEMENT .....	ix
TABLE OF CONTENTS.....	x
LIST OF TABLES.....	xiii
LIST OF FIGURES .....	xv
LIST OF SYMBOLS AND ABBREVIATIONS.....	xix
CHAPTER	
1. INTRODUCTION.....	1
1.1 General View of Fracture and Rock Fracture Mechanics.....	1
1.2 Objective of the Thesis Work.....	4
1.3 Methodology.....	5
1.4 Sign Convention.....	6
1.5 Outline of the Thesis.....	6
2. FRACTURE MECHANICS AND FRACTURE TOUGHNESS.....	7
2.1 History of Fracture Mechanics.....	7
2.2 Linear Elastic Fracture Mechanics (LEFM).....	10
2.3 Fracture Modes.....	10
2.4 Stress Intensity Factor and Crack Tip Stresses.....	12
2.5 Fracture Toughness.....	19
2.6 Elastic Plastic Fracture Mechanics.....	25
3. ROCK FRACTURE TOUGHNESS TESTING METHODS FOR MODE I.....	26
3.1 Short Rod (SR) Method .....	28

3.2 Chevron Bend (CB) Method .....	31
3.3 Cracked Chevron-Notched Brazilian Disc (CNBD) Method .....	32
3.4 Straight Notch Semi-Circular Bending (SNSCB).....	34
4. ESTIMATION OF STRESS INTENSITY FACTORS BY NUMERICAL MODELING.....	39
4.1 Finite Element Method.....	39
4.2 Origins of the Finite Element Method.....	40
4.3 ABAQUS Software.....	42
4.4 ABAQUS Modules.....	42
4.4.1 Part Module.....	43
4.4.2 Property Module.....	43
4.4.3 Assembly Module.....	43
4.4.4 Step Module.....	43
4.4.5 Interaction Module.....	44
4.4.6 Load Module.....	44
4.4.7 Mesh Module.....	44
4.4.8 Job Module.....	44
4.4.9 Visualization Module.....	45
4.4.10 Sketch Module.....	45
4.5 ABAQUS Verification Analysis.....	45
4.5.1 Semi-infinite plate with an edge crack.....	45
4.5.2 Inclined Crack in Tension.....	54
4.6 Method of Application of Distributed Loads to the Boundaries.....	60
4.7 Modeling of Cracks.....	64
4.8 Computation of Stress Intensity Factor for SCB Type Specimens.....	68
5. EXPERIMENTAL STUDIES.....	77
5.1 Mechanical Properties of Pink-Gray Coloured Ankara Andesite.....	77
5.2 SCB Specimen Preparation.....	79
5.3 Experimental Setup.....	83
5.3.1 DaqBook.....	83

5.4 SCB Specimen Geometry.....	84
5.5.1 Notch Thickness Analysis.....	87
5.5.2 Specimen Dimensions of Span Ratio (S/R) Analysis.....	89
5.5.3 Specimen Dimensions of Flattened SCB Analysis.....	89
5.5.4 Effect of Geometrical Variations in Dimensions When Preparing the SCB Specimens.....	91
6. RESULTS & DISCUSSIONS.....	94
6.1 Computation Technique.....	94
6.2 Notch Thickness Results.....	97
6.3 Results for Changing Loading Span of the Beam.....	111
6.4 Flattened Loading Surface Results .....	122
6.5 Effect of Geometrical Variations in Dimensions When Preparing the SCB Specimens.....	133
7. CONCLUSION.....	140
7.1 Recommendations.....	141
REFERENCES.....	142
APPENDICES	
A. SPECIMEN DIMENSIONS TABLES.....	148
A.1 Specimen Dimensions of Notch Thickness Analysis .....	148
A.2 Specimen Dimensions of Span Ratio (S/R) Analysis .....	150
A.3 Specimen Dimensions of Flattened SCB Analysis .....	154
B. SPECIMEN PHOTOS AFTER EXPERIMENTS.....	156
B.1 Notch Thickness Specimen Photos After Experiments .....	156
B.2 Span Ratio (S/R) Analysis Specimens After Experiments .....	157
B.3 Flattened Loading Face Specimens After Experiments .....	158

## LIST OF TABLES

Table 2.1 $K_{IC}$ values some materials and rocks.....	20
Table 4.1 Dimensions and mechanical properties of the semi-infinite plate with an edge through crack.....	46
Table 4.2 Dimensions and mechanical properties of the inclined crack in tension.....	55
Table 4.3 Dimensions and mechanical properties of the rectangular prism.....	60
Table 4.4 Dimensional and mechanical properties of the SCB models.....	71
Table 5.1 Indirect tensile strength test data and results for Brazilian Test.....	79
Table 5.2 Dimensions of $t_n < 1\text{mm}$ , $a/R=0.2$ , $S/R=0.7$ SCB specimens .....	87
Table 5.3 Dimensions of $a/R=0.2$ , $S/R=0.3$ SCB specimens.....	89
Table 5.4 Dimensions of $f \geq 15\text{mm}$ $a/R=0.2$ , $S/R=0.7$ SCB specimens .....	91
Table 5.5 SCB specimen dimensions used in geometrical variations analysis.....	92
Table 5.6 Dimension ratios used in dimension investigation .....	93
Table 6.1 Results of $t_n < 1\text{ mm}$ , $a/R=0.2$ , $S/R=0.7$ SCB specimens.....	98
Table 6.2 Results of $1\text{ mm} < t_n < 2\text{ mm}$ , $a/R=0.2$ , $S/R=0.7$ SCB specimens.....	98
Table 6.3 Results of $2\text{ mm} < t_n < 3\text{ mm}$ , $a/R=0.2$ , $S/R=0.7$ SCB specimens.....	99
Table 6.4 Results of $3\text{ mm} < t_n < 4\text{ mm}$ , $a/R=0.2$ , $S/R=0.7$ SCB specimens.....	99
Table 6.5 Results of $a/R=0.2$ , $S/R=0.3$ SCB specimens .....	111
Table 6.6 Results of $a/R=0.2$ , $S/R=0.4$ SCB specimens .....	112
Table 6.7 Results of $a/R=0.2$ , $S/R=0.5$ SCB specimens .....	112
Table 6.8 Results of $a/R=0.2$ , $S/R=0.6$ SCB specimens .....	113
Table 6.9 Results of $a/R=0.2$ , $S/R=0.7$ SCB specimens .....	113
Table 6.10 Results of $a/R=0.2$ , $S/R=0.8$ SCB specimens .....	114
Table 6.11 Results of $a/R=0.2$ , $S/R=0.9$ SCB specimens .....	114
Table 6.12 Results of $f \geq 15\text{mm}$ SCB specimens .....	123
Table 6.13 Results of $f \geq 20\text{mm}$ SCB specimens .....	123
Table 6.14 Results of $f \geq 22.5\text{mm}$ SCB specimens .....	124

Table 6.15 Results of $f \geq 25\text{mm}$ SCB specimens .....	124
Table 6.16 Results of dimension changes SCB specimens .....	134
Table A.1 Dimensions of $t_n < 1 \text{ mm}$ , $a/R=0.2$ , $S/R=0.7$ SCB specimens.....	148
Table A.2 Dimensions of $1 \text{ mm} < t_n < 2 \text{ mm}$ , $a/R=0.2$ , $S/R=0.7$ SCB specimens.....	149
Table A.3 Dimensions of $2 \text{ mm} < t_n < 3 \text{ mm}$ , $a/R=0.2$ , $S/R=0.7$ SCB specimens.....	149
Table A.4 Dimensions of $3 \text{ mm} < t_n < 4 \text{ mm}$ , $a/R=0.2$ , $S/R=0.7$ SCB specimens.....	150
Table A.5 Dimensions of $a/R=0.2$ , $S/R=0.3$ SCB specimens.....	150
Table A.6 Dimensions of $a/R=0.2$ , $S/R=0.4$ SCB specimens.....	151
Table A.7 Dimensions of $a/R=0.2$ , $S/R=0.5$ SCB specimens.....	151
Table A.8 Dimensions of $a/R=0.2$ , $S/R=0.6$ SCB specimens.....	152
Table A.9 Dimensions of $a/R=0.2$ , $S/R=0.7$ SCB specimens.....	152
Table A.10 Dimensions of $a/R=0.2$ , $S/R=0.8$ SCB specimens.....	153
Table A.11 Dimensions of $a/R=0.2$ , $S/R=0.9$ SCB specimens.....	153
Table A.12 Dimensions of $f \geq 15\text{mm}$ $a/R=0.2$ , $S/R=0.7$ SCB specimens.....	154
Table A.13 Dimensions of $f \geq 20\text{mm}$ $a/R=0.2$ , $S/R=0.7$ SCB specimens.....	154
Table A.14 Dimensions of $f \geq 22.5\text{mm}$ $a/R=0.2$ , $S/R=0.7$ SCB specimens.....	155
Table A.15 Dimensions of $f \geq 25\text{mm}$ $a/R=0.2$ , $S/R=0.7$ SCB specimens.....	155

## LIST OF FIGURES

Figure 1.1 One of the liberty ships broke into two (Banks, 2003).....	2
Figure 1.2 The Aloha Airlines Boeing 737 airplane after the accident (Banks, 2003)....	3
Figure 2.1 Types of fracture.....	11
Figure 2.2 Stress tensor notations in the cartesian co-ordinate system.....	12
Figure 2.3 Stress intensity factor $K_I$ solutions for the known analytical problems .....	16
Figure 3.1 ISRM's suggested Mode I fracture toughness testing methods, (modified from Backers, 2004).....	27
Figure 3.2 Geometry of short rod specimen (Zhao et al., 1990).....	29
Figure 3.3 Definitions for computation of correction factor based on Load-CMOD plot (Sousa & Bittencourt, 2001).....	30
Figure 3.4 Geometry of the CB type specimen (Zhao et al., 1990).....	32
Figure 3.5 CNBD under diametrical compression (Khan and Al-Shayea, 2000).....	33
Figure 3.6 Experimental setup for CNBD type specimen (Khan and Al-Shayea, 2000).....	33
Figure 3.7 Experimental setup for SNSCB type specimens (Khan and Al-Shayea, 2000).....	35
Figure 3.8 A semi-circular specimen containing an angled edge crack under three point-bending (Khan and Al-Shayea, 2000).....	37
Figure 4.1 Semi-infinite plate with an edge through crack under tension .....	46
Figure 4.2 3D ABAQUS view of the semi-infinite plate with an edge through crack under tension .....	47
Figure 4.3 Schematic view of the crack .....	47
Figure 4.4 Boundary conditions and load directions of the model .....	48
Figure 4.5 Schematic view of the 3D undeformed ABAQUS model after meshing ....	49
Figure 4.6 Schematic view of the 3D model .....	51
Figure 4.7 Boundary conditions and load directions of the model .....	52
Figure 4.8 Schematic view of the undeformed model after meshing .....	53

Figure 4.9 Inclined crack in tension .....	54
Figure 4.10 Schematic view of the 3D model .....	55
Figure 4.11 Schematic view of the model and the seam cracks.....	56
Figure 4.12 Boundary conditions and load directions of the model .....	57
Figure 4.13 Schematic view of the undeformed model after meshing .....	58
Figure 4.14 Schematic view of the undeformed seam cracks after meshing .....	59
Figure 4.15 Display of the reference point positions and the couplings .....	61
Figure 4.16 Boundary conditions of the model.....	62
Figure 4.17 Vertical stress distributions in y-direction (S22) after the computation ....	63
Figure 4.18 The displacements in y-direction (U2).....	64
Figure 4.19 Crack front .....	65
Figure 4.20 Points marked for the selection of crack extension direction using q vector.....	66
Figure 4.21 Crack extension direction .....	66
Figure 4.22 Schematic view of the constraints around the crack tip .....	67
Figure 4.23 Schematic view of the crack field after meshing .....	68
Figure 4.24 Load application by steel loading bars .....	69
Figure 4.25 (a) Direct load application from reference points .....	70
Figure 4.25 (b) Finite element mesh used in the analysis of SCB specimens .....	70
Figure 4.26 Boundary conditions of the direct load application through the reference point .....	71
Figure 4.27 (a) S11 ( $\sigma_{xx}$ ) Stress distribution in the model .....	73
Figure 4.27 (b) S11 ( $\sigma_{xx}$ ) Stress distribution at the crack tip (detailed view).....	73
Figure 4.28 (a) S22 ( $\sigma_{yy}$ ) Stress distribution in the model .....	74
Figure 4.28 (b) S22 ( $\sigma_{yy}$ ) Stress distribution at the crack tip (detailed view).....	74
Figure 4.29 (a) U1 ( $U_x$ ) Horizontal displacement distribution .....	76
Figure 4.29 (b) U2 ( $U_y$ ) Vertical displacement distribution.....	76
Figure 5.1 UCS test specimen with circumferential extensometer before the experiment.....	78
Figure 5.2 Smartcut 1004 precision diamond saw and the holding fixture .....	80

Figure 5.3 Half disc after the notch opening .....	81
Figure 5.4 Explanation of specimen codes .....	82
Figure 5.5 DBK 80 analog multiplexor, DBK 43 and DBK43A strain gage cards.....	84
Figure 5.6 SCB specimen with steel rollers before the experiment.....	85
Figure 5.7 SCB specimen sketch .....	86
Figure 5.8 Diamond saws which were used in the notch thickness analysis .....	88
Figure 5.9 Dimensions of flattened SCB specimens.....	90
Figure 6.1 Normalized SIF versus notch thickness .....	100
Figure 6.2 Normalized SIF versus $t_n/a$ .....	101
Figure 6.3 Average normalized SIF versus average notch thickness .....	102
Figure 6.4 Average normalized SIF versus average $t_n/a$ .....	103
Figure 6.5 Fracture toughness versus $t_n/a$ .....	104
Figure 6.6 Average fracture toughness versus average notch thickness .....	106
Figure 6.7 Average fracture toughness versus average $t_n/a$ .....	107
Figure 6.8 Horizontal stress versus distance in y-direction from the notch front.....	108
Figure 6.9 Vertical stress versus distance in y-direction from the notch front .....	109
Figure 6.10 $\sigma_{zz}$ stresses of two different notch thickness values versus distance in z- direction along the notch front .....	110
Figure 6.11 Normalized SIF versus span ratio (S/R) .....	115
Figure 6.12 Average normalized SIF versus average span ratio (S/R) .....	116
Figure 6.13 Average vertical displacement versus average span ratio (S/R) .....	117
Figure 6.14 Average stiffness versus average span ratio (S/R) .....	118
Figure 6.15 Failure load versus span ratio (S/R).....	119
Figure 6.16 Fracture toughness versus span ratio (S/R).....	120
Figure 6.17 Average fracture toughness versus average span ratio (S/R).....	121
Figure 6.18 Normalized SIF versus flattened loading surface width .....	125
Figure 6.19 Average normalized SIF versus average flattened loading surface width.	126
Figure 6.20 Fracture toughness versus flattened loading surface width.....	128
Figure 6.21 Average fracture toughness versus average flattened loading surface width .....	129

Figure 6.22 Horizontal stress distributions of flattened and non-flattened specimens .....	130
Figure 6.23 Vertical stress distribution of flattened and non-flattened specimens .....	131
Figure 6.24 Variation of the $\sigma_{zz}$ at the notch front along the thickness (in z-direction).....	132
Figure 6.25 Normalized SIF versus h .....	135
Figure 6.26 Normalized SIF versus h/D Ratio .....	136
Figure 6.27 Fracture toughness versus h/D Ratio .....	137
Figure 6.28 Fracture toughness versus h/a ratio .....	138
Figure 6.29 Fracture toughness versus a/D Ratio .....	139
Figure B.1 Notch thickness specimens after experiments.....	156
Figure B.2 Span ratio (S/R) analysis specimens after experiments.....	157
Figure B.3 Flattened loading face specimens after experiments.....	158

## SYMBOLS AND ABBREVIATIONS

$a$	: Crack length
A	: Area
B	: Thickness
BDT	: Uncracked Brazilian Disc Test
CB	: Chevron Bend
CCBD	: Central Cracked Brazilian Disc under diametrical compression test
$C_K$	: Correction factor to account for the size variation of the specimen
CMOD	: Crack Mouth Opening Displacement
CMOD <sub>f</sub>	: Crack Mouth Opening Displacement at failure
CNBD	: Chevron-Notched Brazilian Disc
CT	: Compact Tension test
CTOD	: Crack Tip Opening Displacement
D	: Specimen diameter
DOF	: Degrees of Freedom
DT	: Double Torsion
E	: Young's Modulus
EPFM	: Elastic Plastic Fracture Mechanics
f	: Flattened Loading Surface Width
FEM	: Finite Element Method
G	: Strain energy release rate
h	: Height
ISRM	: International Society for Rock Mechanics
J	: J-integral
k	: Stiffness
K	: Stress intensity factor
$K_{Comp.}$	: Computed Stress Intensity Factor
$K_{Anal.}$	: Analytical Solution of the Stress Intensity Factor

$K_{IC}$	: Fracture toughness
$K_I$	: Stress intensity factor in Mode I
$K_{II}$	: Stress intensity factor in Mode II
LEFM	: Linear Elastic Fracture Mechanics
MR	: Modified Ring test
$P$	: Applied load
$P_{max.}$	: Maximum Load at Failure
R	: Specimen Radius
S	: Support Span
SC3PB	: Single edge straight through cracked rectangular plate in three-point bending test
SCB	: Semi-Circular specimen under three-point Bending
SECB	: Single Edge Cracked Beam under three-point bending
SECBD	: Single edge cracked Brazilian disk in diametral compression
SECRBB	: Single Edge Cracked Round Bar Bend
SENRBB	: Single Edge Notched Round Bar in Bending
SNBD	: Straight-Notched Brazilian Disc
SNSCB	: Straight-Notched Semi-Circular Bend
SR	: Short Rod
TBM	: Tunnel Boring Machine
$t_n$	: Notch Thickness
$T_0$	: Tensile strength
U	: Vertical Displacement
w	: Width
$Y_I$	: Normalized stress intensity factor in Mode I
$\varepsilon$	: Strain
$\theta$	: Angle
$\beta$	: Crack Angle
$\Gamma$	: An arbitrary path around the crack tip
$\Pi$	: Potential Energy

$\sigma$  : Stress

$\sigma_{\max}$  : Maximum tangential stress criterion

$\nu$  : Poisson's Ratio

# CHAPTER 1

## INTRODUCTION

### 1.1 General View of Fracture and Rock Fracture Mechanics

Every structure contains small flaws whose size and distribution are dependent upon the material and its processing. These may vary from nonmetallic inclusions and micro voids to weld defects, grinding cracks, quench cracks, surface laps, etc. The objective of a **Fracture Mechanics** analysis is to determine if these small flaws will grow into large enough cracks to cause the component to fail catastrophically, (Dolan, 1970). Fracture mechanics combines the mechanics of cracked bodies and mechanical properties.

Cracks and flaws may occur everywhere therefore application areas of fracture mechanics are extensive, including many sciences and engineering disciplines such as Materials and Medical Sciences, Aerospace Engineering, Mechanical Engineering, Civil Engineering, Geological Engineering, Petroleum Engineering and Mining Engineering. In all these, researchers and designers have to consider fracture mechanics in their applications.

The establishment of fracture mechanics is closely related to some well known disasters in recent history. Several hundred liberty ships fractured extensively during World War II. The failures occurred primarily because of the change from riveted to welded construction and the major factor was the combination of the poor weld properties with stress concentrations, and poor choice of brittle materials in the construction, (Wang, 1996). There were 2,751 Liberty Ships manufactured between 1941-1945. Cracks propagated in 400 of these ships including 145

catastrophic failures; and some broke completely into two. Today only two of these ships still exist, (Banks, 2003).



**Figure 1.1** One of the liberty ships broke into two, (Banks, 2003)

On April 28, 1988 another accident happened because of the cracks. The Aloha Airlines Boeing 737 airplane failed. The central body portion of the airplane failed after 19 years of service. The failure was caused by fatigue (multi-site damage), (Banks, 2003).

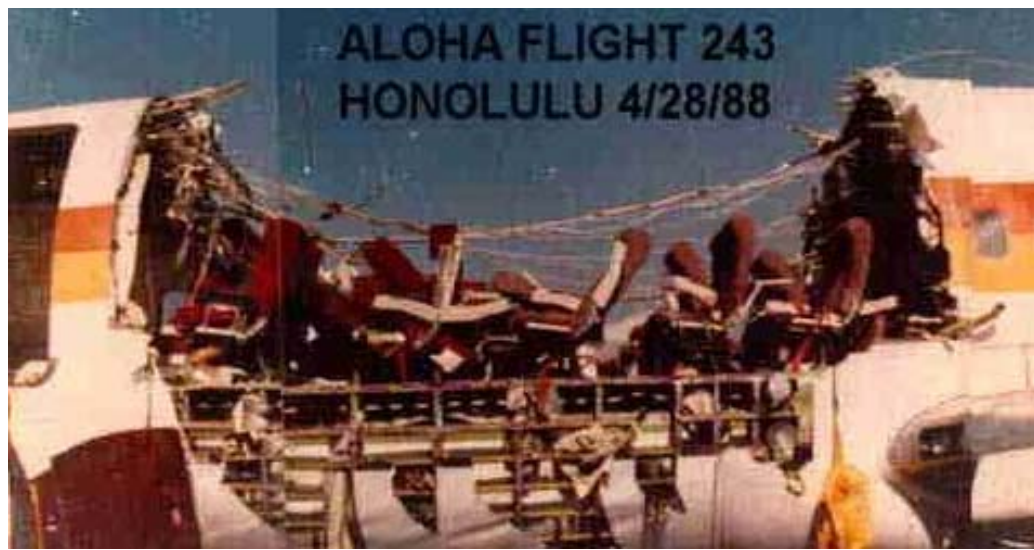


**Figure 1.2** The Aloha Airlines Boeing 737 airplane after the accident,  
(Banks, 2003)

One of the fracture mechanics branches is rock fracture mechanics. In earth sciences like petroleum engineering, geological engineering, civil engineering and mining engineering many applications of rock fracture mechanics can be found.

In rock engineering, rock fracture mechanics has a significant importance, in designing rock structures preventing or minimizing the fracture occurrence or development of cracks. In some situations, predicting the fracture behaviour of rock gives additional information about the structure and its mechanical response.

The recently increasing interest and developments in rock fracture mechanics research have touched many diverse areas including blasting, hydraulic fracturing and in situ stress determination, mechanical fragmentation, rock slope analysis, earthquake mechanics, earthquake prediction, plate tectonics, magmatic intrusions, hot dry rock geothermal energy extraction, fluid transport properties of fracturing rock masses, propagating oceanic rifts, crevasse penetration and other glaciological problems, the development of steeply dipping extension fractures that are nearly ubiquitous at the earth's surface and are formed through folding, upwarping and

rifting and the modeling of time-dependent rock failure, the geological disposal of radioactive waste, terrestrial sequestration of carbon dioxide to ease prejudicial effects on the environment, efficient underground storage of oil, gas or air, enhanced recovery of hydrocarbons and underground constructions at increasing overburden pressure for infrastructure or transport, (Atkinson, 1987; Whittaker et al., 1992; Backers, 2004).

In civil and mining engineering various types of rock cutting machines are used for rock excavation purposes, e.g. tunnel boring machines (TBM), raise borers and longwall shearers. Up to now the rock cutting tools are mounted in some experience-optimised pattern on the cutting heads of the machines, (Backers, 2004). Rock fracture mechanics is used to improve the design of these machines and their efficiency and workability in different types of rocks.

## **1.2 Objective of the Thesis Work**

In this study, semi circular discs were used to determine the fracture toughness of pink-gray Ankara andesite. Experiments were done by using the three point bending specimens, called as SCB (Semi-circular specimen under three point-bending). This specimen type was commonly used before by other researchers. Semi-circular specimen is a common choice in fracture mechanics determination, due to its easiness in specimen preparation, its versatility, its reliability and cost effectiveness. In the previous studies the effects of loading rate, water content of rock, temperature, notch length and notch type were investigated. In this study, new investigations were carried out on SCB type specimens to improve the accuracy and repeatability of fracture toughness determinations with this specimen type. The purpose was to make contributions to the efforts leading to acceptance of this specimen type as a standard or suggested method for fracture toughness determination.

The following was investigated in this research work:

- a) The effect of notch thickness,
- b) The effect of different span ratios (S/R),
- c) The effect of flattened surface,
- d) The effect of little dimensional variations when preparing the specimens.

### **1.3 Methodology**

Middle East Technical University licentiate software ABAQUS (Three dimensional finite element program) was used to determine the stress intensity factors of the specimens. Every specimen was introduced to the software models by its own dimensions. This way, variations in the stress intensity factors due to differences in the specimen dimensions that occurred during specimen preparations were taken into account.

Cylindrical core specimens had an approximately 100 mm diameter and 50 mm radius with thickness around 50 mm. Initial notch introduced to initiate crack propagation had a length around 10 mm.

Effect of notch thickness was studied by using four different rotary diamond saws which cut initial notches with thickness changing between 0.84 mm – 3.66 mm. A total of 24 tests were conducted in this category with 5-6 repeated tests for each notch thickness group.

Load span was changed and effect of variation of span between S/R=0.3 to 0.9 was studied for 7 different S/R value with about 3 tests at each S/R ratio.

Upper loading surface of SCB specimens were machined as flat loading surfaces for uniform load application instead of a concentrated load application of regular

tests. Flat loading ends of widths 15, 20, 22.5 and 25 mm were tried with 3-5 repeated tests for each group.

Fracture toughness values were evaluated by using the stress intensity factors computed from numerical modeling and crack initiation loads of the experiments.

#### **1.4 Sign Convention**

In this study, on the contrary to the general rock mechanics convention, compressive stresses are taken negative and the tensile stresses are taken positive. The reason for this ABAQUS finite element program used extensively in this work is a general engineering program with a regular solid mechanics sign convention. Coordinate axes marked with 1, 2 and 3 in ABAQUS according to the general tensor notation correspond to x, y and z axes, respectively.

#### **1.5 Outline of the Thesis**

After a brief introduction to fracture mechanics and rock fracture mechanics in Chapter I, history of the fracture mechanics, fracture modes, stress intensity factor and fracture toughness are described in Chapter II. In Chapter III rock fracture testing methods for Mode I are mentioned. Numerical modeling, finite element method, ABAQUS software and ABAQUS verification examples are presented in Chapter IV. Experimental studies, laboratory works and the specimen geometries are described in Chapter V. In Chapter VI results and discussions are presented. Consequently, in Chapter VII conclusion and recommendations are given.

## CHAPTER 2

# FRACTURE MECHANICS AND FRACTURE TOUGHNESS

### 2.1 History of Fracture Mechanics

The first milestone of fracture mechanics was performed by Leonardo da Vinci several centuries earlier provided some clues as to the root cause of fracture. He measured the strength of iron wires and found that the strength varied inversely with wire length. These results implied that flaws in the material controlled the strength; a longer wire corresponded to a larger sample volume and a higher probability of sampling a region containing a flaw. These results were only qualitative, however, (Anderson, 1991).

In 1920, a quantitative connection between fracture stress and flaw size came from the work of Griffith (1920) in his famous paper. He applied a stress analysis of an elliptical hole (performed by Inglis (1913) seven years earlier) to the unstable propagation of a crack. Griffith invoked the first law of thermodynamics to formulate a fracture theory based on a simple energy balance. According to this theory, a flaw becomes unstable, and thus fracture occurs, when the strain energy change that results from an increment of crack growth is sufficient to overcome the surface energy of the material, (Anderson, 1991). However, Griffith's approach is too primitive for engineering applications and is only successful for brittle materials.

In 1948, Irwin (1948) extended the Griffith approach to metals by including the energy dissipated by local plastic flow. During the same period Orowan (1948)

independently proposed similar modification to the Griffith theory and Mott (1948) extended the Griffith theory to a rapidly propagating crack, (Anderson, 1991).

In 1956, Irwin (1956) developed the concept of strain energy release rate  $G$ ,  $G$  was defined as the rate of change in potential energy near the crack area for a linear elastic material, ([www.efunda.com](http://www.efunda.com)). This concept is related to the Griffith's theory but is in a form that is more useful for solving engineering problems, (Anderson, 1991).

$$G \equiv \frac{d\Pi}{dA} \quad (2.1)$$

where:

$G$ : Energy release rate,

$d\Pi$  : Potential energy supplied by the internal strain energy and external forces,

$dA$ : Incremental increase in the crack area.

When the strain energy release rate reaches the critical value,  $G_c$ , the crack will grow. Later, the strain energy release rate  $G$  was replaced by the stress intensity factor  $K$  with a similar approach by other researchers, ([www.efunda.com](http://www.efunda.com)).

After the fundamentals of fracture mechanics were established around 1960, scientists turned their attention on the plasticity of the crack tips. During this time period several researchers developed analyses to correct for yielding at the crack tip, including Irwin (1961), Dugdale (1960), Barenblatt (1962) and Wells (1961). The Irwin (1961) plastic zone correction was relatively simple extension of LEFM, while Dugdale (1960) and Barenblatt (1962) each developed somewhat more elaborate models based on a narrow strip of yielded material at the crack tip. On the other hand Wells (1961) proposed the displacement of the crack faces as an alternative fracture criterion when significant plasticity precedes failure. He attempted to apply LEFM to low- and medium-strength structural steels. These materials were too ductile for LEFM to apply, but Wells noticed that the crack

faces moved apart with plastic deformation. This observation led to the development of the parameter now known as the crack tip opening displacement (CTOD), (Anderson, 1991).

In 1968, Rice (1968) modeled the plastic deformation as nonlinear elastic behavior and extended the method of energy release rate to nonlinear materials. He showed that the energy release rate can be expressed as a path-independent line integral, called the  $J$  integral. Rice's theory has since dominated the development of fracture mechanics in United States. During his study was being published, Rice discovered that Eshelby (1956) had previously published several so-called conservation integrals, one of which was equivalent to Rice's  $J$  integral. However, Eshelby (1956) did not apply his integrals to crack problems. In 1971 Begley and Landes (1972) who were research engineers at Westinghouse, came across Rice's article and decided to characterize fracture toughness of these steels with the  $J$  integral. Their experiments were very successful and led to the publication of a standard procedure for  $J$  testing of metals ten years later. In 1976, Shih and Hutchinson (1976) established a fracture design analysis based on the  $J$  integral by providing the theoretical framework for such an approach. In addition to this analysis Shih demonstrated a relationship between the  $J$  integral and the CTOD, implying that both parameters are equally valid for characterizing fracture, (Anderson, 1991).

Thereafter, many experiments were conducted to verify the accuracy of the models of fracture mechanics. Significant efforts were devoted to converting theories of fracture mechanics to fracture design guidelines.

Fracture mechanics basically can be divided into two main categories. These are:

- 1) Linear Elastic Fracture Mechanics (LEFM),
- 2) Elastic-Plastic Fracture Mechanics (EPFM).

## 2.2 Linear Elastic Fracture Mechanics (LEFM)

Linear Elastic Fracture Mechanics (LEFM) first assumes that the material is isotropic and linear elastic. Based on the assumption, the stress field near the crack tip is calculated using the theory of elasticity. When the stresses near the crack tip exceed the material fracture toughness, the crack will propagate.

The crack tip stress field is a function of the location, loading, and geometry:

$$\sigma_{ij}^{Tip} \equiv \sigma_{ij}^{Tip}(Location, Loading, Geometry) \quad (2.2)$$

$$\equiv \sigma_{ij}^{Tip}(r, \theta, K) \quad (2.3)$$

where,

r: Location

$\theta$ : Loading

K: Geometry

Location can be represented by  $r$  and  $\theta$  using the polar coordinate system whereas the loading and geometry terms can be grouped into a single parameter, ([www.efunda.com](http://www.efunda.com)).

## 2.3 Fracture Modes

In fracture mechanics cracks or fractures are usually subdivided into three basic types, namely Mode I, Mode II and Mode III, (Figure 2.1) from a mostly mathematical viewpoint, (Irwin, 1958).

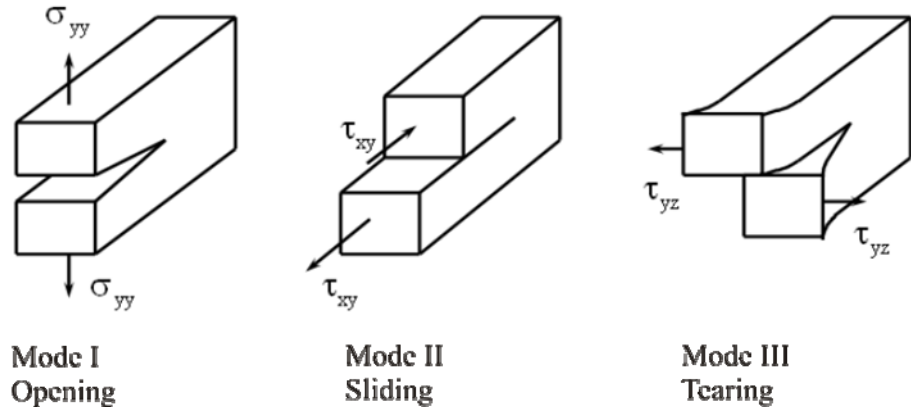


**Figure 2.1** Types of fracture

Mode I which is called as opening (tensile) mode, the crack tip is subjected to displacements perpendicular to the crack plane. The crack propagation is in crack plane direction. The crack carries no shear traction and no record of shear displacement is visible, (Backers, 2004).

Mode II which is called as sliding, the crack faces move relatively to each other in the crack plane. Crack propagation is perpendicular to the crack front. Shear traction parallels the plane of the crack, (Backers, 2004).

Mode III which called as tearing, shear displacement is acting parallel to the front in the crack plane, (Backers, 2004).

If any combination of these modes occurred, this is called as mixed mode.

## 2.4 Stress Intensity Factor and Crack Tip Stresses

Determination of the stresses for Mode I and Mode II cracks is first carried out by Westergaard (1939) who made use of a stress function which is a function of a complex variable. Later, Williams (1957) made use of the equation of elasticity in conventional form and lead to the results which were more general than Westergaard's. Theory of stress intensity factor was developed by Barenblatt (1962) and others in the Soviet Union. A more detailed comparison of the energy and stress intensity approaches has been given by Willis (1967). He showed that they are identical except for the fact that one involves work to separate two planes from an unstrained position and the other the work to separate from a strained position.

Crack tips produce a  $1/\sqrt{r}$  singularity. The stress fields near a crack tip of an isotropic linear elastic material can be expressed as a product of  $1/\sqrt{r}$  and a function of  $\theta$  with a scaling factor  $K$ :

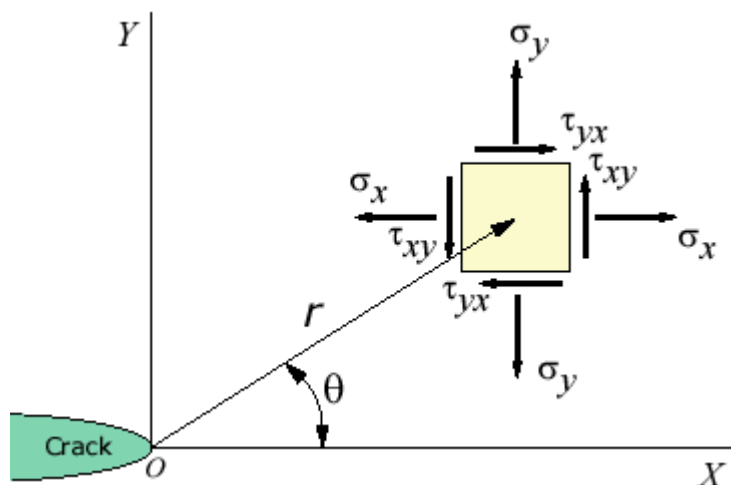


**Figure 2.2** Stress tensor notations in the cartesian co-ordinate system

The simple form of stress and displacement functions near the tip of the crack (as  $r \rightarrow 0$ ) are shown below:

$$\lim_{r \rightarrow 0} \sigma_{ij}^{(I)} = \frac{K_I}{\sqrt{2\pi r}} f_{ij}^{(I)}(\theta) \quad (2.4)$$

$$\lim_{r \rightarrow 0} \sigma_{ij}^{(II)} = \frac{K_{II}}{\sqrt{2\pi r}} f_{ij}^{(II)}(\theta) \quad (2.5)$$

$$\lim_{r \rightarrow 0} \sigma_{ij}^{(III)} = \frac{K_{III}}{\sqrt{2\pi r}} f_{ij}^{(III)}(\theta) \quad (2.6)$$

where:

$\sigma_{ij}$ : Stress tensor in cartesian coordinates,

$f_{ij}$ : Geometric stress factor depending solely on angle  $\theta$ .

Similarly the displacement components have the form where K can be  $K_I$ ,  $K_{II}$  or  $K_{III}$  depending on the mode.

$$\frac{K_I}{\sigma} \left( \frac{r}{2\pi} \right)^{1/2} g(\theta) \quad (2.7)$$

For all three fracture modes (Mode I, Mode II, Mode III) stress and displacement fields near a crack tip of a linear elastic isotropic material are listed below.

where,

$$\kappa = \begin{cases} \frac{3-\nu}{1+\nu} & (\text{Plane Stress}) \\ \frac{3-4\nu}{1+\nu} & (\text{Plane Strain}) \end{cases} \quad (2.8)$$

For linear elastic materials, the principle of superposition applies. A mixed-mode problem can be treated as the summation of each mode (Mode I, Mode II, Mode III).

$$\sigma_{ij}^{(Total)} = \sigma_{ij}^{(I)} + \sigma_{ij}^{(II)} + \sigma_{ij}^{(III)} \quad (2.9)$$

Crack tip displacement components and crack tip stress components of Mode I loading is presented below:

Mode I Crack Tip Stress Components:

$$\sigma_{xx} = \frac{K_I}{\sqrt{2\pi r}} \cos\left[\frac{\theta}{2}\right] \left[ 1 - \sin\left[\frac{\theta}{2}\right] \sin\left[\frac{3\theta}{2}\right] \right] \quad (2.10)$$

$$\sigma_{yy} = \frac{K_I}{\sqrt{2\pi r}} \cos\left[\frac{\theta}{2}\right] \left[ 1 + \sin\left[\frac{\theta}{2}\right] \sin\left[\frac{3\theta}{2}\right] \right] \quad (2.11)$$

$$\sigma_{zz} = \begin{cases} \mathbf{0} & (Plane \quad Stress) \\ \nu(\sigma_{xx} + \sigma_{yy}) & (Plane \quad Strain) \end{cases} \quad (2.12)$$

$$\tau_{xy} = \frac{K_I}{\sqrt{2\pi r}} \cos\left[\frac{\theta}{2}\right] \sin\left[\frac{\theta}{2}\right] \cos\left[\frac{3\theta}{2}\right] \quad (2.13)$$

$$\tau_{yz} = \mathbf{0}, \quad \tau_{xz} = \mathbf{0}$$

Mode I Crack Tip Displacement Components:

$$u_x = \frac{K_I}{2\mu} \sqrt{\frac{r}{2\pi}} \cos\left[\frac{\theta}{2}\right] \left[ \kappa - 1 + 2 \sin^2\left[\frac{\theta}{2}\right] \right] \quad (2.14)$$

$$u_y = \frac{K_I}{2\mu} \sqrt{\frac{r}{2\pi}} \sin\left[\frac{\theta}{2}\right] \left[ \kappa + 1 - 2 \cos^2\left[\frac{\theta}{2}\right] \right] \quad (2.15)$$

$$u_z = \mathbf{0}$$

$K_I, K_{II}, K_{III}$  are the factors depending on the outer boundary conditions, i.e. applied loading and geometry and also called as the stress intensity factor. In fracture mechanics the stress intensity factor gives the grade of stress concentration at the tip of a crack of length at a given loading and has the dimension of stress. In units  $\text{MPa}\sqrt{m}$ , (Backers, 2004).

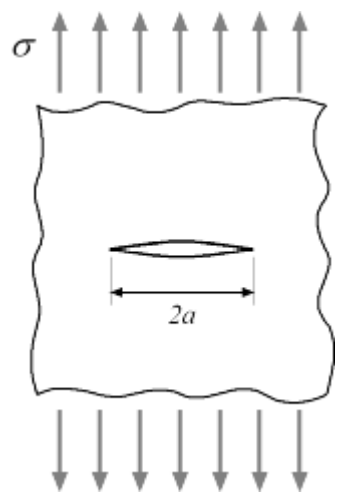
$$K_{I, II, III} = \sigma_A \sqrt{\pi \times a} = \sigma_{ij} \sqrt{2\pi \times r}; \text{ for } \theta = 0 \quad (2.16)$$

where,

$\sigma_A$ : Applied stress

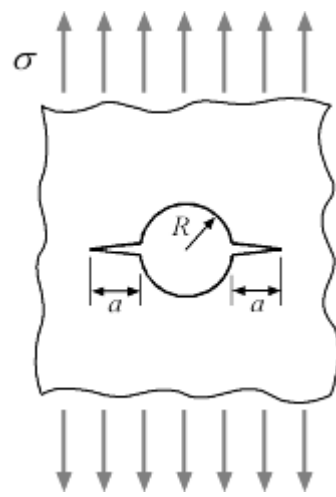
a: Crack length

Some typical stress intensity factor  $K_I$  solutions for the best known loading conditions are shown in Figure 2.3 below:



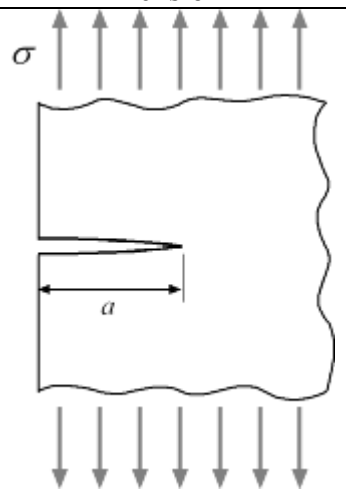
$$K_I = \sigma \sqrt{\pi a}$$

Infinite Plate with a Center Through Crack under Tension



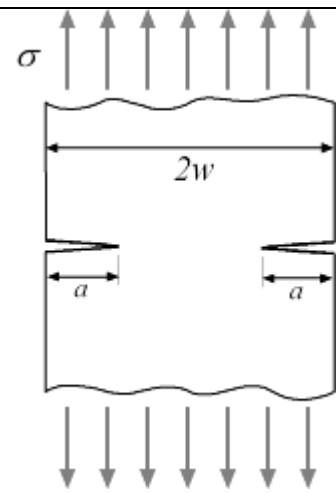
$$K_I = \sigma \sqrt{\pi a} \left[ 1 + 2.365 \left( \frac{R}{R+a} \right)^{2.4} \right]$$

Infinite Plate with a Hole and Symmetric Double Through Cracks under Tension



$$K_I = 1.12 \sigma \sqrt{\pi a}$$

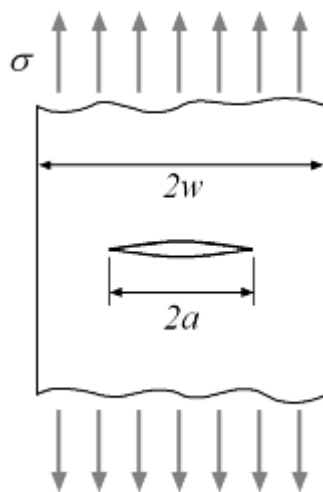
Semi-infinite Plate with an Edge Through Crack under Tension



$$K_I = \sigma \sqrt{\pi a} \left[ \frac{2w}{\pi a} \right]^{\frac{1}{2}} \left[ \tan \left[ \frac{\pi a}{2w} \right] + 0.1 \sin \left[ \frac{\pi a}{w} \right] \right]^{\frac{1}{2}}$$

Infinite Stripe with Symmetric Double Through Cracks under Tension

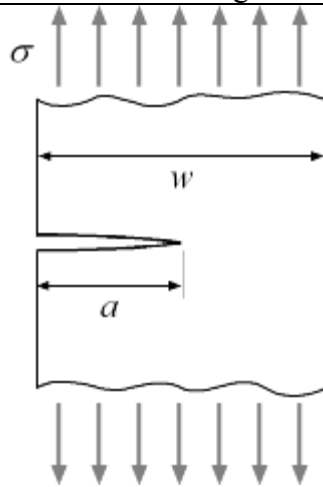
**Figure 2.3** Stress intensity factor  $K_I$  solutions for the known analytical problems



$$K_I = \sigma \sqrt{\pi a} \left[ \frac{2w}{\pi a} \tan \left[ \frac{a}{2w} \right] \right]^{\frac{1}{2}}$$

$$K_I = \sigma \sqrt{\pi a} \left[ \sec \left[ \frac{\pi a}{2w} \right] \right]^{\frac{1}{2}} \left[ 1 - 0.25 \left[ \frac{a}{w} \right]^2 + 0.06 \left[ \frac{a}{w} \right]^4 \right]$$

Infinite Stripe with a Center Through Crack under Tension

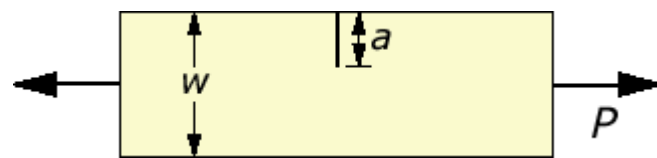


$$K_I = \sigma \sqrt{\pi a} \left[ \frac{2w}{\pi a} \tan \left[ \frac{\pi a}{2w} \right] \right]^{\frac{1}{2}}$$

$$\left[ \frac{0.752 + 2.02 \frac{a}{w} + 0.37 \left[ 1 - \sin \left[ \frac{\pi a}{2w} \right] \right]}{\cos \left[ \frac{\pi a}{2w} \right]} \right]$$

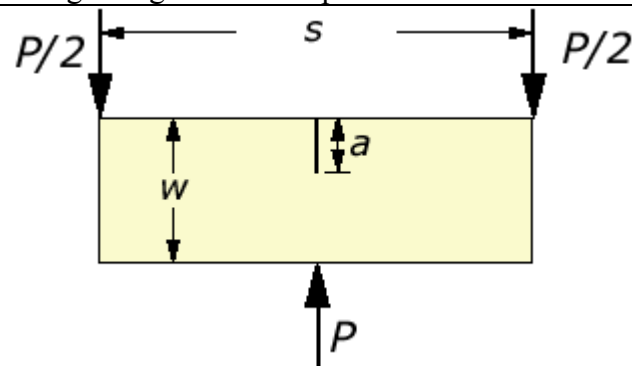
Infinite Stripe with an Edge Through Cracks under Tension

**Figure 2.3 (Cont'd)**



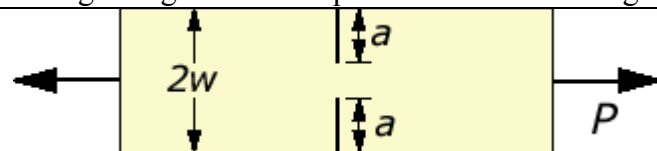
$$K_I = \frac{P}{B\sqrt{w}} \left\{ \frac{\sqrt{2} \tan \left[ \frac{\pi a}{2w} \right]}{\cos \left[ \frac{\pi a}{2w} \right]} \left[ 0.752 + 2.02 \left[ \frac{a}{w} \right] + 0.37 \left[ 1 - \sin \left[ \frac{\pi a}{2w} \right] \right]^3 \right] \right\}$$

Single Edge Notched Specimen under Tension



$$K_I = \frac{P}{B\sqrt{w}} \left\{ \frac{3 \frac{s}{w} \sqrt{\frac{a}{w}}}{2 \left[ 1 + 2 \frac{a}{w} \right] \left[ 1 - \frac{a}{w} \right]^{\frac{3}{2}}} \left\{ 1.99 - \frac{a}{w} \left[ 1 - \frac{a}{w} \right] \left[ 2.15 - 3.93 \frac{a}{w} + 2.7 \left( \frac{a}{w} \right)^2 \right] \right\} \right\}$$

Single Edge Notched Specimen under Bending



$$K_I = \frac{P}{B\sqrt{w}} \left\{ \frac{\sqrt{\frac{\pi a}{2w}}}{\sqrt{1 - \frac{a}{w}}} \left[ 1.122 - 0.561 \frac{a}{w} - 0.205 \left( \frac{a}{w} \right)^2 + 0.471 \left( \frac{a}{w} \right)^3 + 0.190 \left( \frac{a}{w} \right)^4 \right] \right\}$$

Double Edge Notched Specimen under Tension

Figure 2.3 (Cont'd)

By measuring  $\sigma$  and  $a$  at the outset of fracture we obtain  $K_C$  which is usually referred to as the fracture toughness. Knowing  $K_C$  we can then predict the critical combinations of stress and crack length for any other configuration for which the stress intensity factor is known from analytical or numerical solutions. Fracture toughness is a material property.

## 2.5 Fracture Toughness

Fracture toughness can be defined as the ability of rock to resist fracturing and propagation of pre-existing cracks. In other words, it is the fracture energy consumption rate required to create new surfaces. Some applications of such values for rock are as, (Whittaker et al., 1992, Sun and Ouchterlony, 1986):

- A parameter for classification of rock material,
- An index for fragmentation processes such as tunnel,
- Boring and model scale blasting, and
- A material property in the modeling of rock fragmentation like hydraulic fracturing, explosive stimulation of gas wells, radial explosive fracturing, and crater blasting as well as in stability analysis.

Fracture toughness values of some materials and rock types are listed below at Table 2.1. (Testing technique is indicated only for rocks)

**Table 2.1**  $K_{IC}$  values of some materials and rocks

Rock	Test Type of $K_{IC}$	Fracture Toughness $K_{IC}$ (MPa $\sqrt{m}$ )	Reference Source
Ankara Andesite	MR	1.59	Şener, 2002
Isparta Andesite	SECBD	2.92	Altındağ, 2000
Tampomas Andesite	CB	1.26	Abrahamsson et al., 1987
Tampomas Andesite	CB	1.68	Abrahamsson et al., 1987
Whitwick Andesite	CB	2.17	Bearman, 1999
Basalt	SC3PB	2.27	Whittaker, 1992
Basalt	SECBD	1.80	Whittaker, 1992
Basalt	BDT	3.01	Whittaker, 1992
Beryllium (Be)	-	4	<a href="http://www.efunda.com">www.efunda.com</a>
Cast Iron	-	6-20	<a href="http://www.efunda.com">www.efunda.com</a>
Cement-Concrete	-	0.2	<a href="http://www.efunda.com">www.efunda.com</a>
Coal	SC3PB	0.03-0.27	Zhang, 2002
Bolton Hill Diorite	CB	2.22	Bearman, 1999
Cliffe Hill Diorite	CB	2.77	Bearman, 1999
Äspö Diorite	SENRBB	3.21	Nordlund et al., 1999
Äspö Diorite	CB	3.21	Staub et al., 2003
Whin Sill Dolerite	SR	3.26	Meredith, 1983
Falkirk Dolostone	SR	1.66	Gunsallus & Kulhawy, 1984
Kankakee Dolostone	SR	1.66	Gunsallus & Kulhawy, 1984
Markgraf Dolostone	SR	1.78	Gunsallus & Kulhawy, 1984
Oatka Dolostone	SR	1.80	Gunsallus & Kulhawy, 1984
Remeo Dolostone	SR	2.47	Gunsallus & Kulhawy, 1984

**Table 2.1** (Cont'd)

Rock	Test Type of $K_{IC}$	Fracture Toughness $K_{IC}$ (MPa $\sqrt{m}$ )	Reference Source
Kallax Gabbro	SR	2.58-3.23	Yi, 1987
Bohus granite	CB	1.42	Ouchterlony, 1987
Bohus granite	SR	2.40	Ouchterlony, 1987
Cornwall granite	CB	1.32	Müller & Rummel, 1984
Daejeon granite	BDT	1.18	Yoon & Jeon, 2004
Epprechtstein granite	CB	1.74	Müller & Rummel, 1984
Favela granite (Grain plane)	CNBD	0.90	Almeida et al., 2006
Favela granite (Hardway plane)	CNBD	1.16	Almeida et al., 2006
Favela granite (Rift plane)	CNBD	0.97	Almeida et al., 2006
Falkenberg granite	CB	0.65-1.52	Müller & Rummel, 1984
Granite	SECBD	1.65	Whittaker, 1992
Iidate granite	SR	1.12	Takahashi et al., 1986
Iidate granite	CB	1.73	Müller & Rummel, 1984
Iidate granite	CB	2.26	Takahashi et al., 1986
Krakemala granite	CB	2.16	Ouchterlony, 1987
Krakemala granite	SR	2.22	Ouchterlony, 1987
Merrivale granite	SR	1.80	Meredith, 1983
Newhurst granite	SCB	1.72	Whittaker, 1992
Penryn granite	CB	1.83	Bearman, 1999
Pink granite	SR	2.03	Meredith, 1983
Rasjö granite	SR	2.80	Ouchterlony, 1987
Stripa granite	SR	2.70	Ouchterlony, 1987
Stripa granite	SR	2.36	Sun & Ouchterlony, 1986

**Table 2.1** (Cont'd)

Rock	Test Type of $K_{IC}$	Fracture Toughness $K_{IC}$ (MPa $\sqrt{m}$ )	Reference Source
Stripa granite	SECRBB	1.74	Sun & Ouchterlony, 1986
Straht Halladale granite	SR	2.19	Meredith, 1983
TGP granite	SENRBB	2.08	Yu, 2001
Utinga granite (Grain plane)	CNBD	0.73	Almeida et al., 2006
Utinga granite (Hardway plane)	CNBD	0.82	Almeida et al., 2006
Utinga granite (Rift plane)	CNBD	0.60	Almeida et al., 2006
Westerly granite	CT	2.70	Schmidt & Lutz, 1979
Westerly granite	CT	2.70	Sun & Ouchterlony, 1986
Westerly granite	SR	2.27	Ouchterlony, 1987
Westerly granite	SR	1.82	Meredith, 1983
Ingleton greywacke	CB	2.38	Bearman, 1999
Cornish greywacke	CB	3.15	Bearman, 1999
Finnsjön granodiorite	SR	3.35	Ouchterlony, 1987
Johnstone (w =18%)	SECB	0.05	Harberfield & Johnstone, 1990
Johnstone (w =18%)	SCB	0.06	Lim et al., 1994
Fethiye limestone	SECBD	2.18	Altındağ, 2000
Grey limestone	BDT	1.58	Whittaker, 1992
Harrycroft limestone	CB	0.82	Bearman, 1999
Isparta limestone	SECBD	2.48	Altındağ, 2000
Indiana limestone	SECB	0.97	Ingraffea & Schmidt, 1979
Indiana limestone	CCP	0.97	Sun & Ouchterlony, 1986
Indiana limestone	SC3PB	0.99	Whittaker, 1992
Irondequoit limestone	SR	1.36	Gunsallus & Kulhawy, 1984

**Table 2.1** (Cont'd)

Rock	Test Type of $K_{IC}$	Fracture Toughness $K_{IC}$ (MPa $\sqrt{m}$ )	Reference Source
Klinthagen limestone	SR	1.87	Ouchterlony, 1987
Middleton limestone	CB	0.73	Bearman, 1999
Reynales limestone	SR	2.06	Gunsallus & Kulhawy, 1984
Saudi Arabia limestone	SENRBB	0.39	Khan & Al-Shayea, 2000
Shelly limestone	SR	1.44	Meredith, 1983
Welsh limestone	SCB	0.85	Singh & Sun, 1990
White limestone	BDT	1.38	Whittaker, 1992
Wredon limestone	CB	1.70	Bearman, 1999
Carrara marble	CB	1.38	Müller & Rummel, 1984
Coarse grained marble	BDT	1.12	Whittaker, 1992
Ekeberg marble	CB	1.76	Ouchterlony, 1987
Ekeberg marble	SR	2.25	Ouchterlony, 1987
Fine grained marble	BDT	1.00	Whittaker, 1992
İzmir (Torbali Marble)	SECBD	1.74	Altındağ, 2000
Muğla Marble	SECBD	0.94-1.19	Altındağ, 2000
Treuchtlingen marble	CB	1.70	Müller & Rummel, 1984
Grey norite	SR	2.69	Meredith, 1983
Alvdalen sandstone	CB	0.73	Ouchterlony, 1987
Alvdalen sandstone	SR	1.91	Ouchterlony, 1987
Coarse grained sandstone	SCB	0.35	Singh & Sun, 1990
Grimsby sandstone	SR	1.47	Gunsallus & Kulhawy, 1984
Fine grained sandstone	SCB	0.28	Singh & Sun, 1990
Fine grained sandstone	SC3PB	0.56	Whittaker, 1992

**Table 2.1** (Cont'd)

Rock	Test Type of $K_{IC}$	Fracture Toughness $K_{IC}$ (MPa $\sqrt{m}$ )	Reference Source
Fine grained sandstone	CCBD	0.62	Fowell & Chen, 1990
Flechtingen sandstone	CB	1.15	Backers et al., 2003
Isparta sandstone	SECBD	2.85	Altındağ, 2000
Montcliffe sandstone	CB	1.18	Bearman, 1999
Pennant sandstone	CB	2.10	Bearman, 1999
Pennant sandstone	SR	2.56	Meredith, 1983
Ruhr sandstone	CB	1.03	Müller & Rummel, 1984
Ryefield sandstone	SECBD	1.04	Whittaker, 1992
Sandstone	BDT	0.67	Whittaker, 1992
Colorado oil shale	SCB	1.02	Chong et al., 1987
Siltstone	SECBD	0.80	Whittaker, 1992
High-Strength Steel	-	50-154	<a href="http://www.efunda.com">www.efunda.com</a>
Mild Steel	-	140	<a href="http://www.efunda.com">www.efunda.com</a>
Medium-Carbon Steel	-	51	<a href="http://www.efunda.com">www.efunda.com</a>
Dark grey syenite	SC3PB	1.55-1.93	Zhang, 2002
Greyish white syenite	SC3PB	1.21-1.51	Zhang, 2002
Göynük tuff	SR	1.29	Şantay, 1990
Nevada tuff	-	0.41	Zhang, 2002
Ogino tuff	SR	1.06	Matsuki et al., 1987
Ogino tuff	CB	1.08	Matsuki et al., 1987

(\*)

BDT : Uncracked Brazilian Disc test

CB : Chevron Bend

CCBD : Central Cracked Brazilian Disc under diametral compression test

CCP : Centre Cracked Panel

CNBD : Chevron-Notched Brazilian Disc

CT : Compact Tension  
MR : Modified Ring test  
SC3PB : Single edge straight through cracked rectangular plate in three-point bending test  
SCB : Semi-Circular Bend test  
SECB : Single Edge Cracked Beam under three-point bending test  
SECBD : Single Edge Cracked Brazilian Disc in diametral compression  
SECRBB : Single Edge Cracked Round Bar Bend  
SENRRBB : Single Edge Notched Round Bar in Bending  
SR : Short Rod

## 2.6 Elastic Plastic Fracture Mechanics

The linear elastic results predict very high stresses at the crack tip even for vanishingly small applied loads, and plastic flow will always occur there. The ways in which the stress and strain distributions at a crack tip affected by this plastic flow can be determined only by performing the appropriate elastic-plastic analysis.

Linear Elastic Fracture Mechanics (LEFM) applies when the nonlinear deformation of the material is confined to a small region near the crack tip. For brittle materials, it accurately establishes the criteria for catastrophic failure. However, severe limitations arise when large regions of the material are subject to plastic deformation before a crack propagates. Elastic Plastic Fracture Mechanics (EPFM) is proposed to analyze the relatively large plastic zones.

Elastic Plastic Fracture Mechanics (EPFM) assumes isotropic and elastic-plastic materials. Based on the assumption, the strain energy fields or opening displacement near the crack tips are calculated. When the energy or opening exceeds the critical value, the crack will grow.

## CHAPTER 3

### ROCK FRACTURE TOUGHNESS TESTING METHODS FOR MODE I

For the determination of the critical stress intensity factors of the different modes and fracture toughnesses  $K_{IC}$ ,  $K_{IIC}$  and  $K_{IIIC}$ , different laboratory testing methods have been developed. Most common ones are the Mode I testing methods, evidently with three ISRM Suggested Methods, (Backers, 2004).

Several Mode I testing methods for the determination of fracture toughness of rocks are available in literature. Some experiment types used in the previous studies are listed below:

- SCB (Semi-Circular Core in three point Bending)-(Chong & Kuruppu, 1984)
- The Chevron-Notched SCB test (Kuruppu, 1997),
- The BD (Brazilian Disc) test (Guo et al., 1993),
- The RCR (Radial Cracked Ring) test (Shiryaev & Kotkis, 1982),
- The MR (Modified Ring) test (Thiercelin & Roegiers, 1986),
- DT (Double Torsion) test (Evans, 1972). This test has a special importance, as it has been also applied to the study of subcritical crack growth in rock, (e.g. Atkinson, 1984).

Three testing methods for rock have been introduced by the International Society for Rock Mechanics (ISRM) as Suggested Methods, (Ouchterlony, 1988; Fowell, 1995). These are:

- SR (Short Rod Specimens) (Ouchterlony, 1988),
- CB (Chevron Bend) (Ouchterlony, 1988),
- Cracked Chevron-Notched Brazilian Disc (CNBD) Specimens (Fowell, 1995).

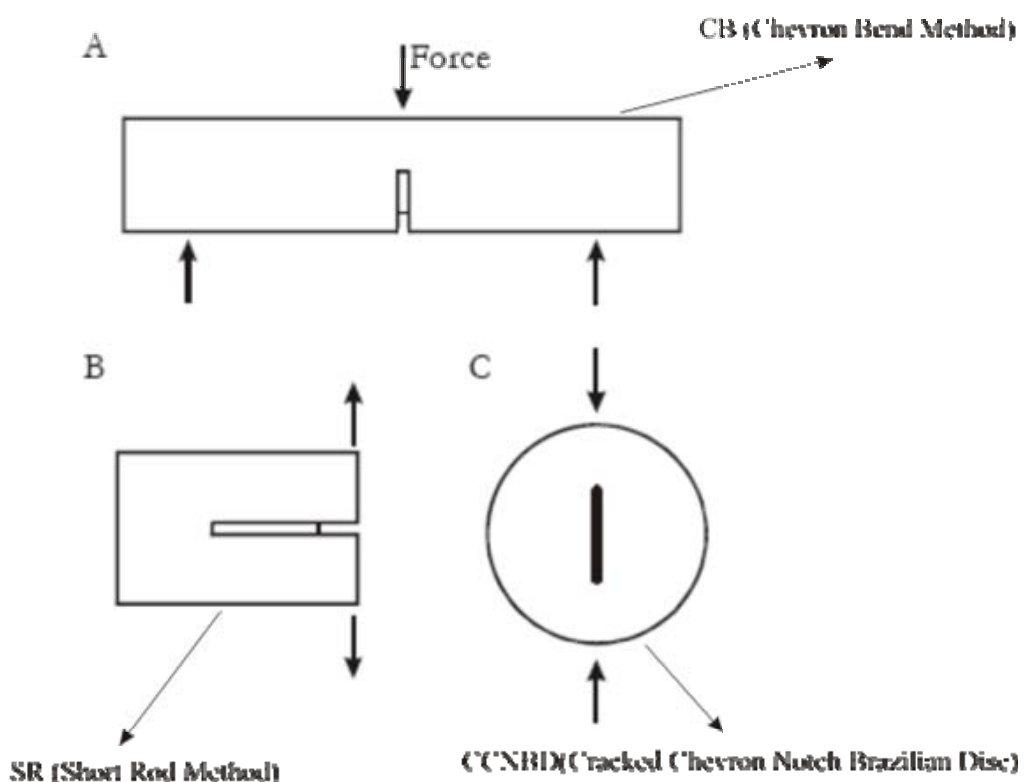


**Figure 3.1** ISRM's suggested Mode I fracture toughness testing methods,  
(Modified From Backers, 2004)

These three methods suggested by the ISRM are shortly described below.

### **3.1 Short Rod (SR) Method**

In 1977 L.M. Barker proposed the Short Rod (SR) test specimen for measuring plane-strain fracture toughness. This new test method was designed to simplify plane-strain fracture toughness procedures and to allow a broader range of materials to be tested successfully. These objectives were accomplished by designing a test specimen which would develop a natural crack in the specimen without the need for fatigue pre-cracking.

As illustrated in Figure 3.2, the general shape of a SR test specimen is a right cylinder. Two narrow slits are cut in the sides of this test specimen such that the two specimen halves are joined by a triangular ligament of material (chevron).

A tensile (opening) load is applied to force the two specimen halves apart (Mode I loading). When this mouth opening load reaches an adequate level, a natural crack is initiated at the tip of the chevron. The geometry of the test specimen is such that as the crack advances, the crack front broadens, thus a crack grows stably, even in very brittle materials. At a crack length known as the “critical crack length”, the crack becomes unstable (requires lower rather than higher loads to advance the crack). A load-displacement record is made during the test. To evaluate fracture toughness, the load to advance a crack of specific length must be known. This may be at the geometry-dependent “critical crack length”, the point at which the load is a maximum, or it may be the load at some other crack length. The crack length at any point during the test may be determined using a compliance technique. During the specimen loading, pairs of unloading - reloading cycles are performed. By comparing the slope of the reloading curves to the initial loading slope, the crack length can be determined. With this technique, fracture toughness can be measured at several different crack lengths as the crack propagates through the test specimen.

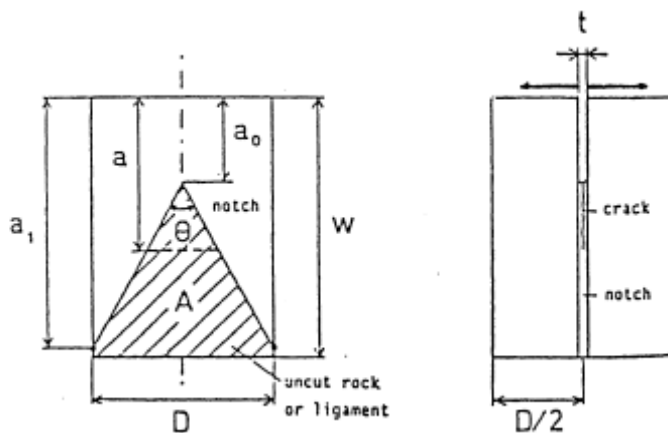


**Figure 3.2** Geometry of short rod specimen, (Zhao et al., 1990)

where:

D: Specimen diameter

W: Specimen length

$\theta$ : Subtended chevron angle

$a_0$ : Distance to chevron notch tip

$W-a_0$ : Chevron length

t: Notch thickness

Fracture toughness is calculated with SR type specimens according to the formulas which are suggested by ISRM (1988). These calculation procedures are shown below:

For Level 1 testing:

$$K_{SR} = C_K \times 24 \times F_{max} / D^{1.5} \quad (3.1)$$

where:

$F_{max}$ : Failure load

D : Specimen diameter

$C_K$ : Correction factor to account for the size variation of the specimen;

$$C_K = \left[ 1 - \frac{0.6\Delta W}{D} + \frac{1.4\Delta a_0}{D} - 0.01\Delta \theta \right] \quad (3.2)$$

where:

$\Delta W$ : Variation in specimen height

$\Delta a_0$ : Initial position of chevron notch apex

$\Delta \theta$  : Chevron notch angle

For Level 2 testing, fracture toughness calculation of the SR specimen begins with Equation 3.1 and Equation 3.2. Afterward a nonlinearity correction factor is calculated and corrected fracture toughness of SR specimen is evaluated as in Equation 3.3 by using Load-CMOD curves (Figure 3.3).

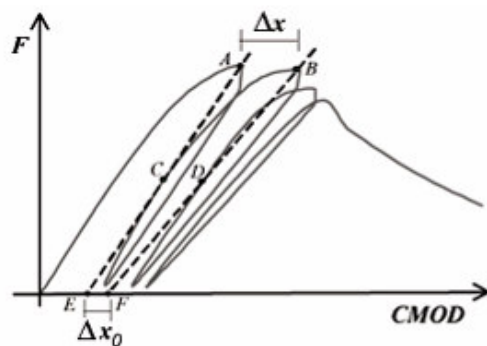


**Figure 3.3** Definitions for computation of correction factor based on Load-CMOD plot, (Sousa & Bittencourt, 2001)

$$K_{SR}^c = \sqrt{\frac{1+p}{1-p}} K_{SR} \quad (3.3)$$

where:

$$p = \Delta x_0 / \Delta x \quad (3.4)$$

### 3.2 Chevron Bend (CB) Method

CB specimen was presented by Ouchterlony (1988). In chevron bend specimen, v-shaped notch is sawed in cylindrical specimen and loaded under three-point bending. Fracture toughness of the CB specimen is evaluated like fracture toughness of the SR specimen. CB method is only used to determine fracture toughness in Mode I like Short Rod Method, (Alkılıçgil, 2006). In Figure 3.4 geometry of the CB type specimen is shown.

Fracture toughness is calculated with CB type specimens with the same formulas of the SR type specimens. However in formulas  $K_{CB}$  is calculated instead of  $K_{SR}$ .

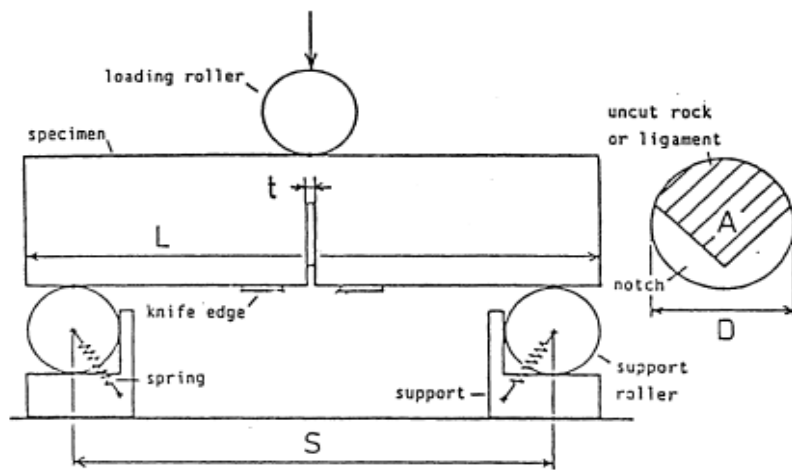


**Figure 3.4** Geometry of the CB type specimen, (Zhao et al., 1990)

where:

S: Span length

D: Specimen diameter

t: Notch thickness

L: Length of the specimen

### 3.3 Cracked Chevron-Notched Brazilian Disc (CNBD) Method

In 1985 Shetty et al. used CNBD firstly specimens to calculate the fracture toughness of ceramics. In CNBD specimen, circular cuts are opened to the centers of both sides of the disc shape specimen. Fracture toughness is calculated by an equation which depends on normalized stress intensity factor. Stress intensity factor is computed with numerical methods and an equation can be evaluated by fitting the numerical results. CNBD specimen is used for both Mode I, Mode II, mixed mode fracture toughness tests, (Alkılıçgil, 2006).

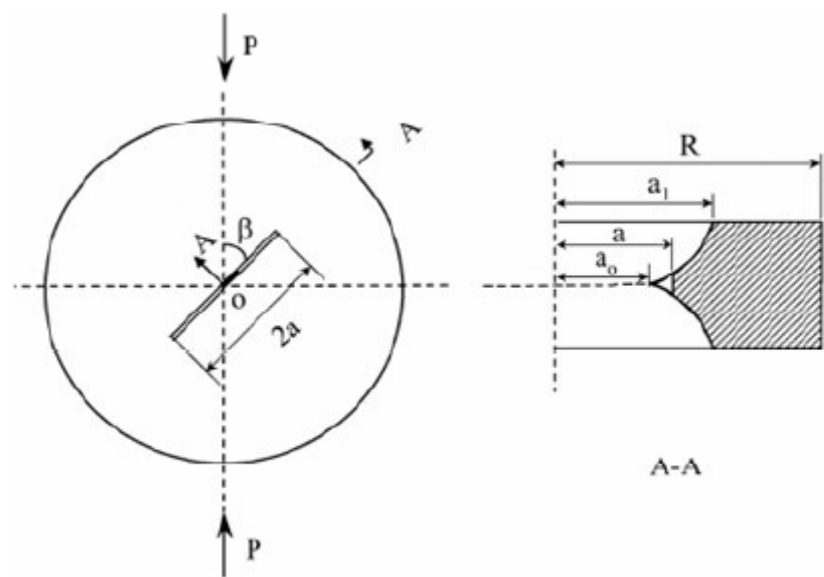


**Figure 3.5** CNBD under diametrical compression, (Khan and Al-Shayea, 2000)

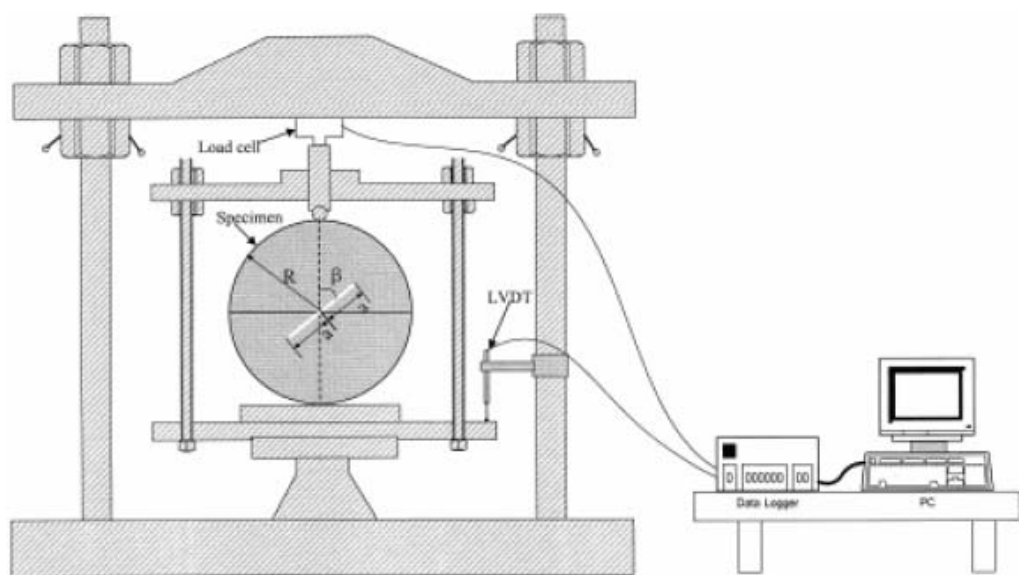


**Figure 3.6** Experimental setup for CNBD type specimen,  
(Khan and Al-Shayea, 2000)

For CNBD type specimens fracture toughness is calculated by using Equation 3.5 suggested by ISRM (1995).

$$K_{IC} = \frac{P_{\max.}}{B\sqrt{D}} Y_{\min.}^* \quad (3.5)$$

where:

$D$ : Diameter of the Brazilian disc

$B$ : Thickness of the specimen

$P_{\max.}$ : Compressive load at failure

$Y_{\min.}^*$  : Critical dimensionless stress intensity factor and equals to:

$$Y_{\min.}^* = ue^{va} \quad (3.6)$$

where:

$u$  and  $v$  are the constants determined by  $a_0/R$  and  $B/R$ .

### 3.4 Straight Notch Semi-Circular Bending (SNSCB)

In this study SNSCB (Straight Notch Semi-Circular Bending) or SCB (Semi-Circular Bending) type specimens were used for all of the experiments. SCB method firstly was introduced by the Chong & Kuruppu 1984. Then, Lim et al.1994 and Khan and Al-Shayea 2000 studied further this type of specimen to determine the fracture toughness of the rocks. The experimental set up and specimen preparation of SCB specimens are included in Chapter V.

SNSCB type specimen testing geometry developed by Chong and Kuruppu (1984), has a single edge notch of length  $a$  and is loaded in a three-point bending configuration (Figure 3.7). SCB is especially suitable for applications requiring duplicate samples having similar composition, as such circular discs provide two duplicate specimens. Furthermore, the SCB can be used to study mixed-mode fracturing, by cutting a crack at an angle, (Chong and Kuruppu, 1988).

There are several advantages of the SCB specimens. Main advantages are listed below:

- Easy to prepare test set- up,
- Only conventional fracture testing equipments are required,
- Very small core-based specimens can be used to obtain valid plane strain fracture toughness. Therefore this specimen type is cost-effective in that it requires minimal rock material and effort to use.
- Finally it produces trustable results.

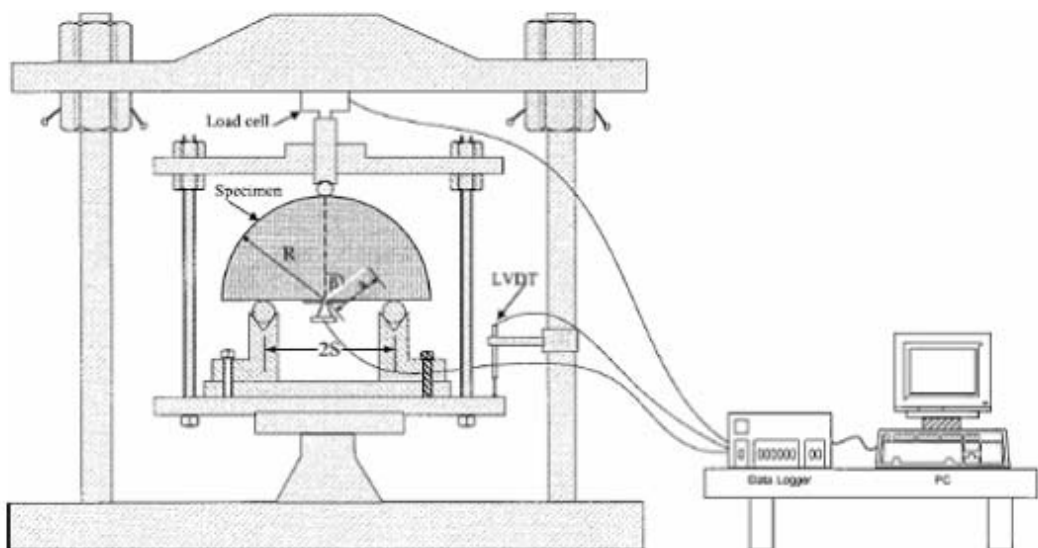


**Figure 3.7** Experimental setup for SNSCB type specimens,  
(Khan and Al-Shayea, 2000)

Fracture toughness is determined from an equation which depends on a numerical constant, which is called as normalized stress intensity factor (Normalized SIF). The normalized stress intensity factor is calculated by using the Equation 3.7 shown below:

$$Y_I = \frac{K_I}{\sigma_0 \sqrt{\pi a}} \quad (3.7)$$

where:

$Y_I$ : Normalized stress intensity factor

$K_I$ : Stress intensity factor (Pa  $\sqrt{m}$ )

$a$ : Notch or crack length

$\sigma_0$ :  $\frac{P}{2RB}$  where:

P: Failure load (kN)

R: Specimen radius

B: Specimen thickness

By using the normalized stress intensity factor, fracture toughness of the rock is calculated with the Equation 3.8.

$$K_{IC} = Y_I \sigma_{cr} \sqrt{\pi a} \quad (3.8)$$

where:

$Y_I$ : Normalized stress intensity factor

$a$ : Notch length

$\sigma_{cr}$ :  $\frac{P_{cr}}{2RB}$

$P_{cr}$ : Critical load when the fracture occurs

R: Specimen radius

B: Specimen thickness

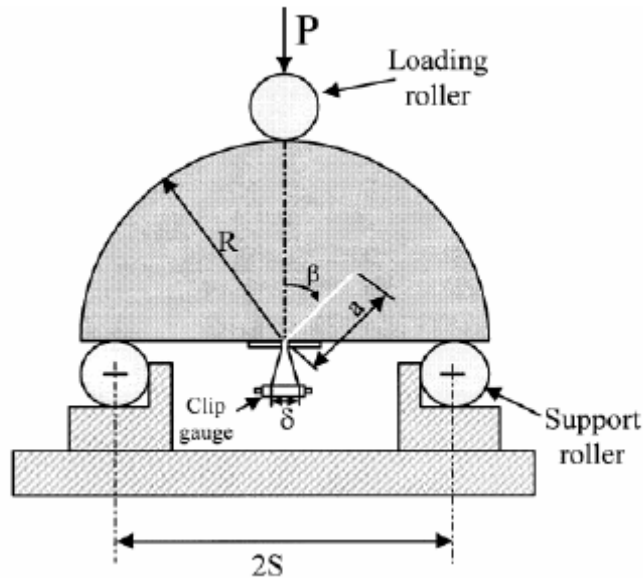


**Figure 3.8** A semi-circular specimen containing an angled edge crack under three point-bending, (Khan and Al-Shayea, 2000)

In the previous studies Khan and Al-Shayea used the SCB specimens with notch angle orientations between  $0^0$ - $60^0$  under three point bending. In these experiments, span ratio ( $S/R$ ) = 0.8 and the notch length ratio ( $a/R$ )=0.3 were used. After experiments, the results of Khan and Al-Shayea showed that specimen diameter and crack type have a substantial influence on the measured fracture toughness; on the other hand, loading rate, crack size, and specimen thickness seem to have a negligible effect on the fracture toughness. Mode I fracture toughness is significantly influenced by specimen diameter and crack type, while their effects on Mode II fracture toughness are generally negligible.

Furthermore Lim et.al (1994) used Johnstone rock in the SCB experiments. In the experiments effect of water content in rock, loading rate, specimen thickness, specimen size and notch length were investigated. According to the results of the experiments, saturated water content is a dominant factor in determining the

fracture toughness of the rock. Generally, with increasing the saturated water content, the  $K_{IC}$  decreases exponentially. The loading rate may also have a considerable effect on the apparent fracture toughness, with high loading rates causing an increase in the fracture toughness. The present results indicate that tests should be conducted at loading rates less than 0.05 mm/min to obtain the  $K_{IC}$  of the rock. Furthermore, fracture toughness is not effected by the specimen thickness, specimen size, and the notch length.

# **CHAPTER 4**

## **ESTIMATION OF STRESS INTENSITY FACTORS BY NUMERICAL MODELING**

In order to calculate stress intensity factors of the samples with different geometries, numerical computations were carried out. In this thesis the package program ABAQUS was preferred for stress and fracture analysis. ABAQUS is a user friendly and powerful finite element modeling program.

### **4.1 Finite Element Method**

Many problems in engineering and applied science are governed by differential or integral equations. The solutions to these equations would provide an exact, closed-form solution to the particular problem being studied. However, complexities in the geometry, properties and in the boundary conditions that are seen in most real-world problems usually means that an exact solution cannot be obtained or obtained in a reasonable amount of time. Current product design cycle times imply that engineers must obtain design solutions in a ‘short’ amount of time. They are content to obtain approximate solutions that can be readily obtained in a reasonable time frame, and with reasonable effort. The FEM is one such approximate solution technique. The FEM is a numerical procedure for obtaining approximate solutions to many of the problems encountered in engineering analysis, (Barton & Rajan, 2000).

In the FEM, a complex region defining a continuum is discretized into simple geometric shapes called elements. The properties and the governing relationships are assumed over these elements and expressed mathematically in terms of

unknown values at specific points in the elements called nodes. An assembly process is used to link the individual elements to the given system. When the effects of loads and boundary conditions are considered, a set of linear or nonlinear algebraic equations is usually obtained. Solution of these equations gives the approximate behavior of the continuum or system. The continuum has an infinite number of degrees-of-freedom (DOF), while the discretized model has a finite number of DOF. This is the origin of the name, finite element method, (Barton & Rajan, 2000).

## **4.2 Origins of the Finite Element Method**

The basic concept studies of finite element method were begun approximately 150 years before. The term finite element method was first introduced by Clough in 1960. At this time period engineers used this method for solution of problems such as stress analysis, fluid flow, heat transfer etc. The first written book on a FEM was published in 1967 by Zienkiewicz and Chung. In the late 1960s and early 1970s, the FEM was applied to a wide variety of engineering problems. The 1970s marked advances in mathematical treatments, including the development of new elements, and convergence studies. Most commercial FEM software packages originated in the 1970s (ABAQUS, ADINA, ANSYS, MARK, PAFEC) and 1980s (FENRIS, LARSTRAN‘80, SESAM‘80). The FEM is one of the most important developments in computational methods to occur in the 20th century. In just a few decades, the method has evolved from one with applications in structural engineering to a widely utilized and richly varied computational approach for many scientific and technological areas, (Barton & Rajan., 2000). Nowadays ABAQUS, ADINA, ANSYS, FRANC3D are the best known finite element softwares.

The FEM offers many significant advantages to the engineers and the companies. Advantages of FEM for design engineers are listed below, (Barton & Rajan, 2000):

- Easily applied to complex, irregular-shaped objects composed of several different materials and having complex boundary conditions.
- Applicable to steady-state, time dependent and eigenvalue problems.
- Applicable to linear and nonlinear problems.
- One method can solve a wide variety of problems, including problems in solid mechanics, fluid mechanics, chemical reactions, electromagnetics, biomechanics, heat transfer and acoustics, to name a few.

Furthermore advantages of FEM for companies are, (Barton & Rajan, 2000):

- Reduced testing and redesign costs thereby shortening the product development time.
- Identify issues in designs before tooling is committed.
- Refine components before dependencies to other components prohibit changes.
- Optimize performance before prototyping.
- Discover design problems before litigation.
- Allow more time for designers to use engineering judgement, and less time “turning the crank.”

On the other hand some disadvantages of the FEM are available. These are, (Barton & Rajan, 2000):

- A specific numerical result is obtained for a specific problem. A general closed-form solution, which would permit one to examine system response to changes in various parameters, is not produced.
- The FEM is applied to an approximation of the mathematical model of a system (the source of so-called inherited errors).
- Experience and judgment are needed in order to construct a good finite element model.
- A powerful computer and reliable FEM software are essential.
- Input and output data may be large and tedious to prepare and interpret.

### **4.3 ABAQUS Software**

ABAQUS is a simulation program based on a finite element method (FEM). It can solve problems ranging from relatively simple linear analyses to the most challenging nonlinear simulations. It includes an extensive library of elements that can model virtually any geometry. ABAQUS can be used to study structural (stress/displacement) problems, heat transfer, mass diffusion, thermal management of electrical components (coupled thermal-electrical analyses), acoustics, soil mechanics (coupled pore fluid-stress analyses), and piezoelectric analysis. ABAQUS contains an extensive list of engineering materials including metals, rubber, polymers, composites, reinforced concrete, crushable and resilient foams, and geotechnical materials such as soils and rock.

ABAQUS is easy to use and offers the user a wide range of capabilities. Even the most complicated analyses can be modeled easily. For an instance, problems with multiple components are modeled by associating the geometry defining each component with the suitable material models. On the other hand with ABAQUS contact between the solids are easily modeled.

ABAQUS was developed and maintained by Habbitt, Karlson and Sorensen, Inc. (HKS) in 1978. The company has several offices around the world, A-Z Tech. Ltd. in İstanbul ('A to Z Advanced Engineering Technologies') is the Turkey Office. ABAQUS version 6.5.4 is used for all the modelings in this thesis.

### **4.4 ABAQUS Modules**

ABAQUS is an user friendly program that divided into functional units called modules. Each module contains only the relevant tools. For example, the Part module contains only the tools needed to create a new part, while the Mesh module contains only the tools for meshing the model.

The order of the modules in the menu are in a logical sequence therefore when creating the model following the logical sequence is required. Before submitting the

model for analyzing, the geometry and other physical properties of the model must be defined step by step by the following list of modules.

#### **4.4.1 Part Module**

The Part module allows to create and edit individual parts by sketching their geometry directly in ABAQUS. On the other hand importing parts which are modeled from other modeling programs are excepted.

#### **4.4.2 Property Module**

Material definitions and material properties of each regions of parts are assigned in this module.

#### **4.4.3 Assembly Module**

This module is used for creating the instances of parts and positioning the instances relative to each other in a global co-ordinate system. Cracks, springs and dashpots are modeled under the assembly module. Cracks are modeled in two ways first one is sharp crack which is called seam the second one is called as blunted crack.

#### **4.4.4 Step Module**

Step module is used for creating and configuring analysis steps and associated output requests. Step module provides a sequence of steps to capture changes in a loading and boundary conditions of each of them. In ABAQUS, output requests are taken from the step module. Two output requests are available in ABAQUS. One of them is Field Output Request and the other one is History Output Request. Generally Field Output Request data are generated from the spatially distributed over the entire model or over a portion of it. On the other hand History Output Request data are generated from at the specific points in the model. In fracture mechanics applications, to calculate the stress intensity factor of a crack, history output request must be defined in the step module.

When forming the history output request of a crack, firstly contour integral domain type is selected and then Stress Intensity Factor type is chosen. Three stress intensity factor criterions are available under Stress Intensity Factor type. These are 1) Maximum tangential stress criterion, 2) Maximum strain energy release rate criterion and 3)  $K_{II} = 0$  criterion. To calculate the crack propagation direction at initiation one of the criterion must be selected. Number of contours around the crack tip after meshing is written in the number of contours dialog box. These contours are taken into consideration for the calculation of the stress intensity factor around the crack tip.

#### **4.4.5 Interaction Module**

This module is used to specify mechanical and thermal interactions between regions of a model, connections between two points, connections between two edges or connections between point and a surface. In the interaction module other interactions are defined as constraints (tie, coupling, rigid body, equation) and connectors.

#### **4.4.6 Load Module**

The Load module is used to specify loads and boundary conditions of the model.

#### **4.4.7 Mesh Module**

The Mesh module is used to generate finite element mesh on an assembly. Seeding, mesh controls, techniques and element types are defined in the mesh module.

#### **4.4.8 Job Module**

After determining and defining all of the modules in the model, the next phase to finalize the analysis by using Job module. The Job Module is used to submit a job for analysis and monitor its progress.

#### **4.4.9 Visualization Module**

The Visualization Module is used to provide graphical display of finite element models and results. Deformed shapes, contours, graphs, animations of analysis are available under this module.

#### **4.4.10 Sketch Module**

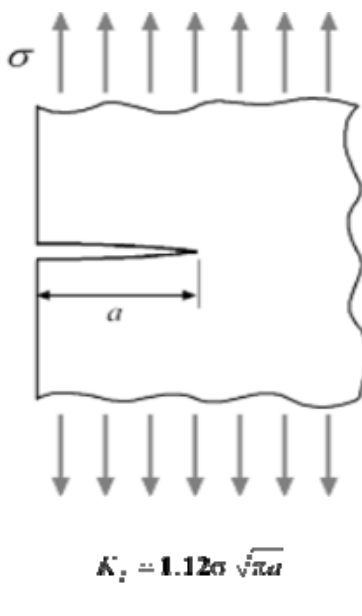
The Sketch Module is used to create two dimensional profiles which are helped to form the geometry when defining an ABAQUS native part.

### **4.5 ABAQUS Verification Analysis**

In order to assess the accuracy of stress intensity factor computations with ABAQUS models, fracture mechanics problems which have known analytical solutions, were studied in the verification work.

#### **4.5.1 Semi-Infinite Plate with an Edge Crack**

First verification model is semi-infinite plate with an edge through crack under tension. Schematic representation of this model is in Figure 4.1.



$$K_I = 1.12\sigma \sqrt{\pi a}$$

**Figure 4.1** Semi-infinite plate with an edge through crack under tension

Dimensions and mechanical properties used in the model of semi-infinite plate with an edge through crack are shown below in Table 4.1. Figure 4.2 and 4.3 show model frame and crack details.

**Table 4.1** Dimensions and mechanical properties of the semi-infinite plate with an edge through crack

Dimensions and Mechanical Properties	Values
Width of the plate, w	400 mm
Height of the plate, h	400 mm
Thickness of the plate, B	1 mm
Crack length of the plate, a	10 mm
Notch thickness, $t_n$	1 mm
Load on the plate in tension, $\sigma$	1 MPa
Young's modulus, E	13000 MPa
Poisson's ratio, $\nu$	0.15

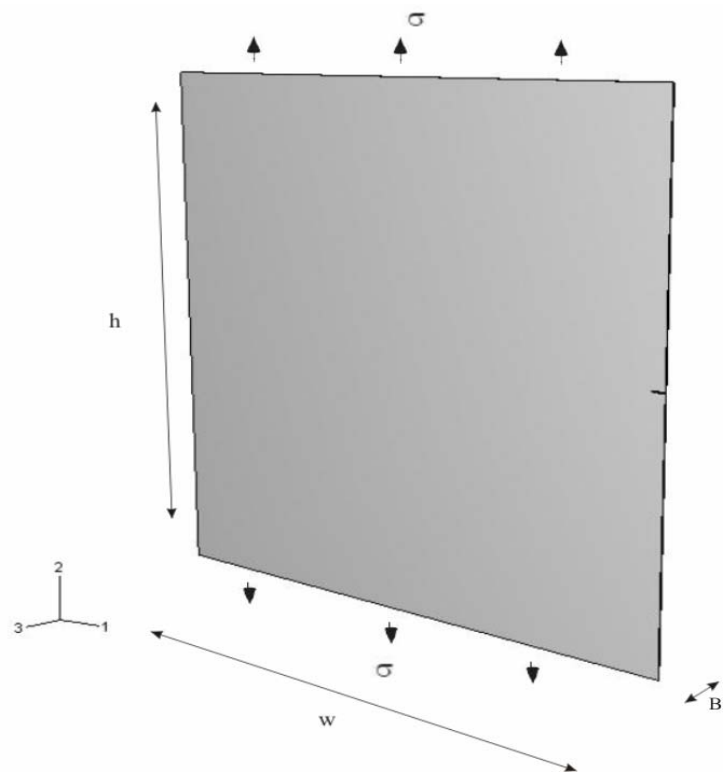


**Figure 4.2** 3D ABAQUS view of the semi-infinite plate with an edge through crack under tension

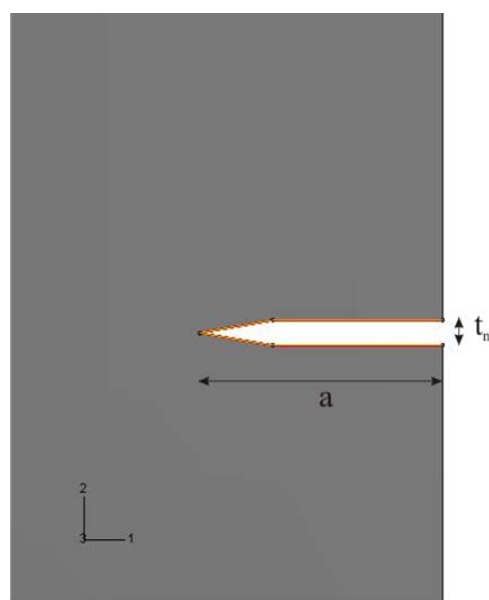


**Figure 4.3** Schematic view of the crack

Analytical solution for stress intensity factor in Mode I for this example is given in Equation 4.1.

$$K_I = 1.12\sigma\sqrt{\pi a} \quad (4.1)$$

For the example above, by using Equation 4.1,  $K_I$  was found as  $6.2775 \text{ MPa}\sqrt{\text{mm}}$ .

This verification example is analyzed by using ABAQUS 3D software. In this verification example firstly analytical and numerical solutions of the problem were compared. Then the effect of young's modulus differences and the effect of poisson's ratio differences on the stress intensity factor were investigated for the same model.

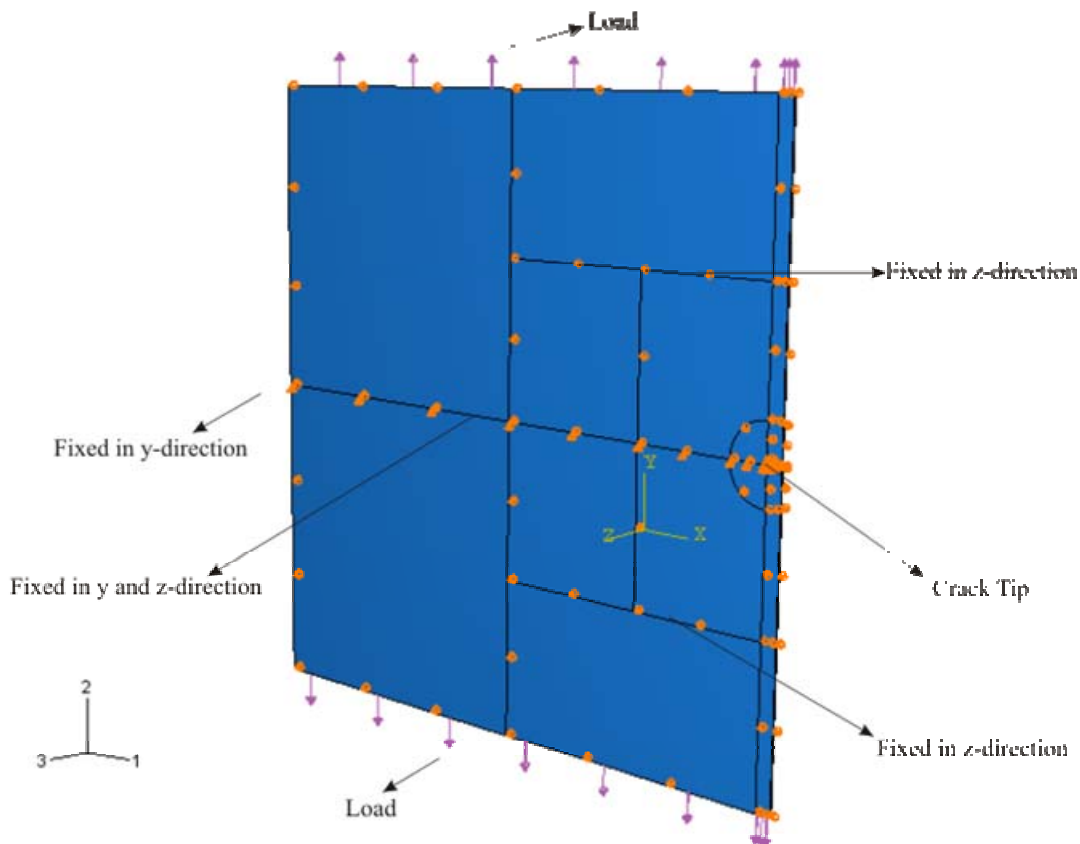


**Figure 4.4** Boundary conditions and load directions of the model

In order to prevent rigid body motions, the whole model was fixed also in y-direction at the mid-side constraints except crack front to allow movements along the crack field. Furthermore, the model's visible surface and the surface at the back were fixed in z-direction, (Figure 4.4). Detailed mesh is seen in Figure 4.5.

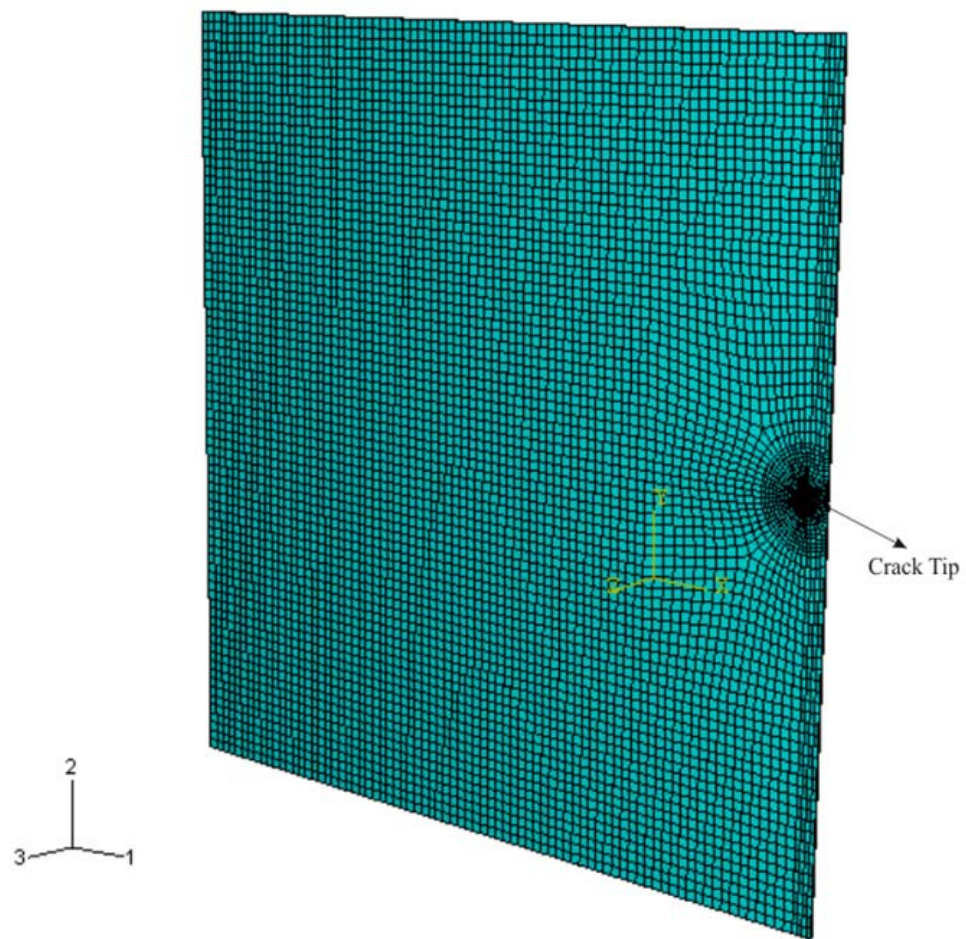


**Figure 4.5** Schematic view of the 3D undeformed ABAQUS model after meshing

After analyzing the model (which has a special mesh configuration around the crack tip) with ABAQUS, the average stress intensity factor  $K_I$  was found as:

$$K_{I \text{ av.}} = 6.32279 \text{ MPa} \sqrt{\text{mm}}$$

Percentage error was calculated from Equation 4.2.

$$\text{Error (\%)} = \frac{K_{comp.} - K_{anal.}}{K_{anal.}} \times 100\% \quad (4.2)$$

where,

$K_{anal.}$ : Analytical solution of the stress intensity factor

$K_{comp.}$ : Computed stress intensity factor

From this equation percentage error for this problem is 0.721%. ABAQUS produced a little error. This error occurred possibly because the analytical solution is for an infinite plate while in this verification example the boundaries of the model are located at a finite distance from the crack plane.

Young's modulus of the material is increased to 20000 MPa. On the other hand Poisson's Ratio and other properties (boundary conditions, dimensions, etc.) of the material were not changed. Mesh of the model is kept the same as in Figure 4.5. After running the model with ABAQUS 3D software, the average stress intensity factor  $K_I$  was found as:

$$K_{I \text{ av.}} = 6.32279 \text{ MPa} \sqrt{\text{mm}}$$

This shows that differences in the Young's Modulus of the material do not affect the stress intensity factor  $K_I$ .

Poisson's ratio of the material is increased 0.30. Young's modulus and other properties (boundary conditions, dimensions, etc.) of the material shown in Table

4.1 were not changed. Mesh of the model is kept the same. After running the model with ABAQUS 3D software, the average stress intensity factor  $K_I$  was found as:

$$K_{I \text{ av.}} = 6.32706 \text{ MPa} \sqrt{\text{mm}} \quad \text{or} \quad K_{I \text{ av.}} = 0.200 \text{ MPa} \sqrt{\text{m}}$$

which shows that the stress intensity factor was not affected by the Poisson's ratio differences of the material.

A 3D analysis was performed by increasing the thickness of the plate to 400 mm as seen in Figure 4.6.

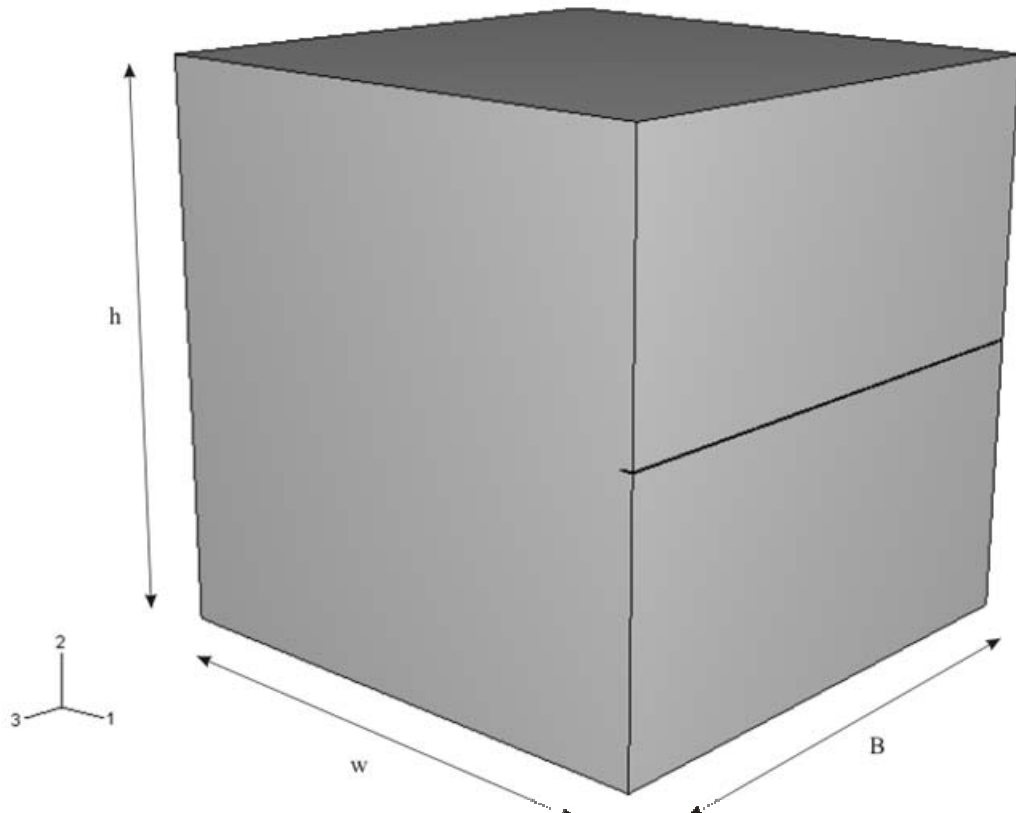


**Figure 4.6** Schematic view of the 3D model

Boundary conditions, load directions and load magnitudes which are the same as the first verification example, are shown in Figure 4.7.

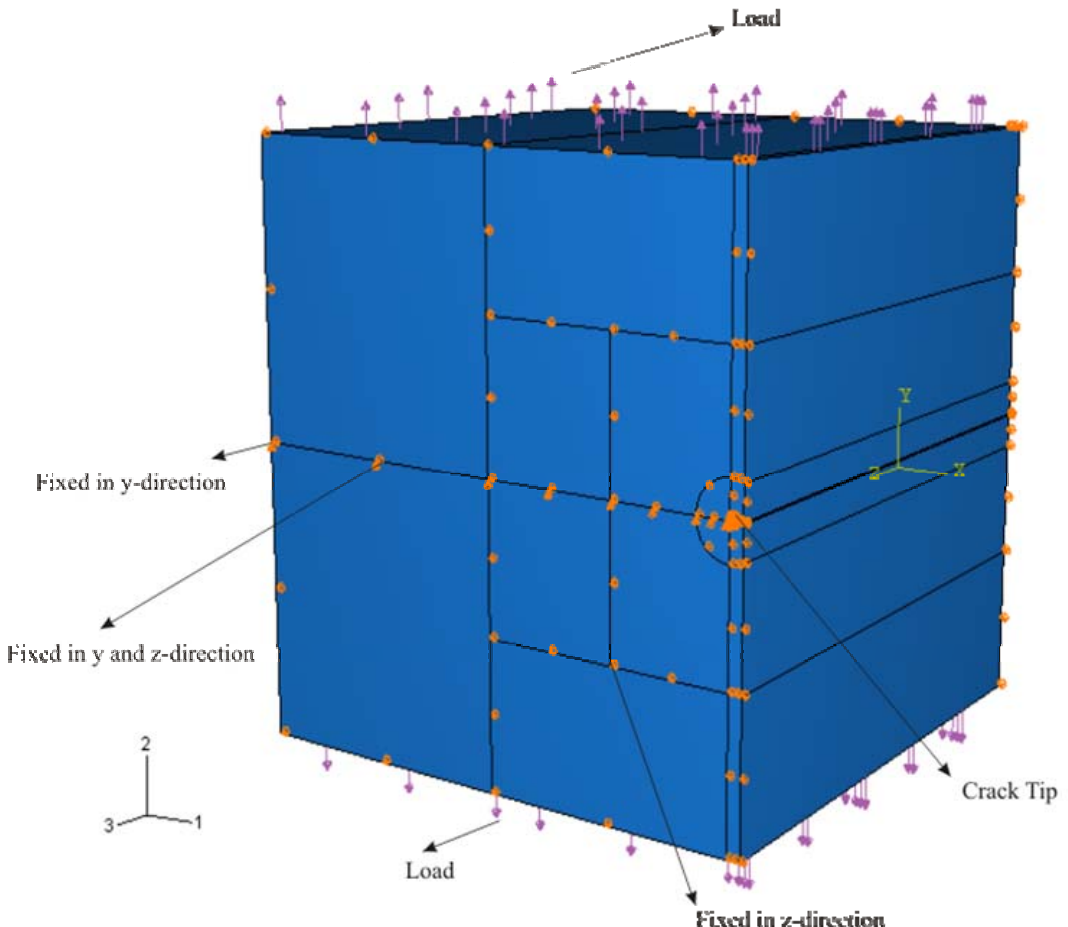


**Figure 4.7** Boundary conditions and load directions of the model

Some changes were made when meshing the model. Mesh density around the crack tip is the same but for other parts mesh density of the model was decreased because of very high number of elements. Schematic view of the undeformed model after meshing is shown in Figure 4.8.

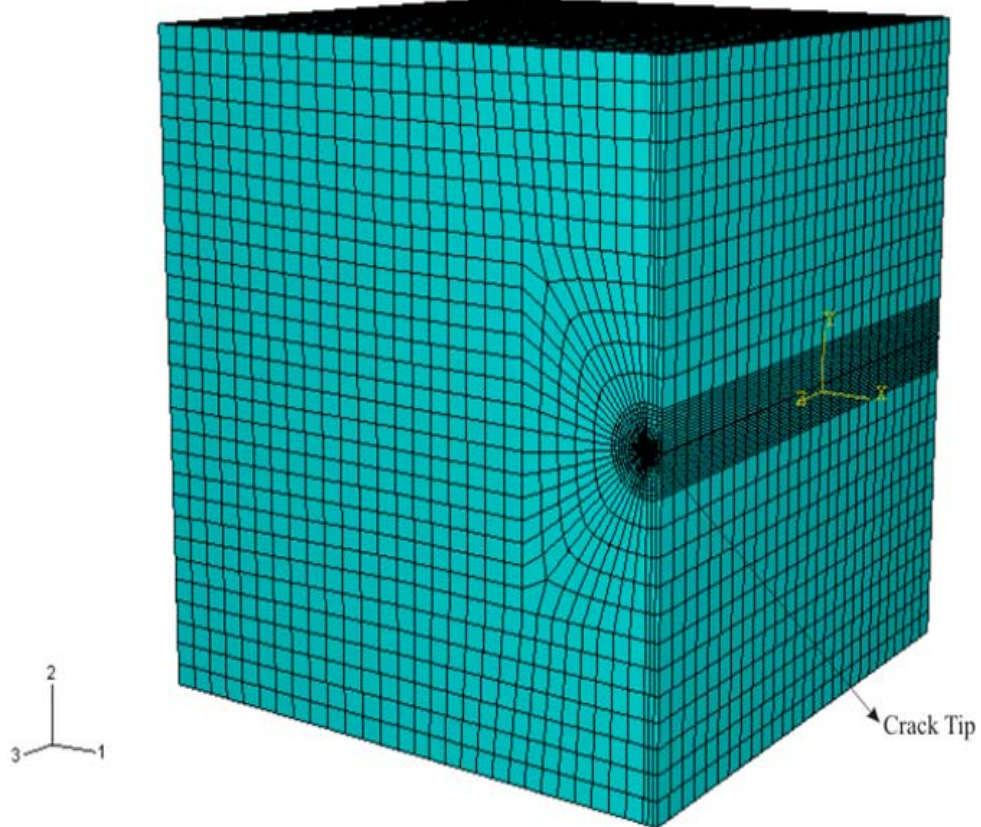


**Figure 4.8** Schematic view of the undeformed model after meshing

After analysing the model with ABAQUS, the average stress intensity factor  $K_I$  was found as:

$$K_{I \text{ av.}} = 6.34122 \text{ MPa} \sqrt{\text{mm}}$$

Percentage error of this problem was 1.015%. Thus, it was concluded that results found by numerical modeling were accurate enough with an error remaining within 1%.

#### 4.5.2 Inclined Crack in Tension

Second verification model is an inclined crack in tension. Model is subjected to a far field uniaxial stress as shown below. Schematic representation of this model is shown in Figure 4.9. Geometry, dimensions and properties are given in Table 4.2. Geometrical parameters and model frame are illustrated in Figure 4.10.

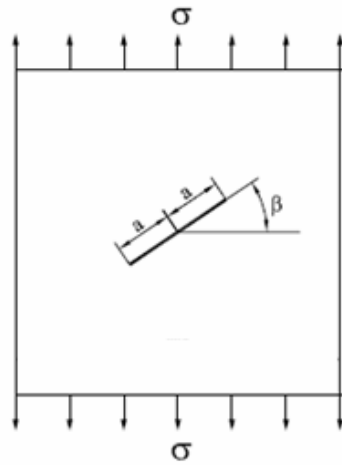


**Figure 4.9** Inclined crack in tension

Analytical solution for stress intensity factor in Mode I and Mode II for this example is given in Equations 4.3.

$$K_I = \sigma \sqrt{\pi a} \cos^2 \beta, \quad K_{II} = \sigma \sqrt{\pi a} \sin \beta \cos \beta \quad (4.3)$$

For the example above, by using Equations 4.3,  $K_I$  and  $K_{II}$  were found as:

$$K_I = 0.42257 \text{ MPa} \sqrt{mm} \quad K_{II} = 1.5791 \text{ MPa} \sqrt{mm}$$

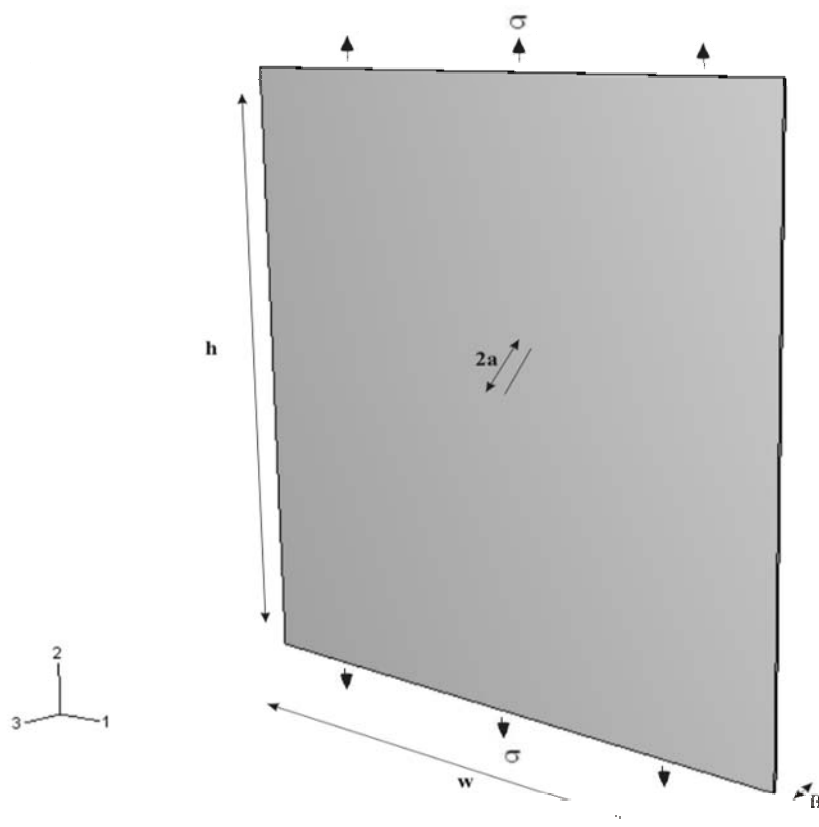


**Figure 4.10** Schematic view of the 3D model

**Table 4.2** Dimensions and mechanical properties of the inclined crack model in tension

Dimensions and Mechanical Properties	Values
Width of the plate, $w$	254 mm
Height of the plate, $h$	254 mm
Thickness of the plate, $B$	1 mm
Crack (seam) length of the plate, $a$	12.7 mm
Crack angle, $\beta$	75°
Load on the plate in tension, $\sigma$	1 MPa
Young's modulus, $E$	13000 MPa
Poisson's ratio, $\nu$	0.15

Seam crack type is introduced into the model (Figure 4.11). Seam crack is the crack type that was used in this ABAQUS analysis. When the crack type is sharp, seam type cracks can be chosen in the models. In ABAQUS, seam crack type choice is available under the crack menu. Boundary conditions, load directions and the display of the model are shown in the Figure 4.12:

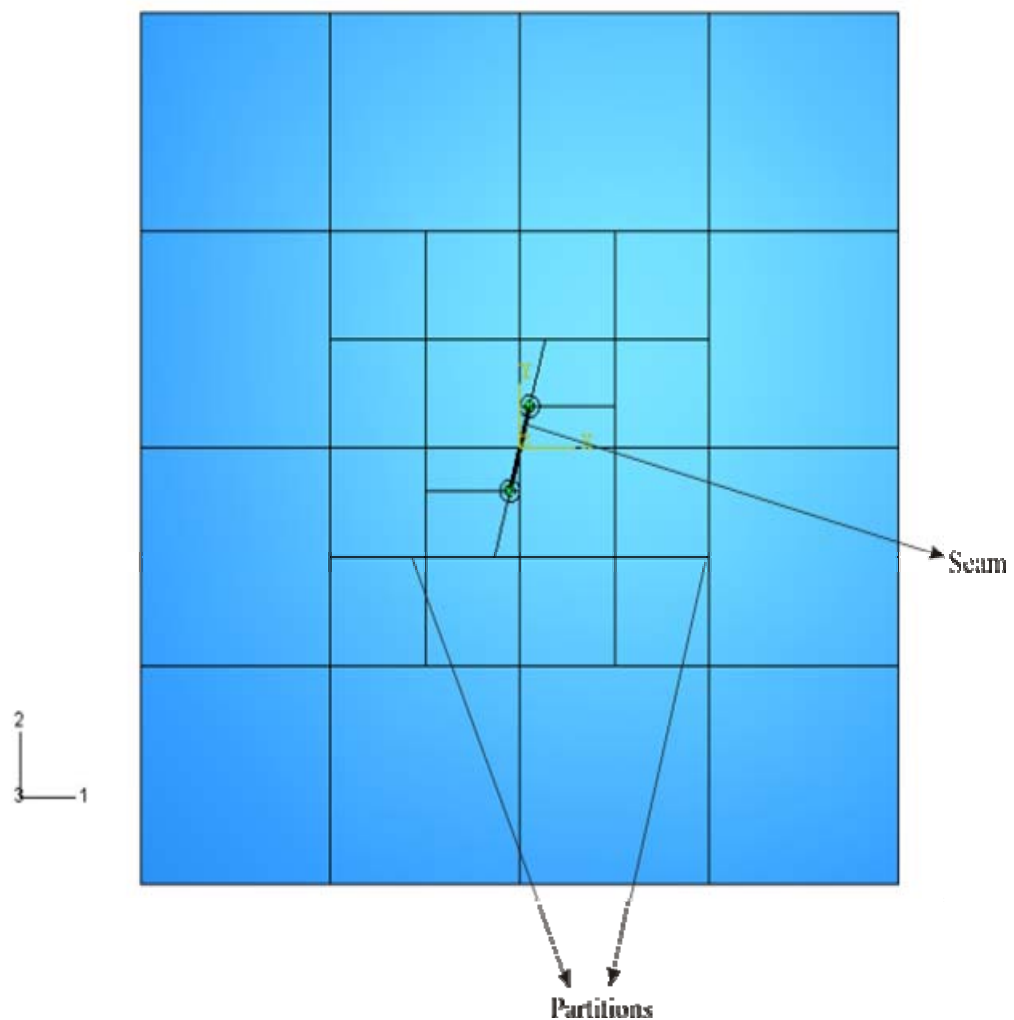


**Figure 4.11** Schematic view of the model and the seam cracks

Explanations of the boundary conditions are:

- B.C. 1: The model is fixed at x-direction along its thickness,
- B.C. 2: The model is fixed at y-direction along its thickness,
- B.C. 3: The model's all visible surface and non-visible surface are fixed at z-direction.

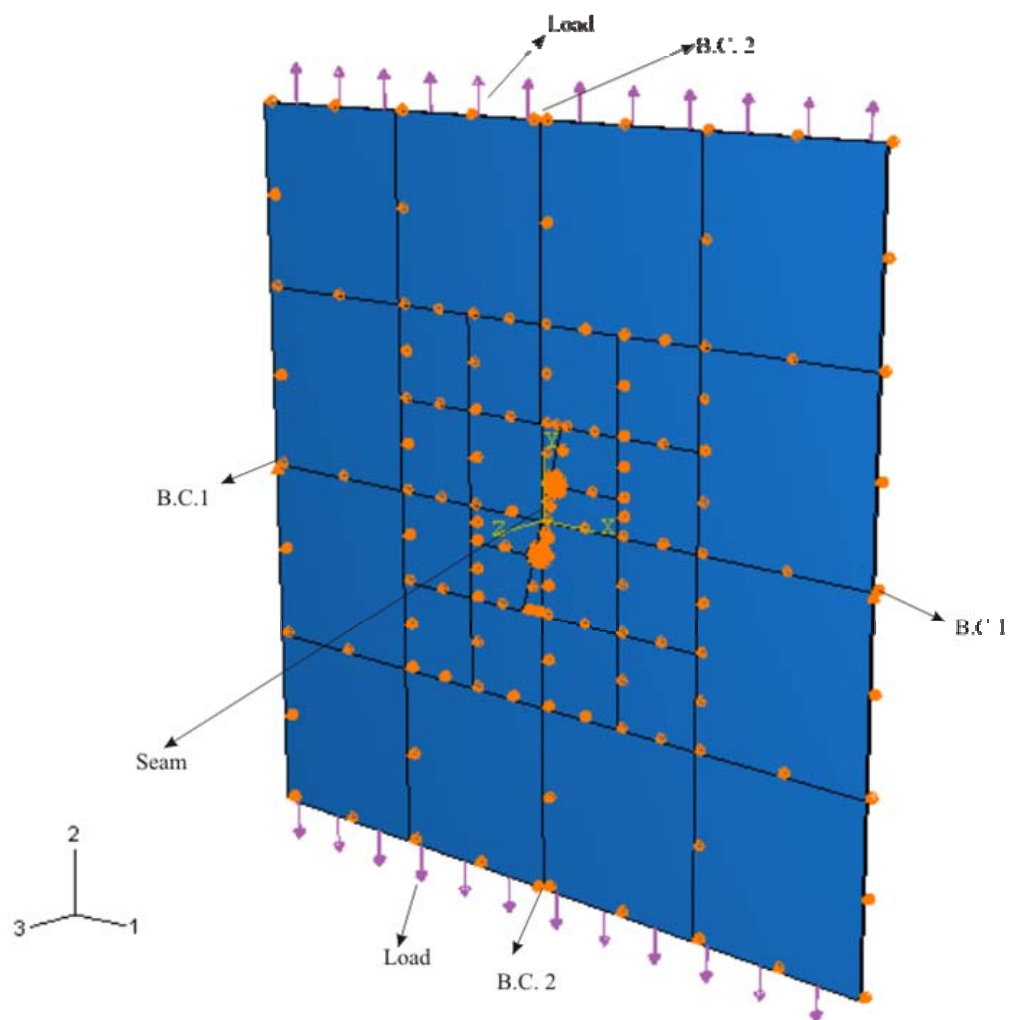


**Figure 4.12** Boundary conditions and load directions of the model

Mesh density around the crack tips and mesh harmony of the whole model are sufficient for this verification model. Schematic view of the undeformed model after meshing is shown below in Figure 4.13 and 4.14.

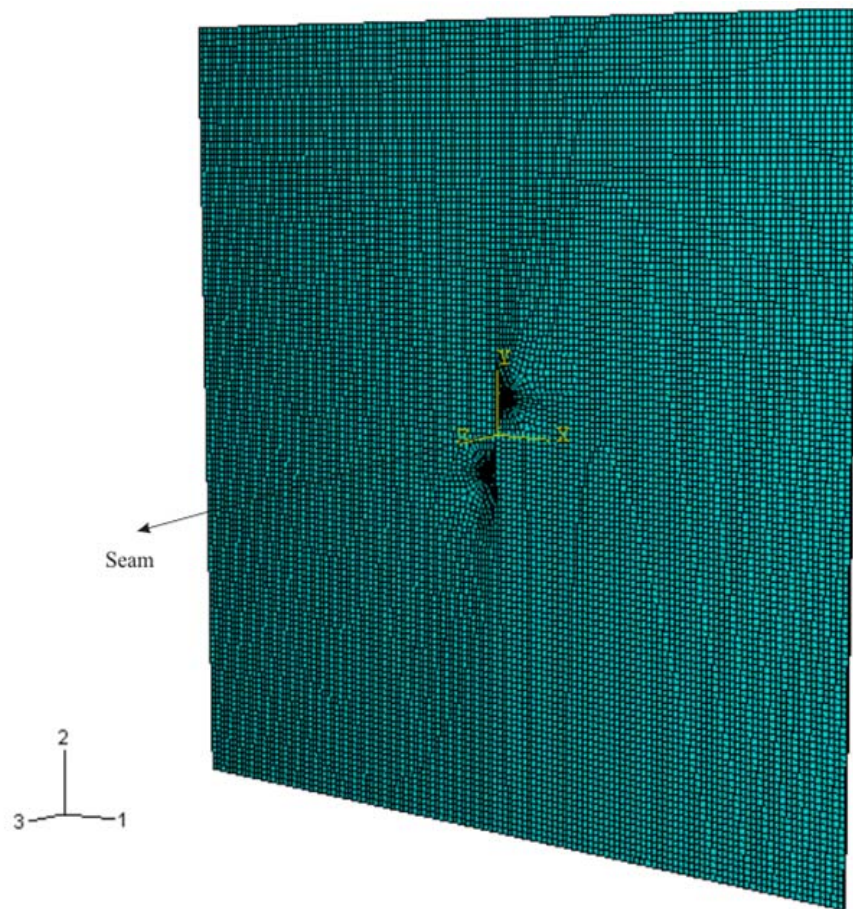


**Figure 4.13** Schematic view of the undeformed model after meshing

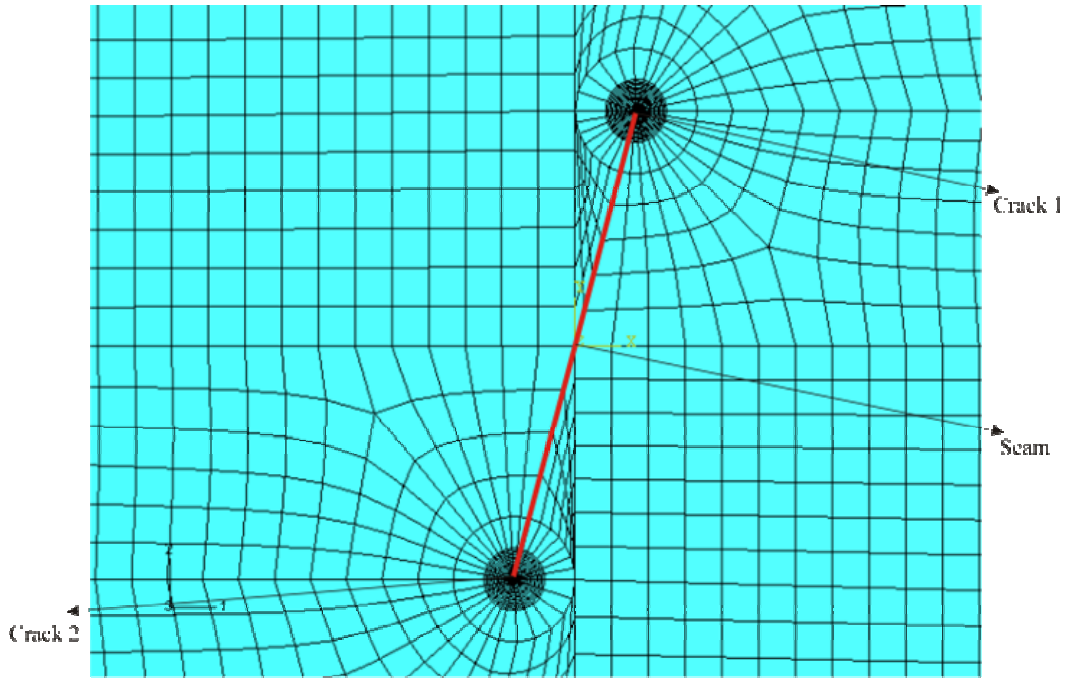


**Figure 4.14** Schematic view of the undeformed seam cracks after meshing

After analysing the model with ABAQUS, the average stress intensity factors  $K_I$  and  $K_{II}$  for Crack 1 (Upper Tip) were found as:

$$K_I \text{ av.} = 0.43011 \text{ MPa} \sqrt{\text{mm}} \quad K_{II} \text{ av.} = 1.61220 \text{ MPa} \sqrt{\text{mm}}$$

The average stress intensity factors  $K_I$  and  $K_{II}$  for Crack 2 (Lower Tip) are found as:

$$K_I \text{ av.} = 0.43069 \text{ MPa} \sqrt{\text{mm}} \quad K_{II} \text{ av.} = 1.61279 \text{ MPa} \sqrt{\text{mm}}$$

Comparing these to the analytical solution percentage errors of the crack 1 and 2 are listed below:

For Crack 1: **Error of  $K_I$ :** 1.784%, **Error of  $K_{II}$ :** 2.096%

For Crack 2: **Error of  $K_I$ :** 1.921 %, **Error of  $K_{II}$ :** 2.133%

Improving the mesh may increase the accuracy. However, as in the previous verification problems, the problem frame is not infinite as in the case of analytical solution, and thus a 2% error in the computation of  $K_I$  and  $K_{II}$  is acceptable.

#### **4.6 Method of Application of Distributed Loads to the Boundaries**

Because of its easy usage and fast application in ABAQUS software, loading with reference point is preferred in this thesis to apply uniformly distributed loads to the boundaries. Simple example in Figure 4.15 with reference points at the top and bottom of a 3D rectangular block illustrates the method of uniform load application to the flat boundaries. This example was chosen to check the validity of the load application method for models including flattened ends.

**Table 4.3** Dimensions and mechanical properties of the rectangular prism

Dimensions and Mechanical Properties	Values
Width of the plate, w	0.5 mm
Height of the plate, h	1 mm
Thickness of the plate, B	1 mm
Loads on the surfaces in uniaxial compressive, $\sigma$	1 N
Young's modulus, E	13000 MPa
Poisson's ratio, $\nu$	0.15
Reference points positions from the bottom and upper surface in y-direction	0.5 mm

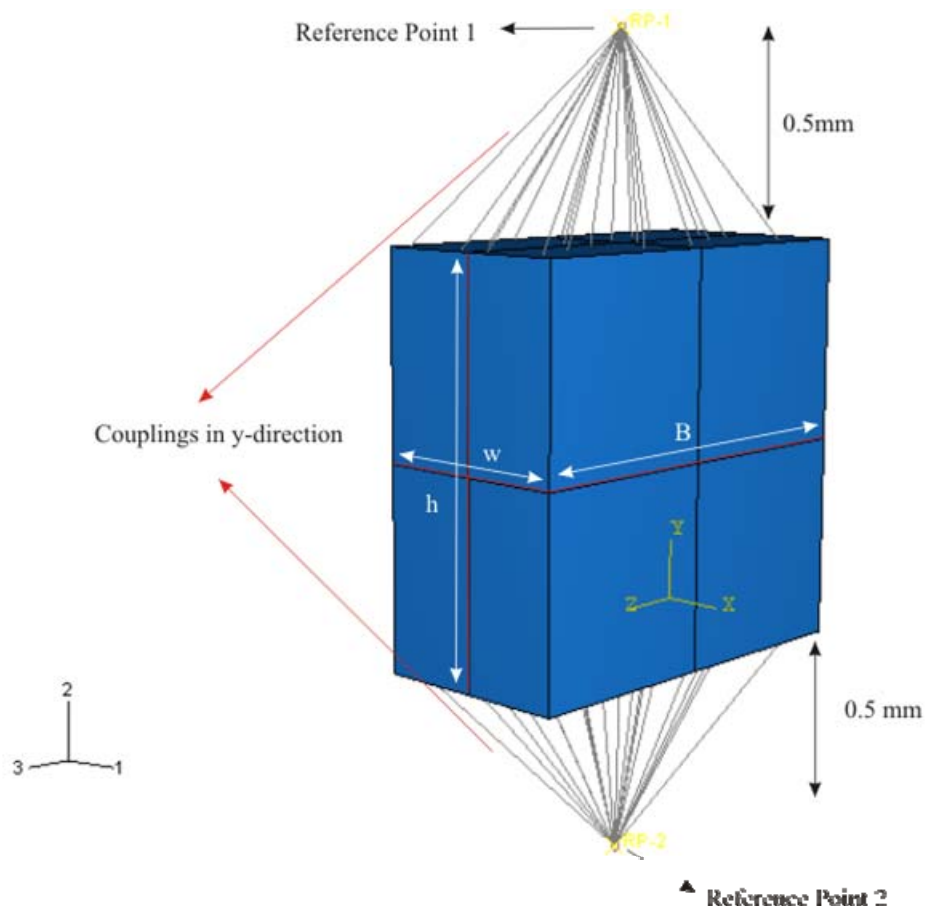


**Figure 4.15** Display of the reference point positions and the couplings

Coupling property (which is under the constraint module) is used to tie the model and the reference point to each other. When using the coupling property of the ABAQUS for this type of load application, kinematic type loading box is clicked in the constraint editor. In this study, model is loaded at y-direction therefore U2 direction box is clicked in the constraint editor. Thus, loads are applied to the model's upper and lower surfaces uniformly in y-direction.

Boundary conditions are shown in Figure 4.16. Explanations of the boundary conditions are:

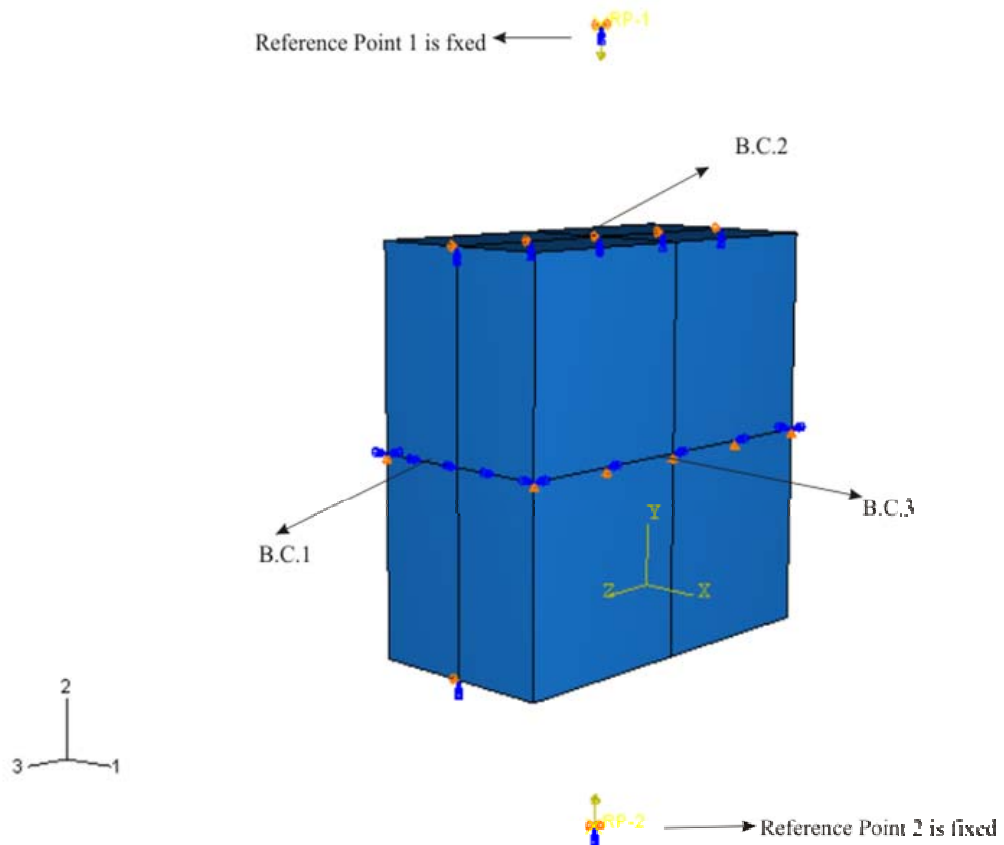


**Figure 4.16** Boundary conditions of the model

B.C.1: The model is fixed against a rotation around x-direction (UR1) along its width on the front and back faces and the opposite side of the non-visible partition line,

B.C.2: The model is fixed in x-direction (U1) and against a rotation around y-direction (UR2) along its thickness at the upper and lower surfaces,

B.C.3: The model is fixed in y-direction (U2), and against a rotation around of z-direction (UR3) along its thickness on the front and back faces.

In order to prevent rigid body motion and rotation of reference points, they are fixed in x-direction (U1), z-direction (U3) and against a rotation along y-direction (UR2). All reference points used in this thesis will have the same boundary conditions described here.

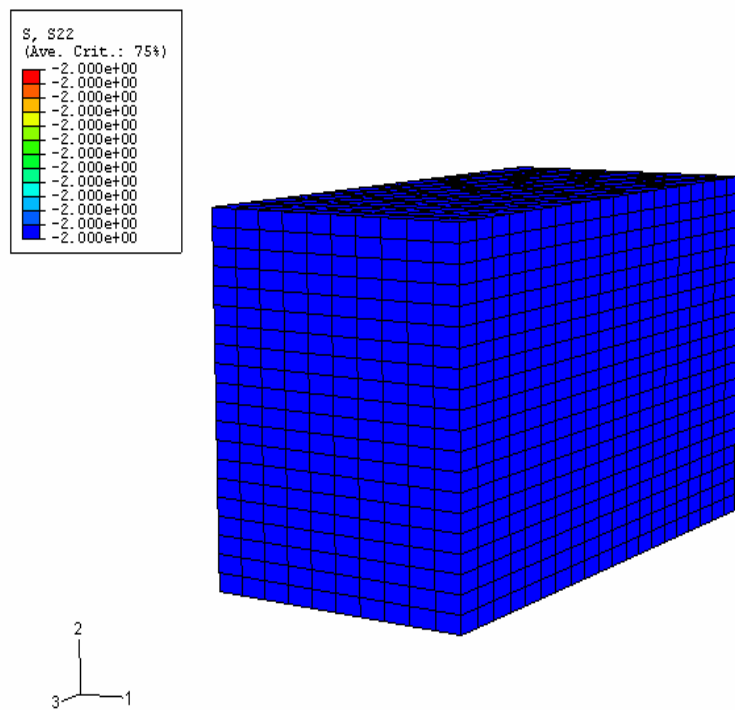


**Figure 4.17** Vertical stress distributions in y-direction (S22) after the computation

Stress is equally distributed to the whole model as shown above Figure 4.17. Everywhere in the model is seen to be under 2 MPa pressure because 1 N load applied at the reference points is distributed to the top and bottom surface having an area of  $0.5 \text{ mm}^2$  which corresponds to a uniform stress or pressure of  $2 \text{ N/mm}^2$  or  $2 \text{ MN/m}^2$ .

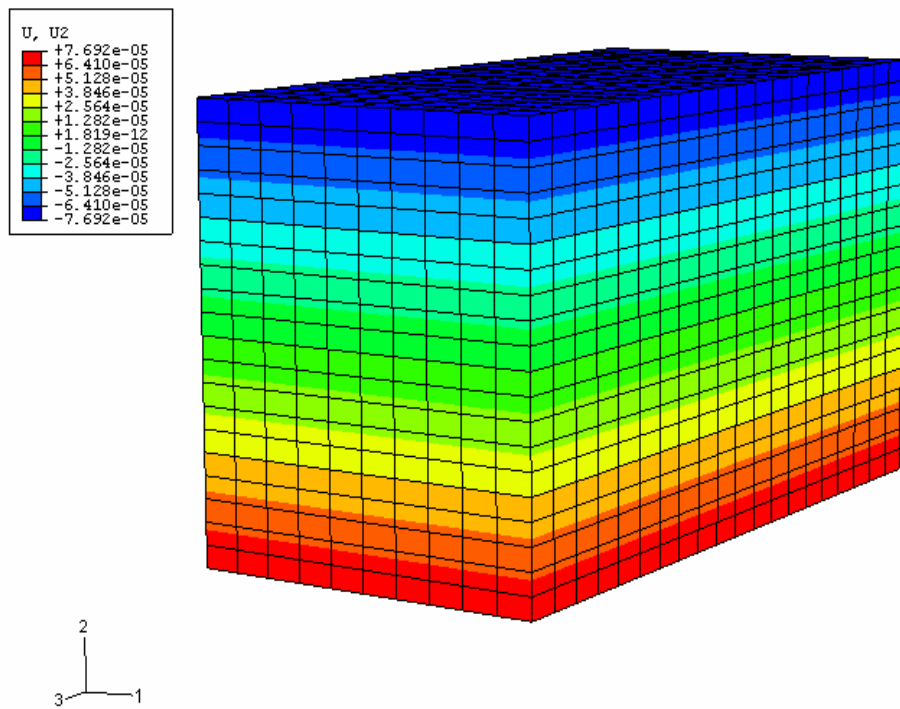


**Figure 4.18** The displacements in y-direction (U2)

Y-displacements of the model are seen to be equally distributed around the center of the block. This shows that uniform loads to the flattened ends can be applied successfully with this method, (Figure 4.18).

#### 4.7 Modeling of Cracks

Crack tips will be introduced to the end of the notches representing the saw cut initial notches in the experiments. When modeling fracture mechanics problems with ABAQUS, defining the crack front and crack extension direction is very important. While creating the crack, the first step is defining the crack front. For this, firstly the line which you want to be modeled as a crack front is selected, (Figure 4.19).

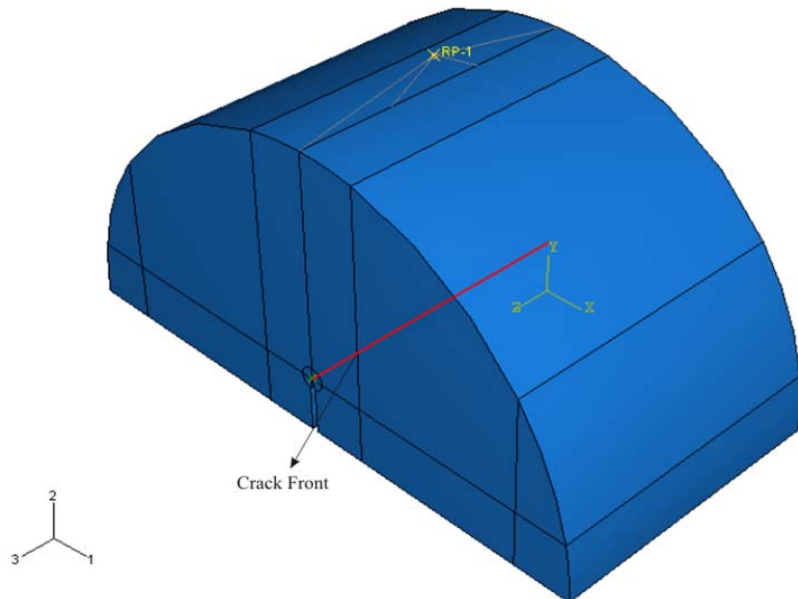


**Figure 4.19** Crack front

After that, estimated crack extension direction is chosen by using  $q$  vector module, (Figure 4.20). Different crack extension directions can be selected in the module which will yield different combinations of stress intensity factors  $K_I$  and  $K_{II}$ . In our case crack extends in the vertical direction parallel to the applied load or in the direction of the maximum principle stress. Crack tip loading is supposed to be pure Mode I loading for our specimens. Therefore crack extension direction is attached in the vertical direction to the front of the initial vertical notch.

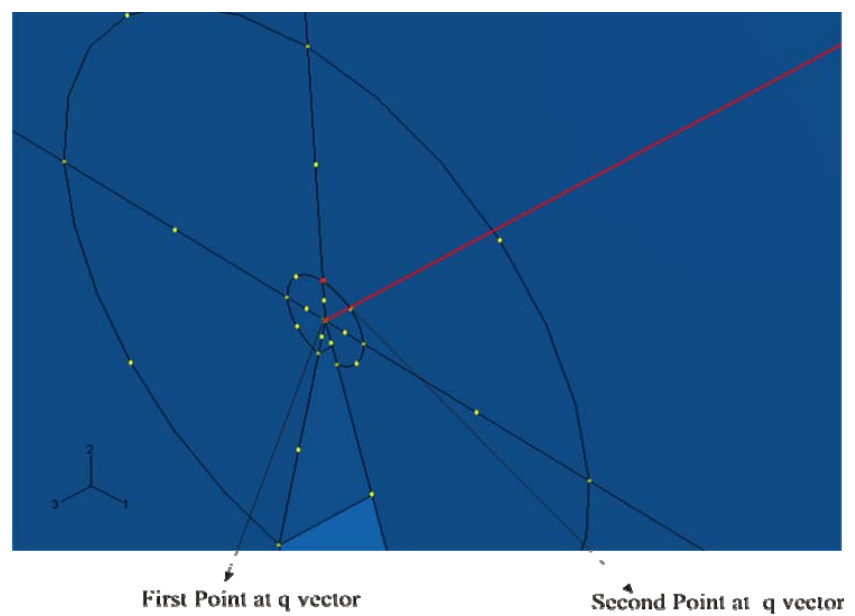


**Figure 4.20** Points marked for the selection of crack extension direction using  $q$  vector

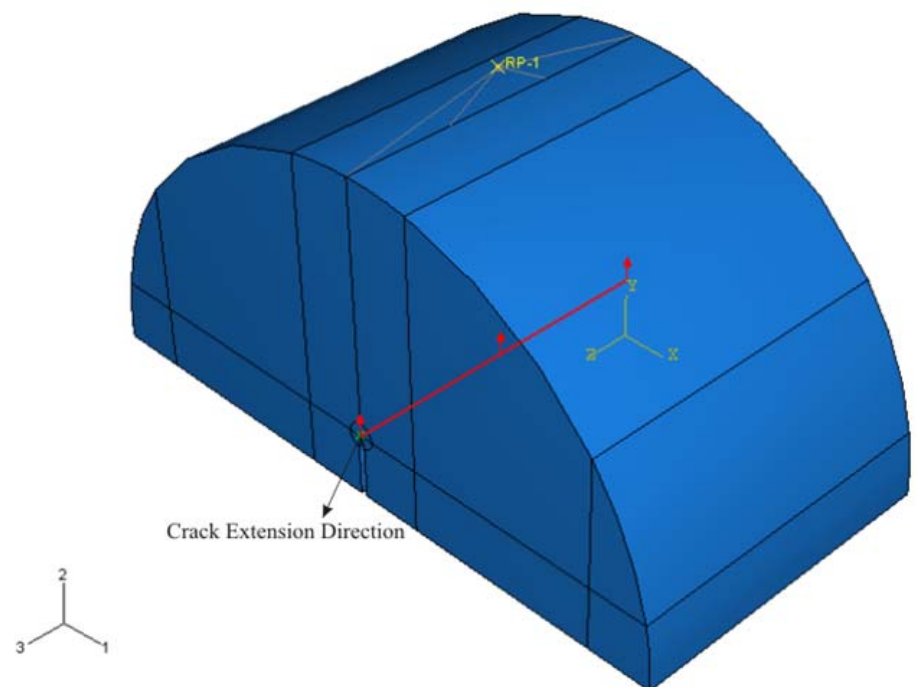


**Figure 4.21** Crack extension direction

After completing the above procedure, crack is created and ready for the analysis as shown in Figure 4.21.

When solving the fracture mechanics problems with ABAQUS, for getting the best  $K_I$  results, a relatively large concentric tube is applied around the crack tip. Generally this concentric tube is connected to the points around which the crack becomes sharp. Then, a small circle which will form the small tube is applied at the crack tip.

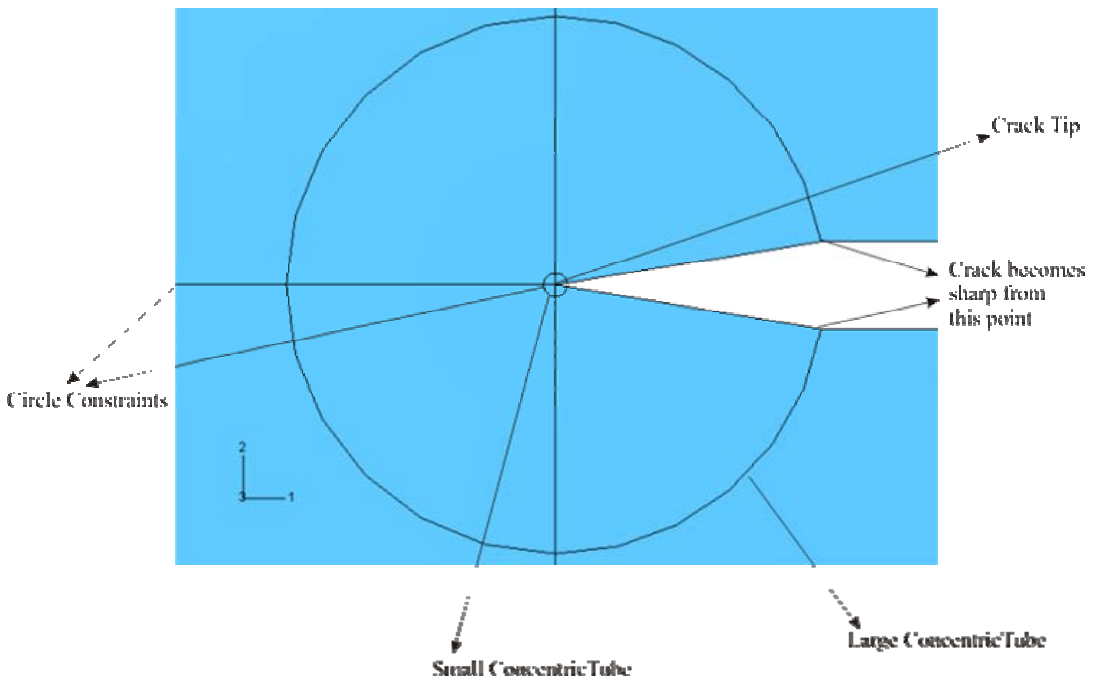


**Figure 4.22** Schematic view of the constraints around the crack tip

In Figure 4.22 model includes the larger concentric tube around the crack tip which is connected to the mesh by Hex Elements. The small tube is connected by or formed by Hex Dominated elements. On the other hand the whole model is meshed by Hex elements. These elements shapes can be found in ABAQUS user manual.

When solving crack problems with ABAQUS software, mesh density around the crack field must be fine, (Figure 4.23). Suitable mesh density increases the accuracy of the stress intensity factor computations. With the assistance of the larger concentric tube and the small tube, a focused mesh is obtained after meshing the model. Thus, accuracy of the  $K_I$  computations is increased.

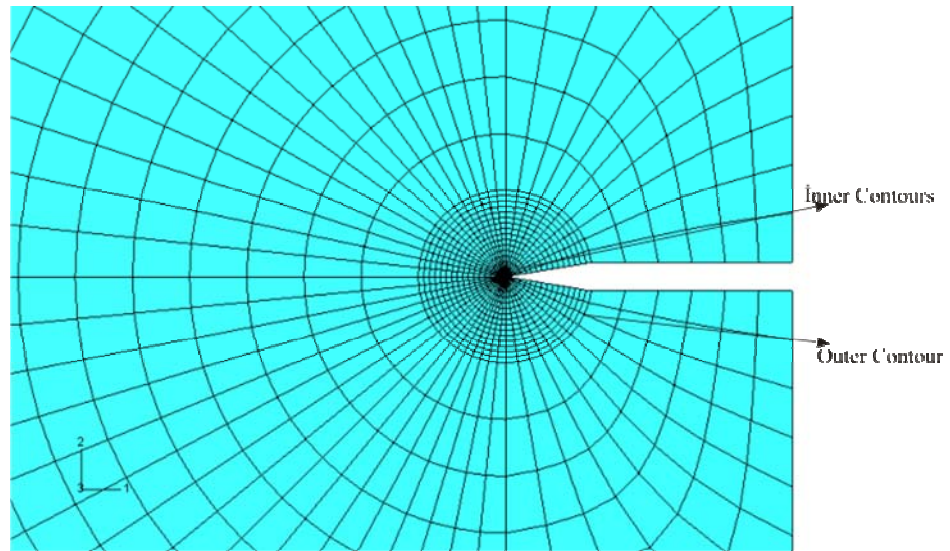


**Figure 4.23** Schematic view of the crack field after meshing

Before running the model, mesh contours around the crack tip must be counted correctly, this number is written to the number of contours space in the contour integral editor under the history output request for the computation of stress intensity factors.

#### 4.8 Computation of Stress Intensity Factor for SCB Type Specimens

In order to assess the effect of using different boundary conditions on ABAQUS models. Two different load application cases were tried. First steel rollers used in

the experiments were modeled directly as rigid loading units, and load was applied to these from the reference point located above the model as in Figure 4.24. In the second case, load was applied to the specimen models directly from the reference points, as discussed before, (Figure 4.25). Mechanical and geometrical input parameters are given in Table 4.4. Boundary conditions of the second case are illustrated in the sketch presented in Figure 4.26. Applied load was 1N at the reference point.

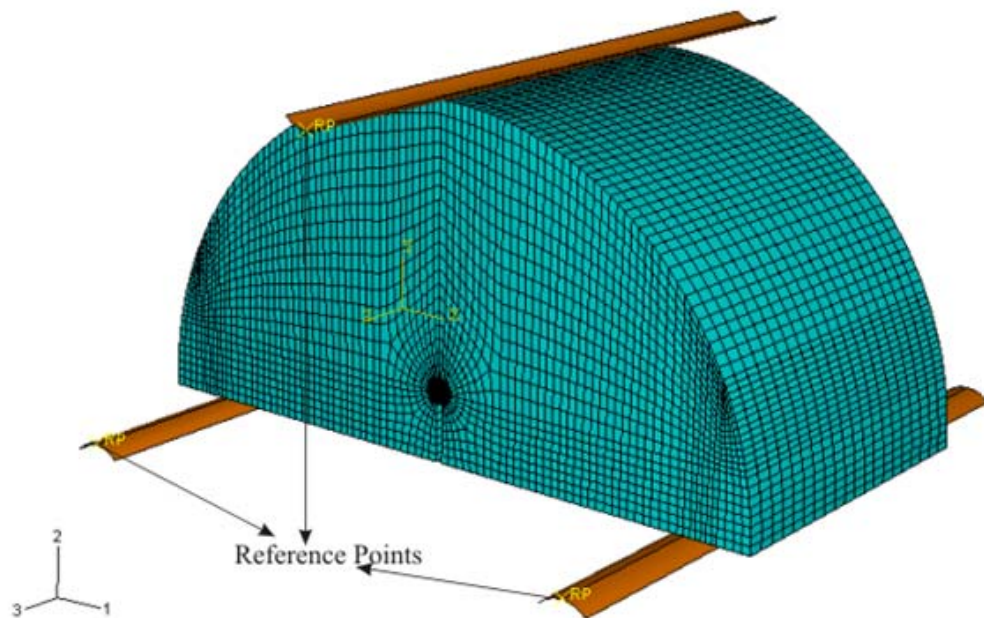


**Figure 4.24** Load application by steel loading bars

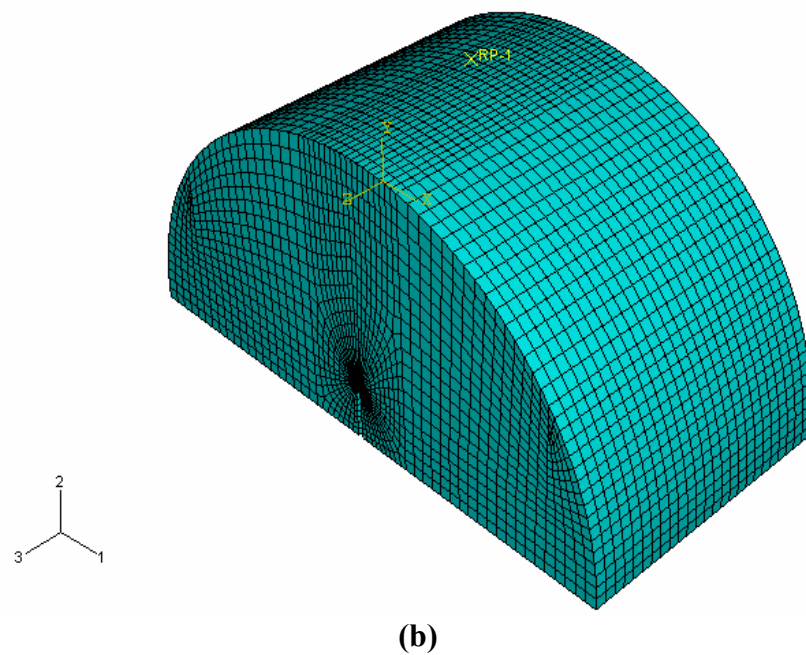
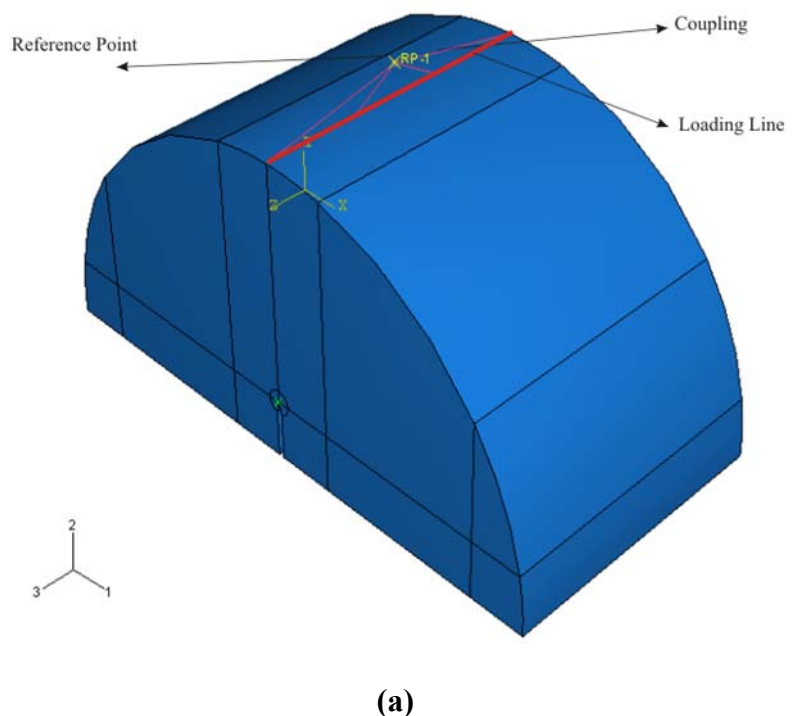


**Figure 4.25** (a) Direct load application from reference points (b) Finite element mesh used in the analysis of SCB specimens

**Table 4.4** Dimensional and mechanical properties of the SCB models

Dimensions and Mechanical Properties	Values
Radius of the specimen, R	0.05 m
Thickness of the specimen, B	0.05 m
Height of the specimen, h	0.05 m
Notch thickness, $t_n$	0.001 m
Notch length, a	0.01 m
Span length, S	0.04 m
Load , $\sigma$	-1 N
Young's modulus, E	1.3 E10 Pa
Poisson's ratio, $\nu$	0.15
a/R	0.2
S/R	0.8

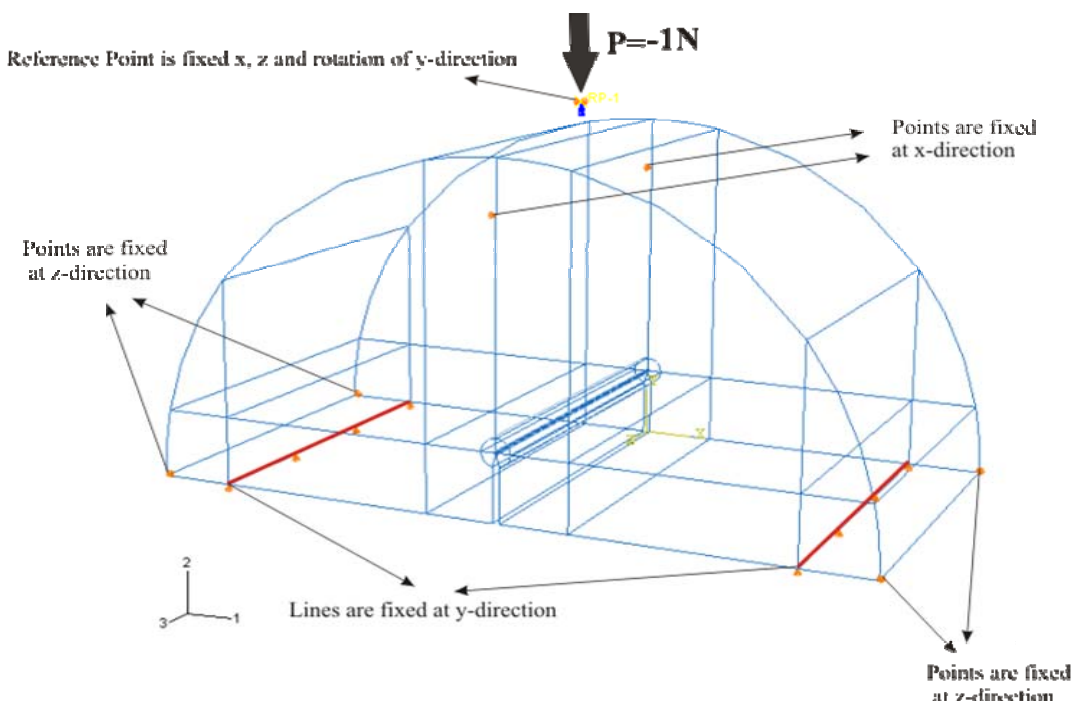


**Figure 4.26** Boundary conditions of the direct load application through the reference point

The results for both cases were very close as below:

$$K_I \text{ of SCB with steel bars} : 161.833 \text{ Pa} \sqrt{m}$$

$$K_I \text{ of SCB without steel bars} : 162.200 \text{ Pa} \sqrt{m}$$

Therefore, the load application method tried in the second case was adopted for all modeling work throughout the thesis due to its simplicity and easiness.

Stress distribution  $\sigma_{xx}$  perpendicular to the plane of the crack is given in Figure 4.27. High compressive stresses at the load application point which are designated as negative turn to very high tensile stresses close to the crack tip indicated as positive. This stress causes the crack to propagate and used mainly in the computation  $K_I$ . Stress  $\sigma_{yy}$  parallel to the crack plane is given in Figure 4.28. Around the crack this stress is also seen to be tension, indicating that crack tip is in a tensile stress field regarding all directions.

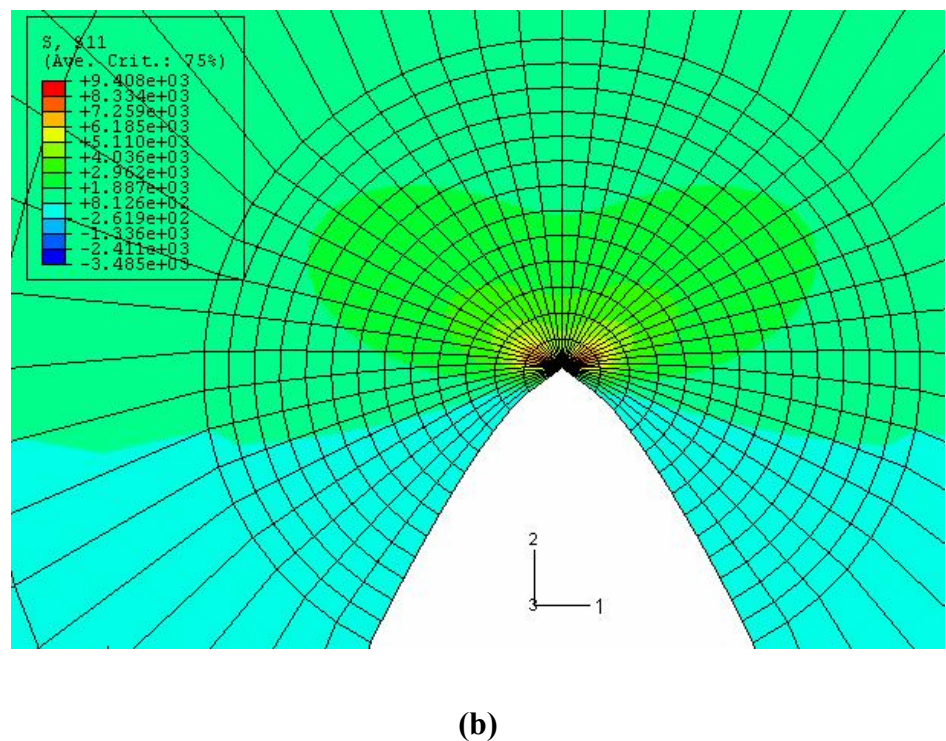
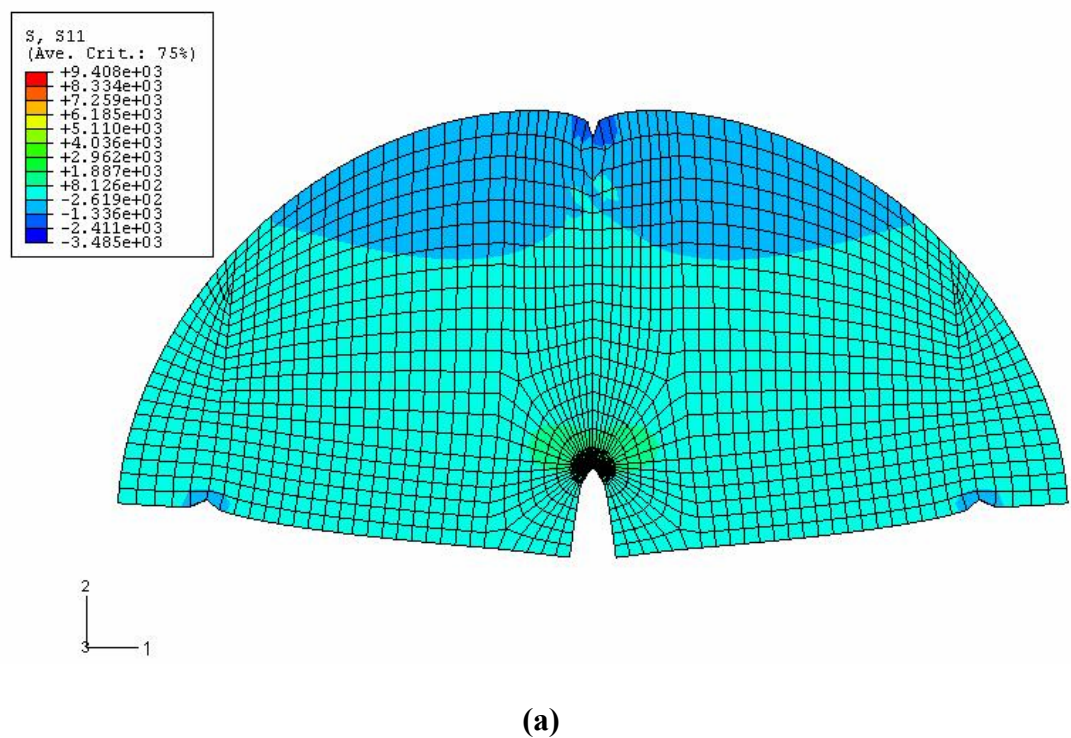
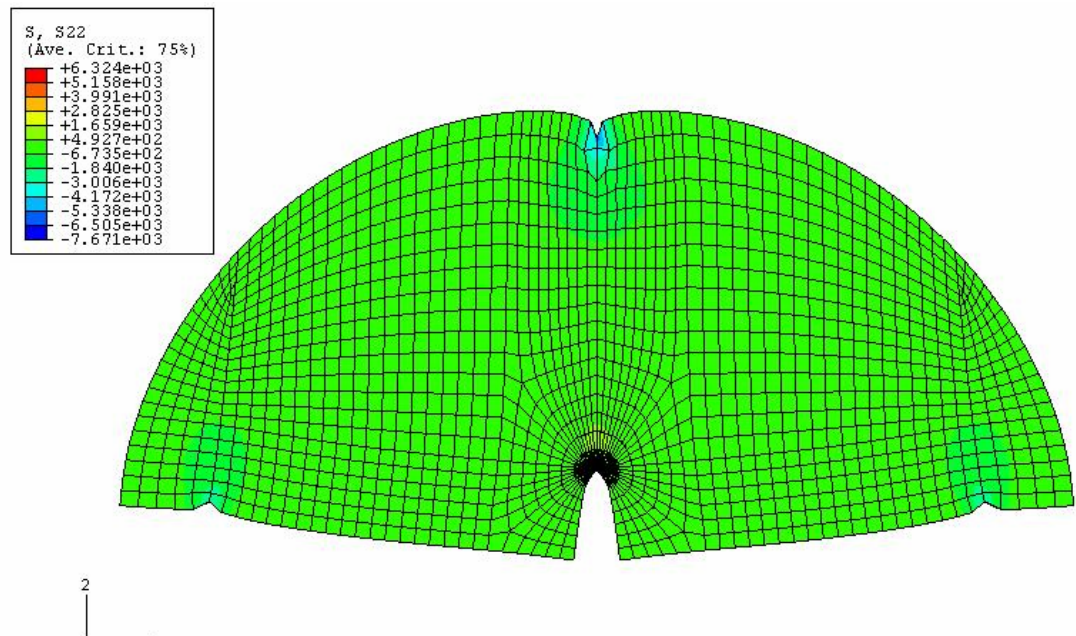
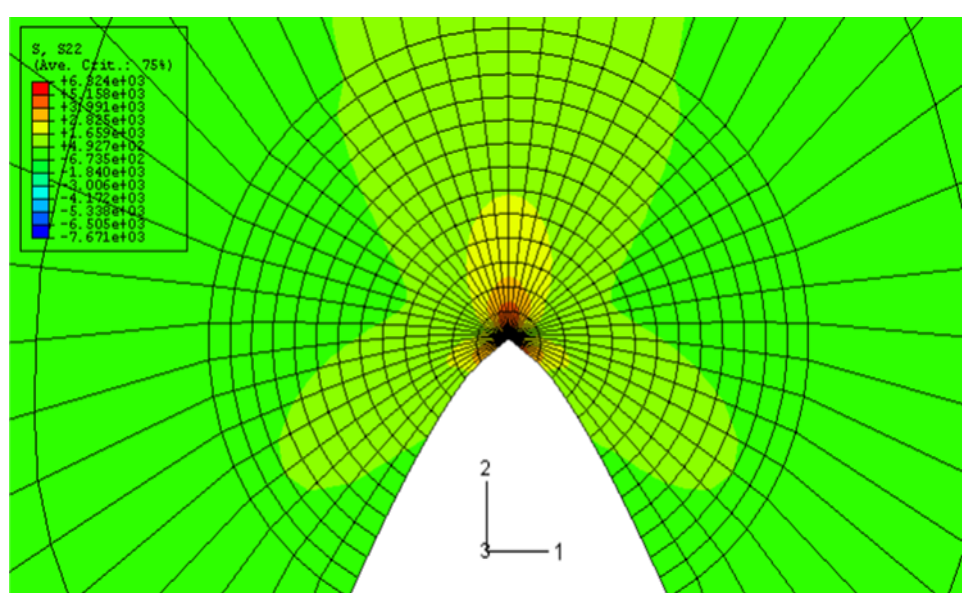


**Figure 4.27 (a)**  $S_{11} (\sigma_{xx})$  Stress distribution in the model **(b)**  $S_{11} (\sigma_{xx})$  Stress distribution at the crack tip (detailed view)



(a)



(b)

**Figure 4.28** (a)  $S_{22} (\sigma_{yy})$  Stress distribution in the model (b)  $S_{22} (\sigma_{yy})$  Stress distribution at the crack tip (detailed view)

Displacement distributions with no rigid body motions and rotations as shown in Figure 4.29 confirm the validity of the modeling work.

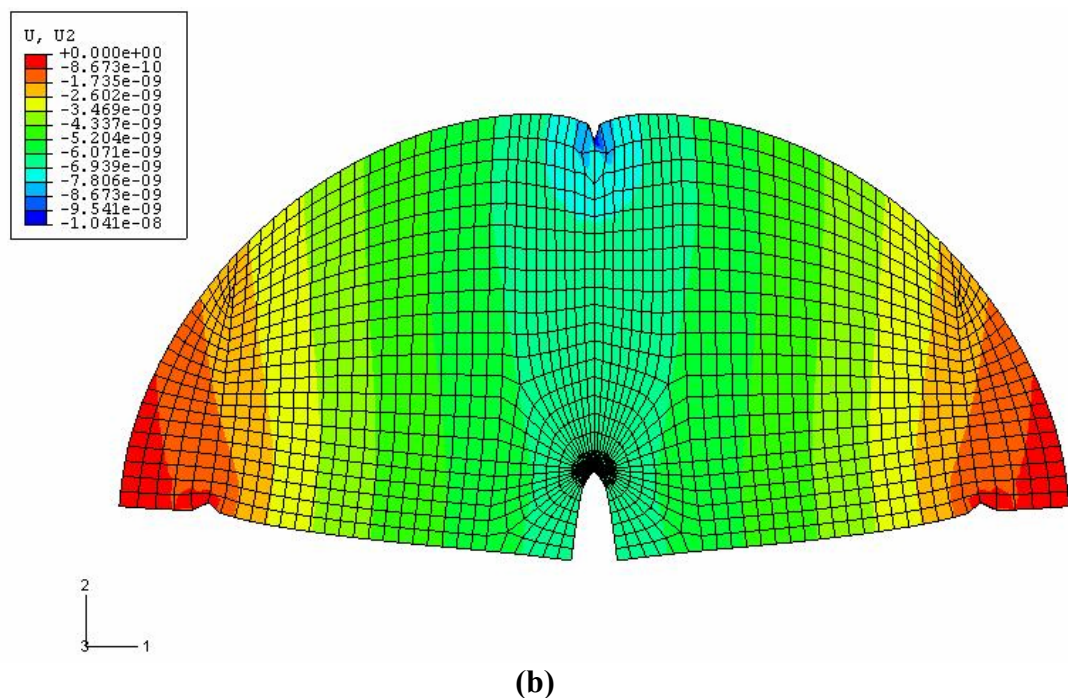
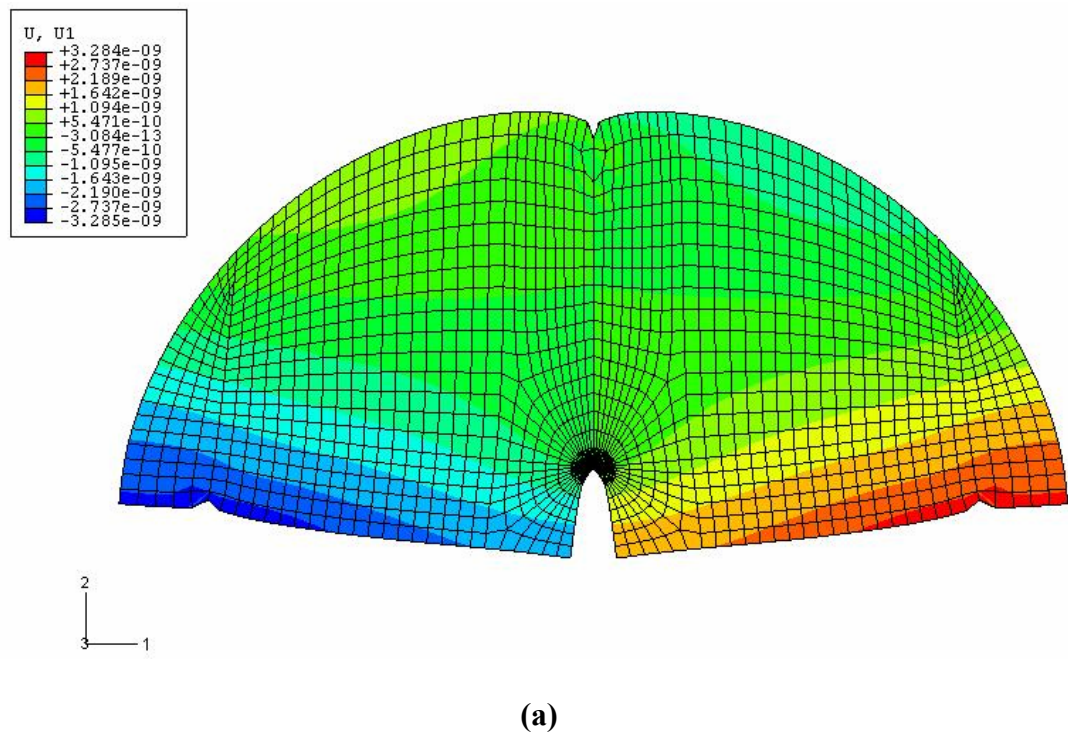
Stress and displacement magnitudes seem to be small because all the modeling work here was conducted by a unit load application of 1 N in order to carry out stress intensity factor analysis in a general way. Once stress intensity factors for different specimen geometries are obtained in a normalized way for unit loads, failure load magnitudes obtained from the experiments can be applied easily to these normalized stress intensity factors for the fracture toughness computations of different tests.

A normalized stress  $\sigma$  which is  $\sigma = \frac{P}{2RB}$  where P is the applied load is used in the stress intensity computations. This stress in a way corresponds to the tensile stress trying to open the crack. Using  $\sigma = 1$  MPa for generalizing the computed stress intensity factor  $K_I = 162.200 \text{ Pa} \sqrt{m}$ , with more commonly used  $\text{MPa} \sqrt{m}$  unit choice,  $K_I$  becomes:

$$K_I = 0.804 \text{ MPa} \sqrt{m}$$

Compared to the infinite plate under  $\sigma = 1$  MPa tension computations where  $K_I = 0.200 \text{ MPa} \sqrt{m}$ , the stress intensity factor is about four times higher under these beam type loading conditions.

After completing the verification runs successfully, each specimen used in the experiments was introduced to the ABAQUS models with its own dimensions. This way sensitivity of stress intensity computations against little dimensional variations was investigated. In the previous studies a common stress intensity factor relation was provided for average specimen dimensions without considering possible variations due to dimensional differences which might occur during preparations.



**4.29 (a)**  $U_1$  ( $U_x$ ) Horizontal displacement distribution **(b)**  $U_2$  ( $U_y$ ) Vertical displacement distribution

# **CHAPTER 5**

## **EXPERIMENTAL STUDIES**

In laboratory studies, mixture of pink-gray coloured Ankara andesite blocks were used. These blocks were taken from a private andesite quarry near Gölbaşı region in Ankara. When taking rock cores andesite blocks having similar characteristics were used in the experimental studies. Therefore, heterogenities due to the different rock blocks were minimized. All of the experiments were performed on Semi-Circular Specimen under Three-Point Bending (SCB), which was commonly used before by other researchers. The reason for this choice is that the simplicity of specimen preparation, laboratory setup and test procedure, (Lim et. al., 1994). In the experimental studies by keeping the  $a/R=0.2$  ratio constant for all specimens, three groups of SCB specimens were prepared:

- SCB specimens with different notch thicknesses,
- SCB specimens with different (S/R) span ratios,
- SCB specimens with flat ends of varying width.

### **5.1 Mechanical Properties of Pink-Gray Coloured Ankara Andesite**

In order to determine the mechanical properties (Young's Modulus, Poisson Ratio) of pink-gray coloured Ankara andesite, uniaxial compressive strength (UCS) tests were done. During the experiments ISRM's (1979) suggested methods were considered. NX size specimens ( $54 \approx \text{mm}$ ) and  $L/D \geq 2$  were used in these tests. In tests The MTS 815 Material Testing System was used. In experiments two external LVDT transducers were used to measure vertical displacement and vertical strain

and circumferential extensometer was used to measure circumferential displacement and strain.



**Figure 5.1** UCS test specimen with circumferential extensometer before the experiment

As a result of 5 tests average elasticity modulus of the andesite rock was found as 21000 MPa, the poisson ratio was found as 0.147 and the UCS of the andesite rock was found as 53.1 MPa.

Indirect tensile (Brazilian) tests were done to measure tensile strength of the pink-gray Ankara andesite in accordance with ISRM (1978). NX specimens were used in Brazilian tests ( $\approx 54$  mm). All specimens thickness and diameter ratio are approximately  $t/D=1/2$ .

As a result of 4 tests the tensile strength of the Ankara Andesite was found as 6.75 MPa, (Table 5.1).

**Table 5.1** Indirect tensile strength test data and results for Brazilian Test

Specimen Code	D (mm)	L(mm)	T <sub>0</sub> (MPa)
Brazilian 1	52.79	26.41	6.53
Brazilian 2	53.12	26.56	6.86
Brazilian 3	52.70	28.77	6.38
Brazilian 4	52.83	26.80	7.24
Average ± STD	26.17 ± 3.70	27.14 ± 1.10	6.75 ± 0.38

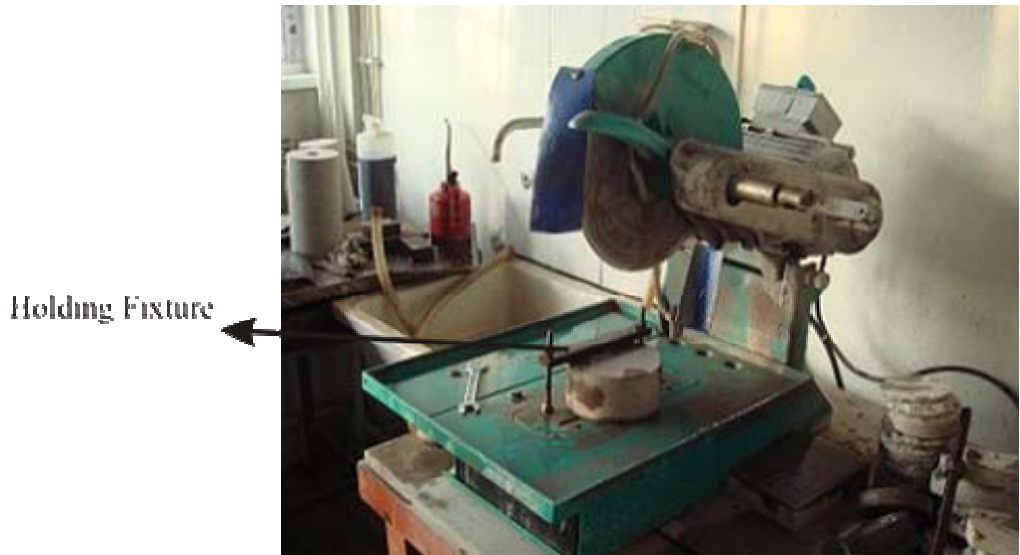
## 5.2 SCB Specimen Preparation

The big andesite blocks which were brought from the andesite quarry, were put on the cutting saw table. Then these big blocks were cut to form smaller ones by using the rotary cutting saw.

The diameter of the coring bit was 102 mm, and the diameter of the cores was approximately 100 mm.

After that, cores were sliced to 55 mm thickness by using the rotary saw. Discs were polished by using the grinding machine. This operation reduced the thickness of the discs approximately to 50 mm.

By using Smartcut 1004 precision diamond saw (Figure 5.2), the discs were cut into halves. During the disc cutting operation, disc was subjected to high vibration. It was very difficult to hold the disc with hand, therefore a holding fixture was used to fix the discs at the desired position, (Figure 5.2 a).



(a)



(b)



(c)

**Figure 5.2** Smartcut 1004 precision diamond saw and the holding fixture

Next stage is the notch cutting operation. In this operation the specimen was fixed on the apparatus (Figure 5.3). By using this apparatus cutting operation was assured to be at the centerline of the specimen which was drawn on the specimen before.

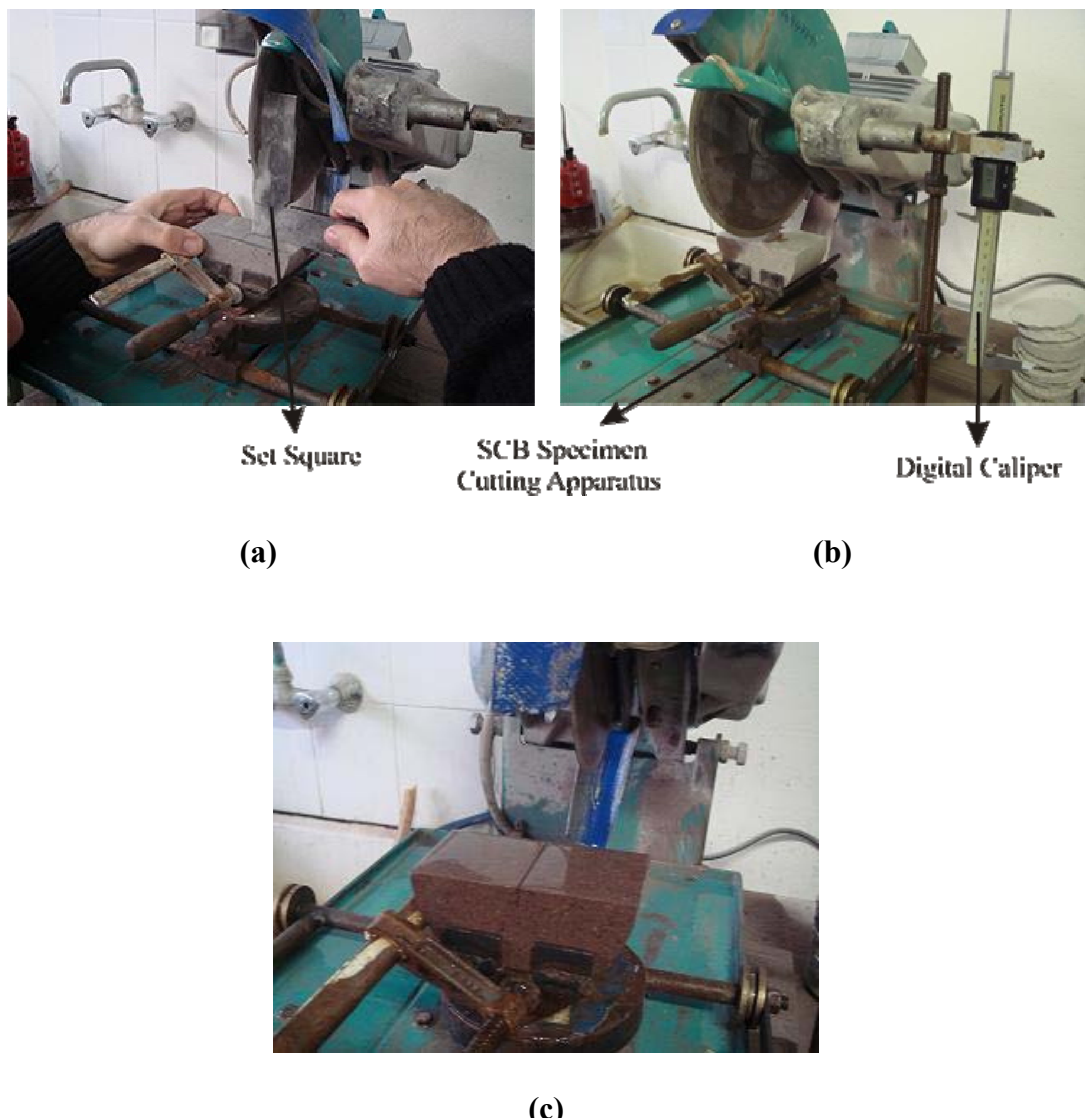


**Figure 5.3** Half disc after the notch opening

The last stage before the experiments is the specimen coding. Each specimen has a code for separating specimen from the other specimens. The coding indicated the notch thickness, span ratio and the flattened surface SCB specimens, (Figure 5.4 ).

**SCB-0<NT<1 mm-02-07-1**

**1<NT<2 mm**

**2<NT<3 mm**

**3<NT<4 mm**

Semi Circular Specimen Under Three Point Bending	Notech Thickness, (mm)	a/R	S/R	Specimen Number
--	------------------------	-----	-----	-----------------

(a)

**SCB-02-07-15 -1**

**20**

**22.5**

**25**

Semi Circular Specimen Under Three Point Bending	a/R	S/R	Flattened Loading Surface Width, (mm)	Specimen Number
--	-----	-----	---------------------------------------	-----------------

(b)

**SCB-02-03-1**

**04**

**05**

**06**

**07**

**08**

**09**

Semi Circular Specimen Under Three Point Bending	a/R	S/R	Specimen Number
--	-----	-----	-----------------

(c)

**Figure 5.4** Explanation of specimen codes

### **5.3 Experimental Setup**

In experiments MTS 815, servo-controlled hydraulic testing machine, was used as loading system. This machine is available at Middle East Technical University Rock Mechanics Laboratory.

MTS system consists of:

- A MicroConsole and its associated AC and/or DC controllers
- A programming device (which maybe mounted in the MicroConsole, mounted in another chassis in the console, or externally connected)

Servohydraulic Devices

- A hydraulic actuator and its associated servovalves and transducers, mounted in load frame
- A hydraulic power supply (HPS)

In operation of the system, the MicroConsole and its associated electronic products control the servohydraulic devices. The servohydraulic devices use hydraulic pressure, supplied by the HPS, to apply forces, displacement and/or strain to specimen.

#### **5.3.1 DaqBook**

Data acquisition system was 16-bit 200 kHz IOTech Daqbook/2000 series. DBK 80 device attached to the system is a low-noise, high-speed, unity-gain multiplexer card that provides 16 channels of differential voltage input. Load signal was processed and sent to the PC by this module. Signals of strain gage type displacement transducers were processed and transferred to the PC by DBK 43A module, (Figure 5.5).



**Figure 5.5** DBK 80 analog multiplexor, DBK 43 and DBK43A strain gage cards

#### 5.4 SCB Specimen Geometry

Set up and loading fixtures are shown in Figure 5.6 for a typical SCB specimen under three point bending. 10 mm diameter steel rollers apply the bending load to the specimen.



**Figure 5.6** SCB specimen with steel rollers before the experiment

In the experimental work, notch thickness ( $t_n$ ), span ratio (S/R), and the size of the flattened loading face experiments were changed. Schematic view in Figure 5.7 shows the symbols used for geometrical parameters of SCB specimens.

During the specimen preparation little variations of the dimensions were unavoidable in the critical geometrical parameters. In order to study the effect of little dimensional differences on the stress intensity factors and fracture toughness, each specimen was modeled with its own dimensions in the computer models. Before the tests, careful dimensional measurements of the geometrical parameters illustrated in Figure 5.7 were carried out. A typical table illustrating the dimensional variations, averages and deviations are included in Table 5.2. Rest of the tables showing the specimen dimensions are presented in Appendix A. When taking dimensions with a digital caliper, all front and back side dimensions were noted separately. Dimensions in the tables are the average values of the front-side and the back-side of the specimens. The \* sign adjacent to some of the specimens means that specimen has a joint or fissure inside, therefore exact critical failure

load value was not taken into consideration in the computations of averages, since specimens like these broke around the joints or natural fractures.

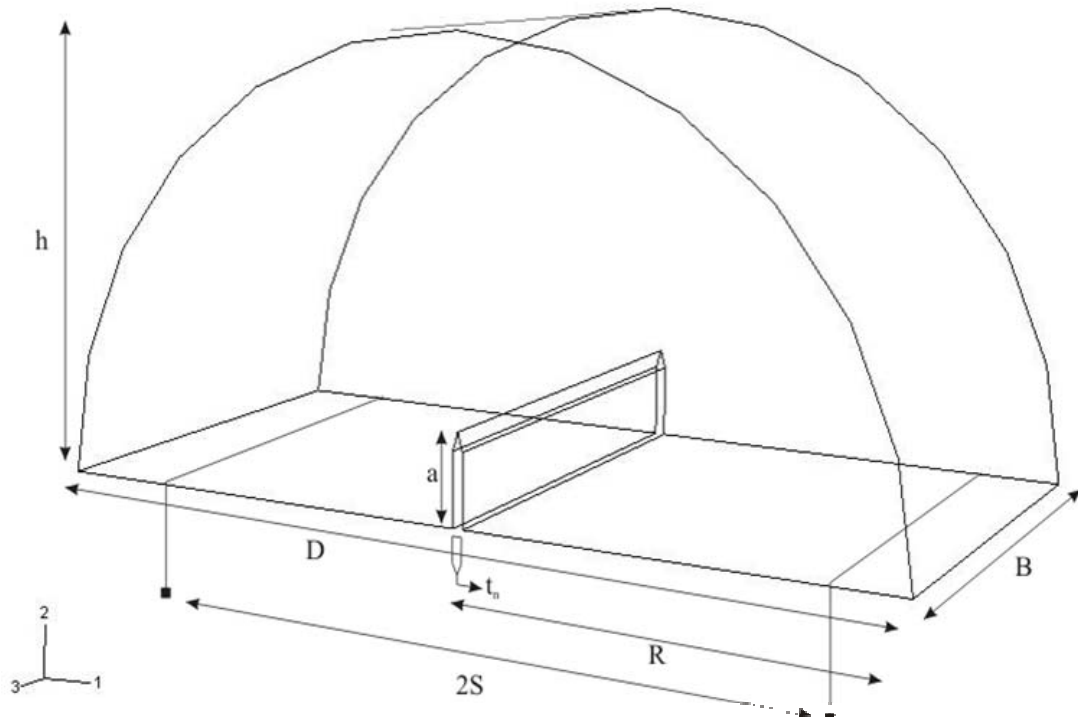


**Figure 5.7** SCB specimen sketch

The geometrical parameters related to the SCB specimens are:

h: Height of the specimen, D: Diameter of the specimen,

S: Span length, B: Thickness of the specimen,

a: Saw-cut notch length, R: Radius of the specimen,

t<sub>n</sub>: Notch thickness.

**Table 5.2** Dimensions of  $t_n < 1 \text{ mm}$ ,  $a/R=0.2$ ,  $S/R=0.7$  SCB specimens

Specimen Code	h mm	D mm	B mm	a mm	R mm	a/R	$t_n$ mm	$t_n/a$	S/R
1	50.71	102.01	50.25	10.00	51.01	0.196	0.80	0.080	0.686
2	48.89	99.21	50.62	10.00	49.61	0.202	0.84	0.084	0.706
3	49.14	99.82	50.51	10.00	49.92	0.200	0.82	0.082	0.701
4	49.95	99.94	50.52	10.00	49.97	0.200	0.91	0.091	0.700
5	49.20	99.88	50.47	10.50	49.95	0.210	0.85	0.081	0.701
6*	48.59	99.15	50.23	10.50	49.58	0.212	1.00	0.095	0.706
Average	49.58	100.17	50.47	10.10	50.09	0.202	0.84	0.084	0.699
$\pm$	$\pm$	$\pm$	$\pm$	$\pm$	$\pm$	$\pm$	$\pm$	$\pm$	$\pm$
STD	0.75	1.07	0.14	0.22	0.53	0.005	0.04	0.004	0.007

### 5.5.1 Notch Thickness Analysis

First analysis for SCB type specimens is the investigation of the effect of notch thickness ( $t_n$ ) on the SIF and fracture toughness. Four different saws with varying thickness were available, and thus four different saw-cut notch sizes ( $t_n < 1 \text{ mm}$ ,  $1 \text{ mm} < t_n < 2 \text{ mm}$ ,  $2 \text{ mm} < t_n < 3 \text{ mm}$ ,  $3 \text{ mm} < t_n < 4 \text{ mm}$ ) were obtained in the experiments. These notch sizes were formed by using rotary diamond saws in the laboratory. The diamond saw's thickness values are shown below in Figure 5.8. All of the notch thickness experiments are prepared keeping the notch length at  $a/R=0.2$  and span at  $S/R=0.7$ .

Real thicknesses of the notches cut by different saws were measured carefully after cutting operations. As seen in Table 5.2 the thinnest rotary diamond saw with a thickness 0.55 mm resulted in notches with thicknesses varying from 0.80 to 1.00 mm, average thickness being  $0.84 \pm 0.04 \text{ mm}$ . This case was named as  $t_n < 1 \text{ mm}$ .

Second one was  $1 \text{ mm} < t_n < 2 \text{ mm}$  case with thicknesses between 1.06-1.31 mm with an average of  $1.20 \pm 0.09$  mm. Thicknesses were between 2.13-2.29 for the third case ( $2 \text{ mm} < t_n < 3 \text{ mm}$ ), and the average was  $2.22 \pm 0.07$  mm.  $3 \text{ mm} < t_n < 4 \text{ mm}$  case was the fourth case with  $t_n$  varying between 3.48-3.96 mm with an average of  $3.66 \pm 0.21$  mm.

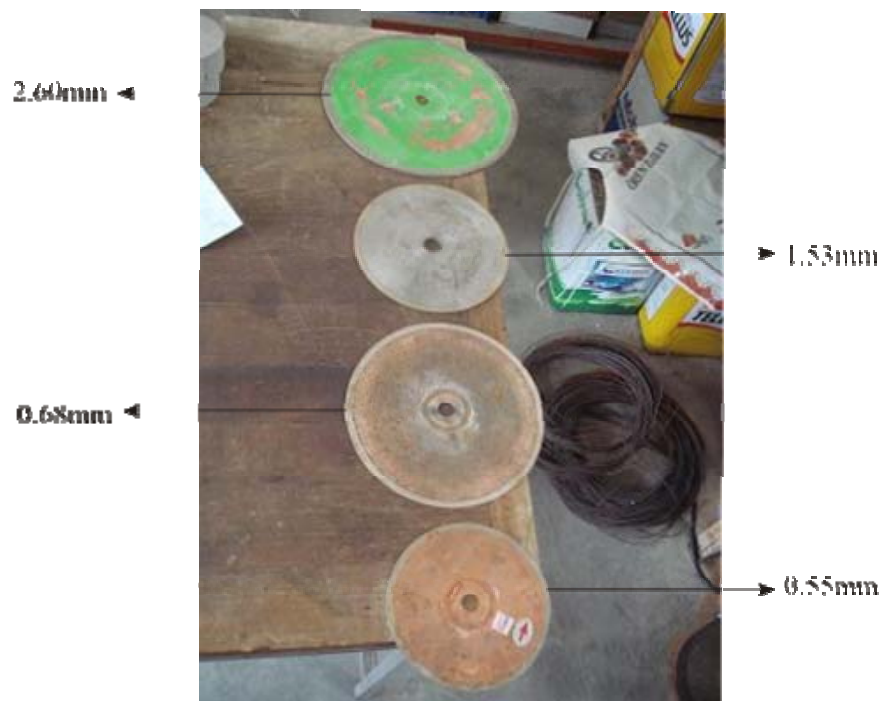


**Figure 5.8** Diamond saws which were used in the notch thickness analysis

### 5.5.2 Specimen Dimensions of Span Ratio (S/R) Analysis

In the investigation of effect of loading span on the SIF's and fracture toughness experiments with seven different S/R ratios were conducted. These are S/R=0.3, 0.4, 0.5, 0.6, 0.7, 0.8 and 0.9. For the span investigations, a/R ratio for all of the specimens is kept at 0.2, and Table 5.3 shows the typical dimensions of the specimens for S/R=0.3. The dimensions of the rest of the specimens are given in Appendix A.

**Table 5.3** Dimensions of a/R=0.2, S/R=0.3 SCB specimens

Specimen Code	h mm	D mm	B mm	a mm	R mm	a/R	t <sub>n</sub> mm	t <sub>n</sub> /a	S/R
1	49.17	99.18	50.27	9.50	49.59	0.192	1.00	0.105	0.302
2	49.40	99.69	50.85	9.50	49.85	0.191	0.98	0.103	0.301
3	49.52	99.90	50.84	10.00	49.95	0.200	1.07	0.107	0.300
Average	49.36	99.59	50.65	9.67	49.80	0.194	1.02	0.105	0.301
±	±	±	±	±	±	±	±	±	±
STD	0.18	0.37	0.33	0.29	0.19	0.005	0.05	0.002	0.001

### 5.5.3 Specimen Dimensions of Flattened SCB Analysis

Sketch in Figure 5.9 shows the general view of the flattened SCB specimens. In flattened surface experiments four different flattened loading surface width (f) sizes were used. These are f $\cong$  15 mm, 20 mm, 22.5 mm and 25 mm. For all of the specimens, a/R ratio is kept at 0.2, span ratio is kept at 0.7 and the notch thicknesses (t<sub>n</sub>) were nearly the same at 1 mm. Table 5.4 shows the typical

dimensions of the flattened specimens for  $f \leq 15$  mm. The dimensions of the rest of the flattened specimens are given in Appendix A. The characters which were used in Table 5.4 are:

$h$ : Height of the specimen,  $D$ : Diameter of the specimen,  $S$ : Span length,  
 $B$ : Width of the specimen,  $a$ : Notch length,  $R$ : Radius of the specimen,  
 $t_n$ : Notch thickness  $f$ : Flattened loading surface width,  $A$ : Area of loading surface.

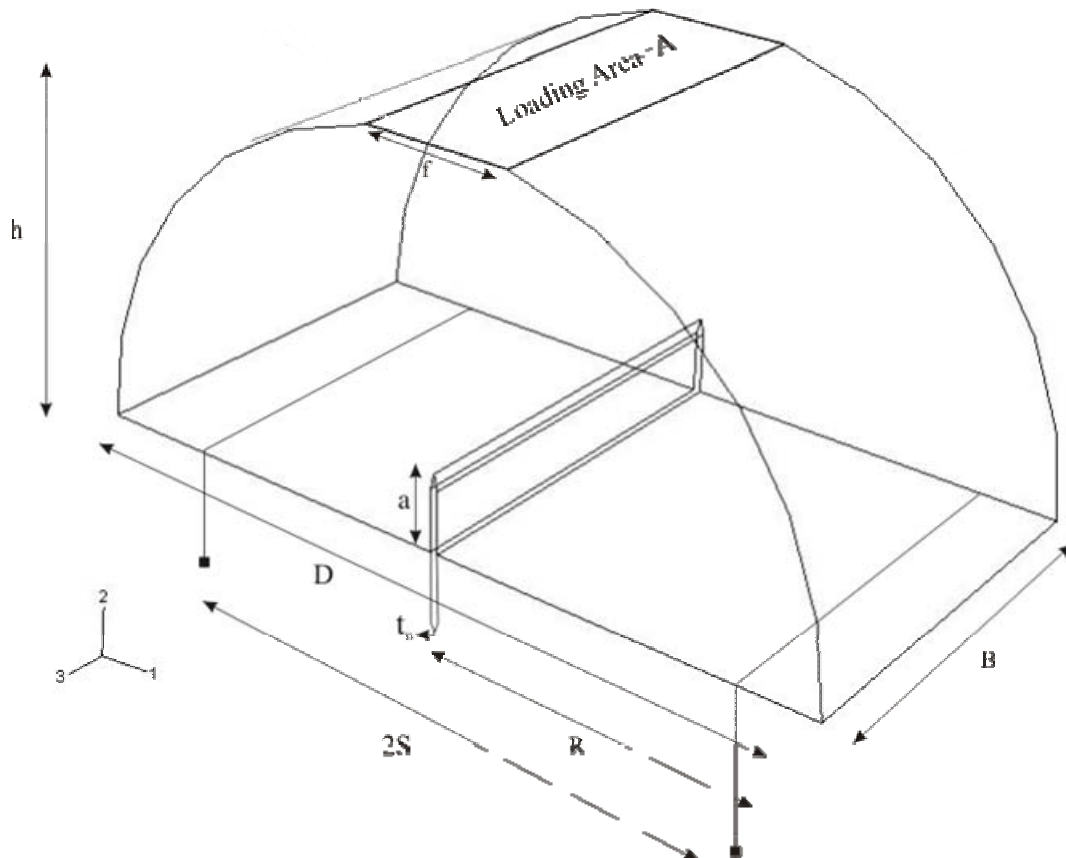


**Figure 5.9** Dimensions of flattened SCB specimens

**Table 5.4** Dimensions of  $f \cong 15\text{mm}$   $a/R=0.2$ ,  $S/R=0.7$  SCB specimens

Specimen Code	h mm	D mm	B mm	a mm	R mm	a/R	t <sub>n</sub> mm	t <sub>n</sub> /a	S/R	f mm	A mm <sup>2</sup>
1	48.47	99.32	50.04	9.50	49.66	0.191	1.04	0.109	0.705	15.18	759.6
2	48.45	99.98	51.20	10.00	49.99	0.200	1.08	0.108	0.700	15.54	795.4
3	48.92	99.92	48.33	9.50	49.96	0.190	0.98	0.103	0.701	14.32	692.1
4	48.96	99.92	50.27	10.00	49.96	0.200	1.06	0.106	0.701	14.71	739.2
5	48.37	99.94	50.22	10.00	49.98	0.200	0.98	0.098	0.700	15.31	768.9
Average	48.63	99.81	50.01	9.80	49.91	0.196	1.03	0.105	0.701	15.01	751.0
±	±	±	±	±	±	±	±	±	±	±	±
STD	0.28	0.28	1.04	0.27	0.14	0.005	0.05	0.005	0.002	0.49	38.6

#### 5.5.4 Effect of Geometrical Variations in Dimensions When Preparing The SCB Specimens

When preparing the SCB specimens for the experiment, some dimension changes were unavoidable because of the preparation processes. Therefore, as another part of this thesis effect of dimension changes of the specimens on fracture toughness were investigated. In this investigation specimens were chosen with same  $a/R = 0.2$ ,  $S/R = 0.7$  and  $t_n \cong 1.20$  values. In Table 5.5 dimensions of the SCB specimens used were presented. Three of these eleven specimens were taken from the  $S/R = 0.7$  span ratio analysis, other five specimens were taken from the  $1 \text{ mm} < t_n < 2 \text{ mm}$  notch thickness analysis. The remaining three of the specimens were additional to increase the quality of the results statistically. The characters which were used in Table 5.5 are:

h: Height of the specimen, D: Diameter of the specimen, S: Span length,  
 B: Thickness of the specimen, a: Notch length, R: Radius of the specimen,  
 $t_n$  = Notch thickness

**Table 5.5** SCB specimen dimensions used in geometrical variations analysis

Specimen Code	h mm	D mm	B mm	a mm	R mm	$t_n$ mm	S/R
1*	49.09	101.80	50.92	10.50	50.93	1.35	0.687
2*	51.63	101.83	50.95	10.50	50.92	1.30	0.687
3*	50.79	101.52	51.63	10.50	50.76	1.26	0.690
4**	49.20	99.86	49.89	10.00	49.94	1.30	0.701
5**	48.75	99.68	47.99	10.50	49.85	1.24	0.702
6**	49.51	99.85	50.03	10.00	49.93	1.35	0.701
7***	50.53	101.95	49.94	10.00	50.98	1.17	0.687
8***	49.99	101.92	49.86	10.00	50.97	1.17	0.687
9***	49.56	99.67	48.03	10.50	49.84	1.18	0.702
10***	49.58	99.69	49.36	10.00	49.85	1.31	0.702
11***	49.39	99.66	50.51	10.00	49.83	1.28	0.702
Average $\pm$ STD	49.82 $\pm$ 0.85	100.68 $\pm$ 1.09	49.92 $\pm$ 1.14	10.23 $\pm$ 0.26	50.34 $\pm$ 0.55	1.26 $\pm$ 0.07	0.695 $\pm$ 0.008

\*: Additional specimens

\*\*: Span ratio analysis specimens (S/R=0.7)

\*\*\*: Notch thickness analysis specimens ( $1 \text{ mm} < t_n < 2 \text{ mm}$ )

In Table 5.6, dimension ratios of the SCB specimens are given.

**Table 5.6** Dimension ratios used in dimension investigation

Specimen Code	$t_n/a$	$a/R$	$h/D$	$h/a$	$a/D$	$h/t_n$
1*	0.129	0.206	0.482	4.675	0.103	36.36
2*	0.124	0.206	0.507	4.917	0.103	39.72
3*	0.120	0.207	0.500	4.837	0.103	40.31
4**	0.130	0.200	0.493	4.920	0.100	37.85
5**	0.118	0.211	0.489	4.643	0.105	39.31
6**	0.135	0.200	0.496	4.951	0.100	36.67
7***	0.117	0.196	0.496	5.053	0.098	43.19
8***	0.117	0.196	0.490	4.999	0.098	42.73
9***	0.112	0.211	0.497	4.720	0.105	42.00
10***	0.131	0.201	0.497	4.958	0.100	37.85
11***	0.128	0.201	0.496	4.939	0.100	38.59
Average ± STD	0.124 ± 0.007	0.203 ± 0.005	0.495 ± 0.006	4.874 ± 0.137	0.102 ± 0.003	39.51 ± 2.35

\*: Additional specimens

\*\*: Span ratio analysis specimens ( $S/R=0.7$ )

\*\*\*: Notch thickness analysis specimens ( $1 \text{ mm} < t_n < 2 \text{ mm}$ )

# **CHAPTER 6**

## **RESULTS & DISCUSSIONS**

By using the values in the dimension tables, specimens were modeled with ABAQUS software. After modeling and analysing the model, ABAQUS gave the  $K_I$  and  $K_{II}$  values for each specimen. Then,  $K_I$  values were firstly normalized ( $Y_1$ ) by using the Equation 6.1. These normalised stress intensity values were used to determine the fracture toughness values of each specimen by using the critical failure load which was taken from the experiments. While SCB tests were performed data was recorded to the computer and this data was used for plotting the Load-Displacement and Load-CMOD (Crack Mouth Opening Displacement) curves. By using these graphs the maximum critical load, maximum vertical displacement and maximum CMOD ( $CMOD_f$ ) values were determined. By the help of the normalized stress intensity factor and the maximum critical load, effect of different testing parameters on fracture toughness of Ankara andesite was investigated. Fracture toughness  $K_{IC}$  values, normalized stress intensity, experimental data and the ABAQUS raw stress intensity values were tabulated. Each of the table is categorized by the type of the analysis.

### **6.1 Computation Technique**

Calculation technique of the normalized stress intensity factor and fracture toughness  $K_{IC}$  was shown through Equations 6.1 and 6.4.

Normalized stress intensity factor  $Y_I$ :

$$Y_I = \frac{K_I}{\sigma_0 \sqrt{\pi a}} \quad (6.1)$$

where:

$K_I$ : Mode I stress intensity factor

$a$ : Notch length

$$\sigma_0 = \frac{P}{2RB} \quad (6.2)$$

$P$ : Applied load (when modeling it is 1N)

$R$ : Specimen radius

$B$ : Specimen thickness

On the other hand fracture toughness  $K_{IC}$ :

$$K_{IC} = Y_I \sigma_{cr} \sqrt{\pi a} \quad (6.3)$$

$Y_I$ : Normalized stress intensity factor,

$$\sigma_{cr} = \frac{P_{cr}}{2RB} \quad (6.4)$$

where:

$P_{cr}$ : Load at fracture.

By using the equations above, sample calculation procedure of normalized stress intensity factor and the fracture toughness of one specimen is shown below. This procedure is for the specimen SCB-NT<1 mm-02-07-1.

By using Table 5.2 and Table 6.1, R, B, a and the  $K_I$  value of the specimen's are obtained.

where:

R: 0.051 m

B: 0.050 m

$K_I$ : 133.926 Pa  $\sqrt{m}$

a: 0.010 m

Substituting the values to the Equation 6.1,  $Y_I$  is:

$$Y_I = \frac{133.926 Pa \sqrt{m}}{\sigma_0 \sqrt{\pi} \times 0.010 m} \quad (6.5)$$

Calculation of the  $\sigma_0$  from Equation 6.4 is below:

$$\sigma_0 = \frac{1N}{2 \times 0.051m \times 0.050m} \quad (6.6)$$

$$\sigma_0 = 195.1 N/m^2$$

By applying the  $\sigma_0$  value to the first Equation 6.5,  $Y_I$  is:

$$Y_I = \frac{133.926 Pa \sqrt{m}}{195.1 N/m^2 \sqrt{\pi} \times 0.010 m} \quad (6.7)$$

$Y_I$  is found as 3.873 according to this calculation procedure. After that fracture toughness is calculated by using Equations 6.4 and 6.3.

$$\sigma_{cr} = \frac{P_{cr}}{2RB} = \frac{11.7kN}{2 \times 0.051m \times 0.050m} = 2282.5 \times 10^3 N/m^2$$

Then, the fracture toughness is:

$$K_{IC} = Y_I \sigma_{cr} \sqrt{\pi a} = 3.873 \times 2282.5 \times 10^3 N/m^2 \sqrt{\pi 0.010m}$$

$$K_{IC} = 1566.9 \times 10^3 Pa\sqrt{m}$$

$$K_{IC} = 1.567 MPa\sqrt{m}$$

## 6.2 Notch Thickness Results

First analysis for SCB type specimens is the investigation of the notch thickness effect on the normalized SIF and fracture toughness values. Four different notch sizes were considered in this study. These notch sizes were obtained by using rotary diamond saws in the laboratory. All of the notch thickness experiments were at  $a/R=0.2$  and  $S/R=0.7$ . Three dimensional ABAQUS analysis results, experimental results and graphical analysis of these results are presented below in Tables 6.1, 6.2, 6.3 and 6.4. The labels used in tables are:

$P_{max}$ : Failure load, (kN),

$U$ : Vertical displacement, (mm),

CMOD: Crack mouth opening displacement, (mm),

$K_I$ : Stress intensity factor calculated with ABAQUS, ( $Pa\sqrt{m}$ ),

$K_{II}$ : Stress intensity factor calculated with ABAQUS, ( $Pa\sqrt{m}$ ),

$Y_I$ : Normalized stress intensity factor,

$K_{IC}$ : Fracture toughness, ( $MPa\sqrt{m}$ ),

$k$ : Stiffness (kN/mm),

$t_n$ : Notch thickness.

**Table 6.1** Results of  $t_n < 1$  mm,  $a/R=0.2$ ,  $S/R=0.7$  SCB specimens

Specimen Code	$P_{max}$ . kN	U mm	CMOD mm	$K_I$ $Pa\sqrt{m}$	$K_{II}$ $Pa\sqrt{m}$	$Y_I$	$K_{IC}$ $MPa\sqrt{m}$	k kN/mm
1	11.70	0.175	-	133.926	0.003630	3.873	1.567	65.18
2	9.05	0.149	-	144.143	0.003900	4.085	1.304	61.91
3	9.35	0.232	0.030	141.935	0.001140	4.038	1.327	38.62
4	8.90	0.285	0.020	136.295	0.000306	3.882	1.213	32.42
5	8.62	0.153	-	145.307	0.001114	4.034	1.252	56.98
6*	8.82	0.184	0.026	149.141	0.000328	4.091	1.315	36.44
Average	9.52	0.199	0.025	140.321	0.002018	3.982	1.333	51.02
$\pm$	$\pm$	$\pm$	$\pm$	$\pm$	$\pm$	$\pm$	$\pm$	$\pm$
STD	1.24	0.058	0.007	4.979	0.001632	0.098	0.138	14.62

\*=Specimen has a joint inside (These specimens were not considered when calculating the averages and standart deviations)

**Table 6.2** Results of  $1 \text{ mm} < t_n < 2$  mm,  $a/R=0.2$ ,  $S/R=0.7$  SCB specimens

Specimen Code	$P_{max}$ . kN	U mm	CMOD mm	$K_I$ $Pa\sqrt{m}$	$K_{II}$ $Pa\sqrt{m}$	$Y_I$	$K_{IC}$ $MPa\sqrt{m}$	k kN/mm
1	10.70	0.239	-	134.446	0.003336	3.862	1.438	43.43
2	10.10	0.172	0.027	136.962	0.000862	3.927	1.383	56.08
3	8.51	0.230	-	143.434	0.003900	4.074	1.220	48.62
4	7.77	0.180	0.032	149.179	0.001655	3.932	1.159	41.95
5	9.17	0.145	-	139.769	-0.000017	3.880	1.281	63.09
6	10.30	0.160	0.039	137.364	0.000027	3.901	1.414	64.34
Average	9.43	0.188	0.033	140.192	0.001627	3.929	1.316	52.92
$\pm$	$\pm$	$\pm$	$\pm$	$\pm$	$\pm$	$\pm$	$\pm$	$\pm$
STD	1.14	0.038	0.006	5.346	0.001669	0.076	0.113	9.72

**Table 6.3** Results of  $2 \text{ mm} < t_n < 3 \text{ mm}$ ,  $a/R=0.2$ ,  $S/R=0.7$  SCB specimens

Specimen Code	$P_{\max.}$ kN	U mm	CMOD mm	$K_I$ $\text{Pa}\sqrt{\text{m}}$	$K_{II}$ $\text{Pa}\sqrt{\text{m}}$	$Y_I$	$K_{IC}$ $\text{MPa}\sqrt{\text{m}}$	k kN/mm
1	9.87	0.167	-	123.776	0.000414	3.688	1.221	63.52
2	11.30	0.219	0.027	123.401	0.000382	3.663	1.394	51.91
3	10.20	0.196	0.027	138.144	0.000431	3.803	1.409	53.39
4	10.00	0.172	0.033	131.711	0.000341	3.656	1.317	59.17
5	9.46	0.241	0.039	138.150	0.000346	3.662	1.307	39.67
6	9.31	0.186	-	134.745	0.000379	3.718	1.254	50.85
Average	10.02	0.197	0.031	131.655	0.000382	3.698	1.317	53.08
$\pm$	$\pm$	$\pm$	$\pm$	$\pm$	$\pm$	$\pm$	$\pm$	$\pm$
STD	0.71	0.029	0.006	6.694	0.000036	0.056	0.074	8.15

**Table 6.4** Results of  $3 \text{ mm} < t_n < 4 \text{ mm}$ ,  $a/R=0.2$ ,  $S/R=0.7$  SCB specimens

Specimen Code	$P_{\max.}$ kN	U mm	CMOD mm	$K_I$ $\text{Pa}\sqrt{\text{m}}$	$K_{II}$ $\text{Pa}\sqrt{\text{m}}$	$Y_I$	$K_{IC}$ $\text{MPa}\sqrt{\text{m}}$	k kN/mm
1	7.77	0.225	-	112.292	-0.000247	3.180	0.872	34.44
2	8.18	0.219	0.032	106.540	-0.000096	3.148	0.871	36.95
3	10.30	0.224	0.023	111.851	0.000026	3.256	1.152	44.83
4	10.20	0.218	0.029	112.667	0.000110	3.033	1.149	45.30
5*	5.20	0.317	0.013	112.333	0.000039	3.233	0.584	15.75
Average	9.11	0.221	0.028	110.838	-0.000052	3.154	1.011	40.38
$\pm$	$\pm$	$\pm$	$\pm$	$\pm$	$\pm$	$\pm$	$\pm$	$\pm$
STD	1.32	0.003	0.005	2.884	0.000155	0.093	0.161	5.51

\*=Specimen has a joint inside (These specimens were not considered when calculating the averages and standart deviations)

By using the table above, Figure 6.1 shows the normalized SIF versus the notch thickness and the Figure 6.2 shows the normalized SIF versus  $t_n/a$ . It is seen from the figures that, SIF values decreased with increasing notch thickness and  $t_n/a$ . These plots were generated by considering all experiments.

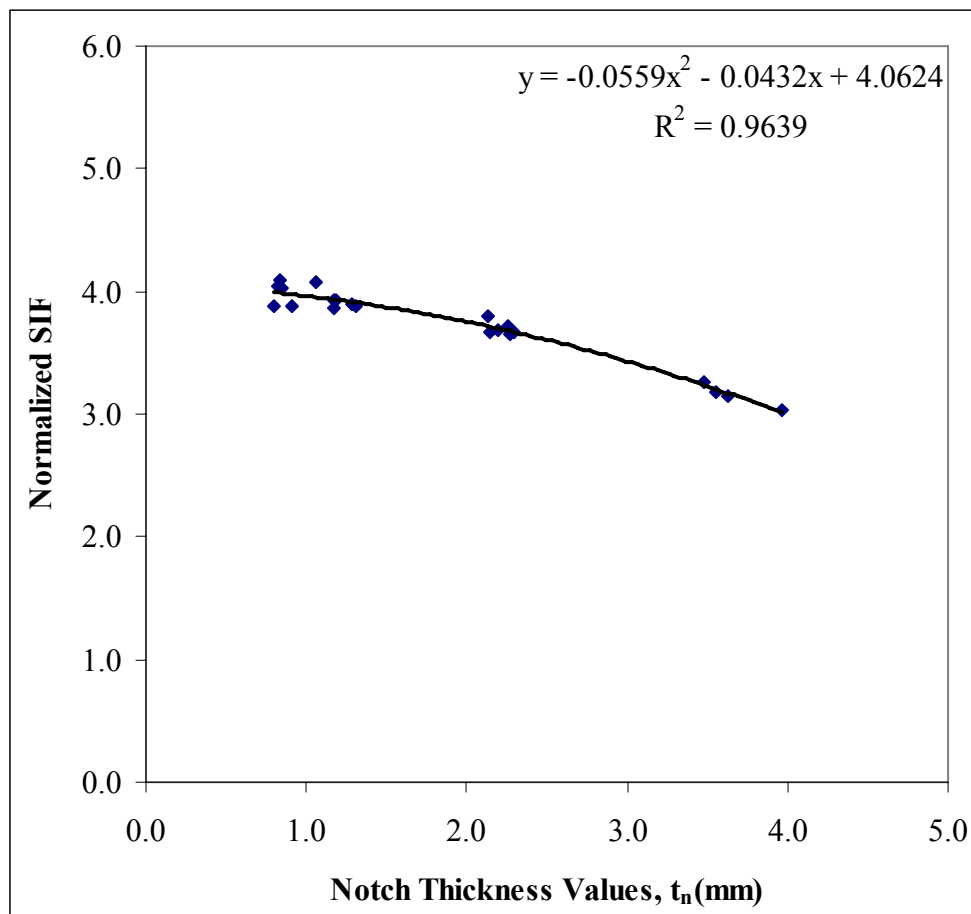


**Figure 6.1** Normalized SIF  $\left[ Y_I = \frac{K_I}{\sigma_0 \sqrt{\pi a}} \right]$  versus notch thickness

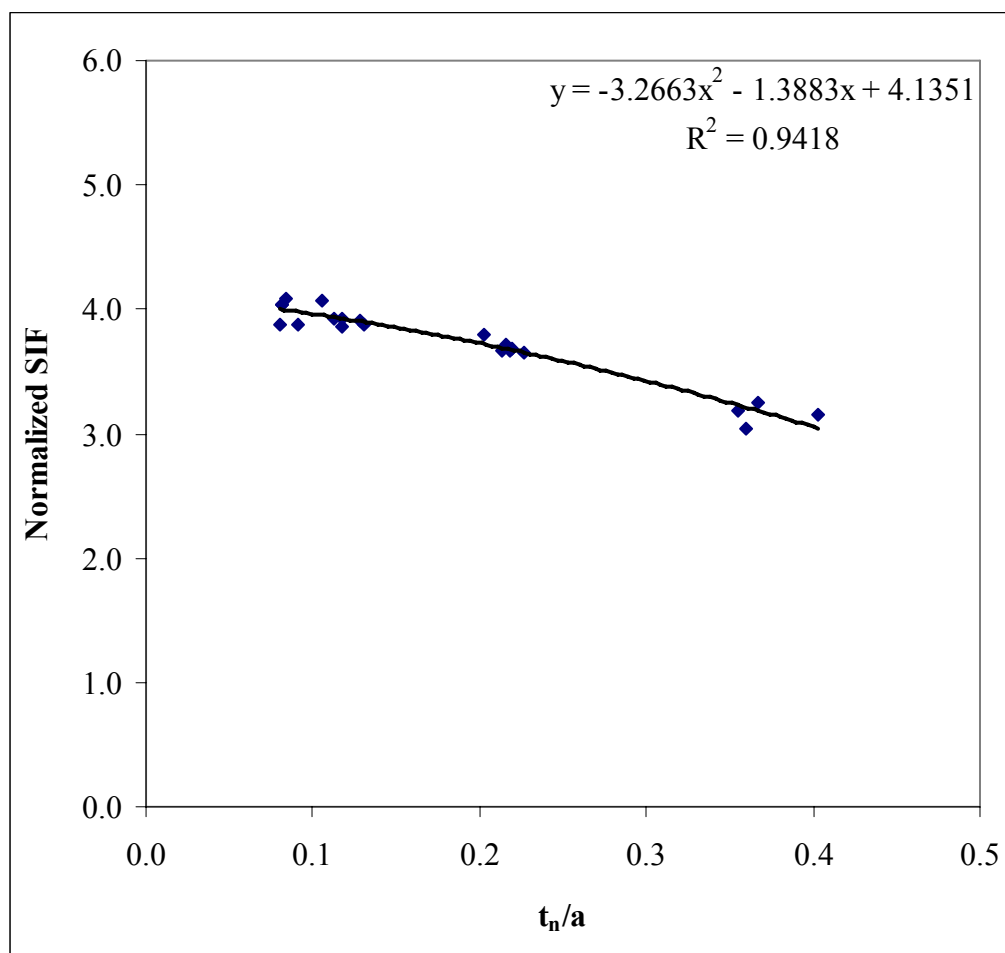


**Figure 6.2** Normalized SIF  $\left[ Y_I = \frac{K_I}{\sigma_0 \sqrt{\pi a}} \right]$  versus  $t_n/a$

Grouping the specimens in each of the four notch thickness categories and averaging them in their own group, the results are given in Figure 6.3 and 6.4. It is important to note that there was a significant drop in the stress intensity factors with increasing notch thickness. The SIF value which is above 4.0 for the notch thicknesses tending to zero goes down to about 3.1 corresponding to a decrease of about 20%. This means that a new SIF computation is needed for a particular set of experiments with a saw of particular diameter, instead of using a common general SIF relation as suggested by the other researchers.

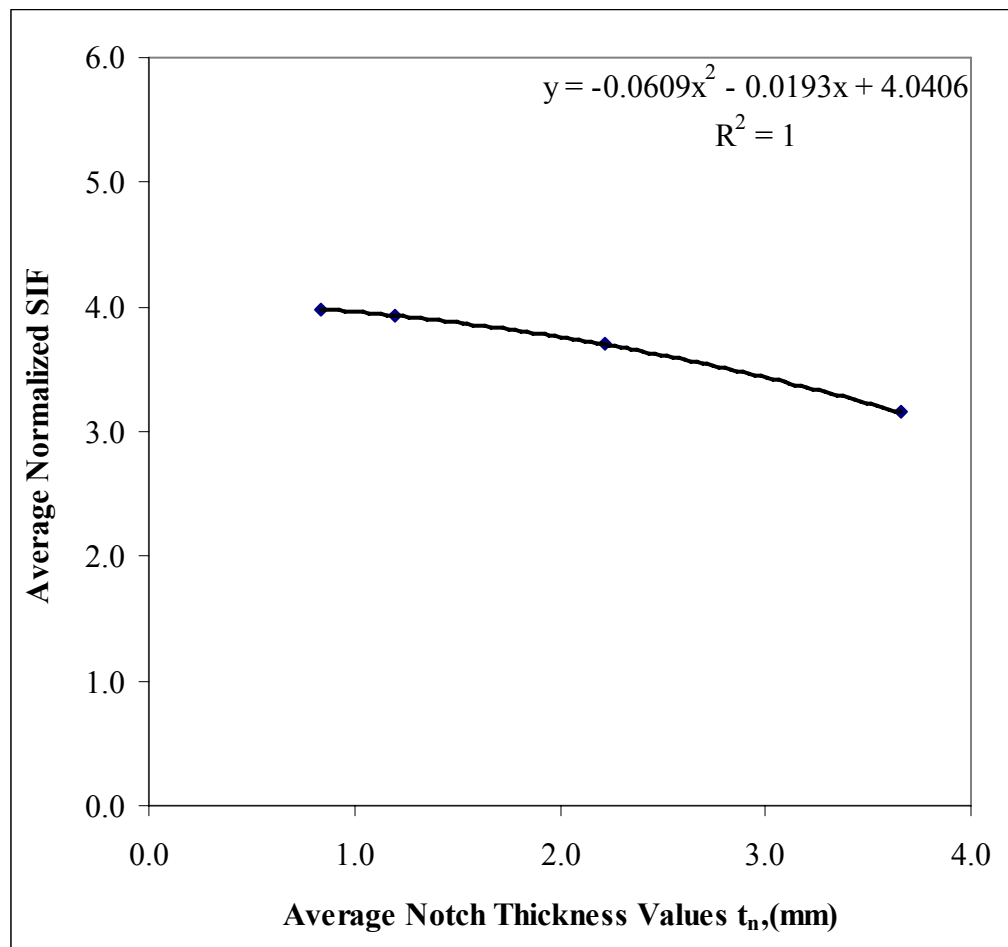


**Figure 6.3** Average normalized SIF  $\left[ Y_I = \frac{K_I}{\sigma_0 \sqrt{\pi a}} \right]$  versus average notch thickness

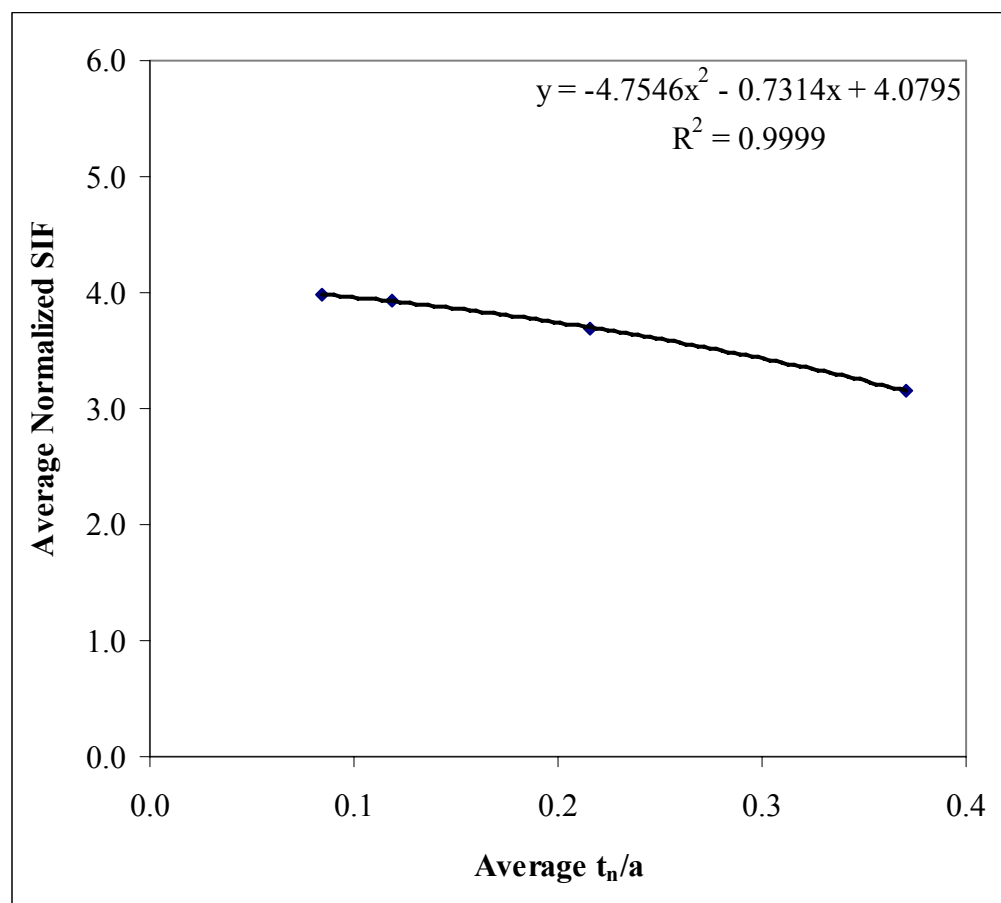


**Figure 6.4** Average normalized SIF  $\left[ Y_I = \frac{K_I}{\sigma_0 \sqrt{\pi a}} \right]$  versus average  $t_n/a$

If all the specimens are included in the evaluation of fracture toughness versus  $t_n/a$ , graph in Figure 6.5 shows a wide scatter although a decreasing trend is observed with increasing  $t_n/a$ .

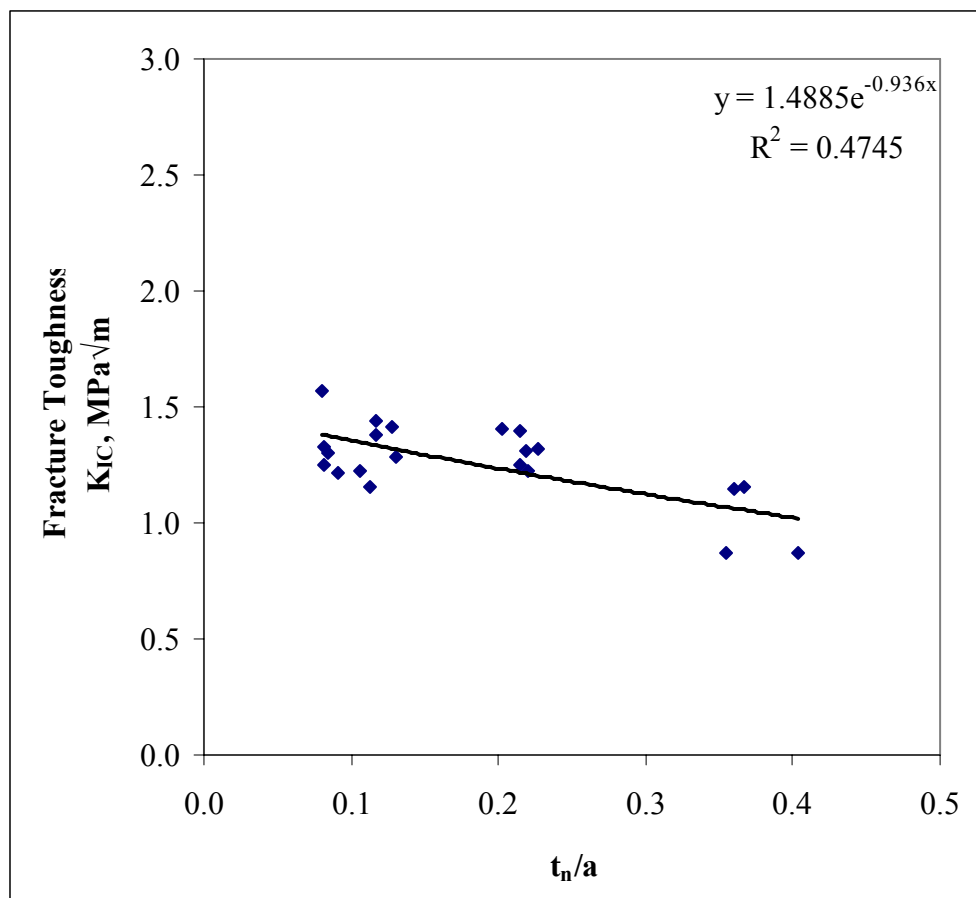


**Figure 6.5** Fracture toughness versus  $t_n/a$

However, if an average is obtained for a particular group such as  $t_n < 1$  mm, a better trend for  $K_{IC}$  variation can be observed as shown in Figures 6.6 and 6.7. If notch thickness experiments for different  $t_n$  groups are treated together, a linear fit shows that  $K_{IC}$  decreases with increasing notch thickness. Considering that quality of the fit is rather low with  $R^2=0.81$ , another way of handling problem is to treat first three  $t_n$  groups with  $t_n$  values around 1-2mm together. In this case a perfect match is obtained for fracture toughness of Ankara andesite and it is found as  $1.32 \text{ MPa}\sqrt{\text{m}}$ .  $3 \text{ mm} < t_n < 4 \text{ mm}$  value is however found as  $1.01 \text{ MPa}\sqrt{\text{m}}$  which is about 25% less than the value of first three. This means that fracture toughness decreases with too large notch thicknesses, that is more than about 2.5mm. Fracture toughness experiments with preliminary saw cut notches can safely be conducted with saws of diameters up to 2mm.

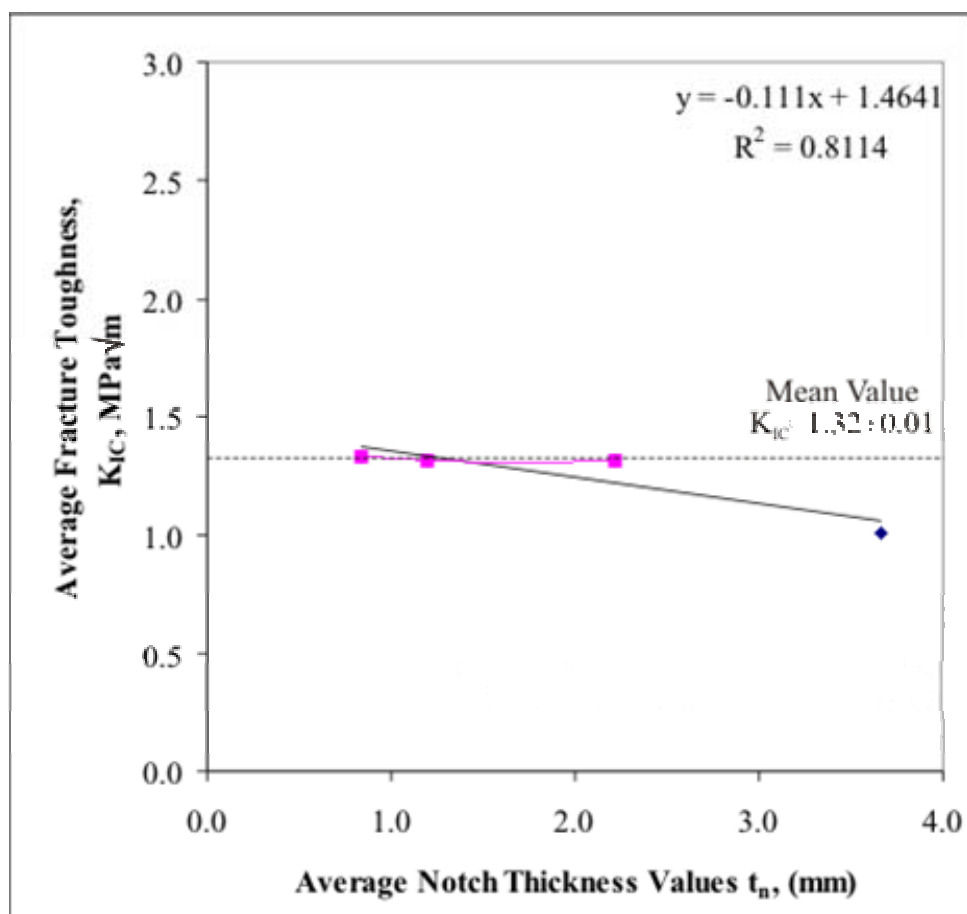


**Figure 6.6** Average fracture toughness versus average notch thickness

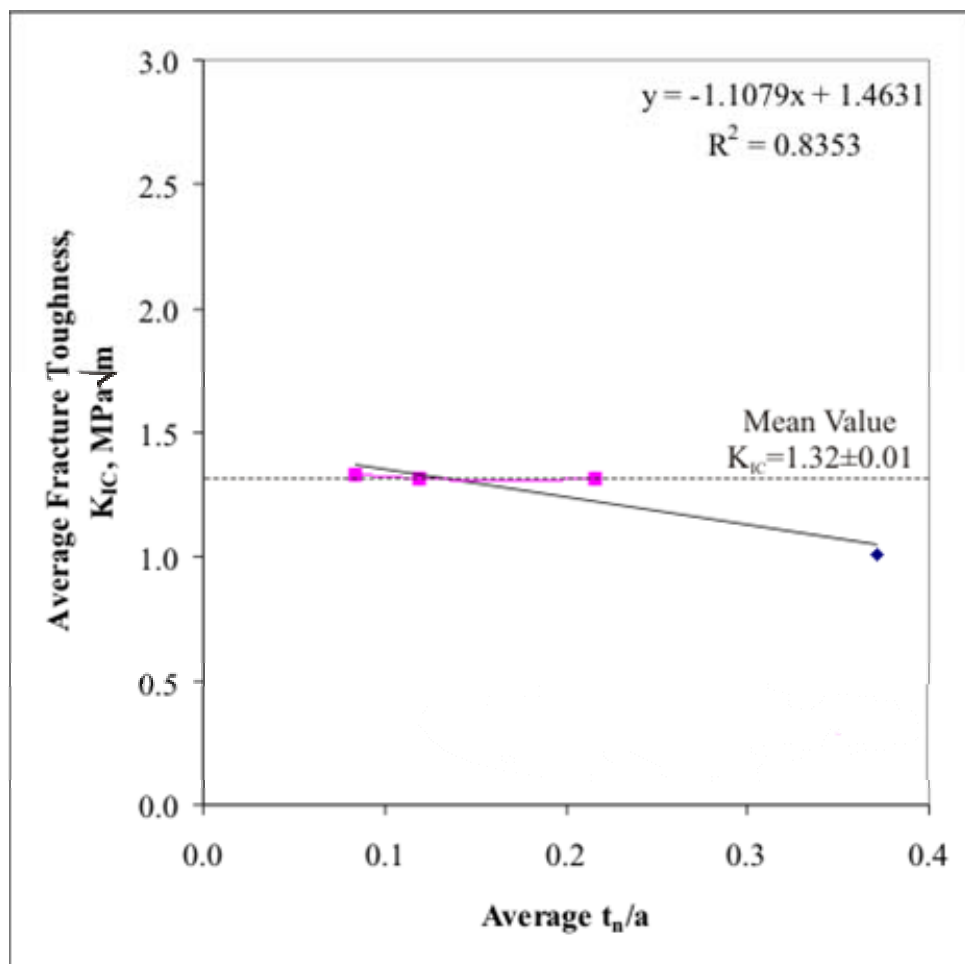


**Figure 6.7** Average fracture toughness versus average  $t_n/a$

In order to investigate the decreasing trend of fracture toughness with increasing notch thickness, stress distributions around the crack front were studied. Stress distributions right around the tip of the notch are given in Figure 6.8, 6.9 and 6.10.  $\sigma_{xx}$  is the major component and it is tensile as expected leading to the Mode I loading.  $\sigma_{xx}$  stress for large notch thickness has a lower tensile value. Similarly,  $\sigma_{zz}$  and  $\sigma_{yy}$  stresses take lower tensile values. This might be the explanation of obtaining a fracture toughness value of about 25% lower than narrow notch thickness case. Large notch thickness case reduces the complex tensile stresses around the notch tip and provides an easy path for crack find its way towards the maximum principal stress.

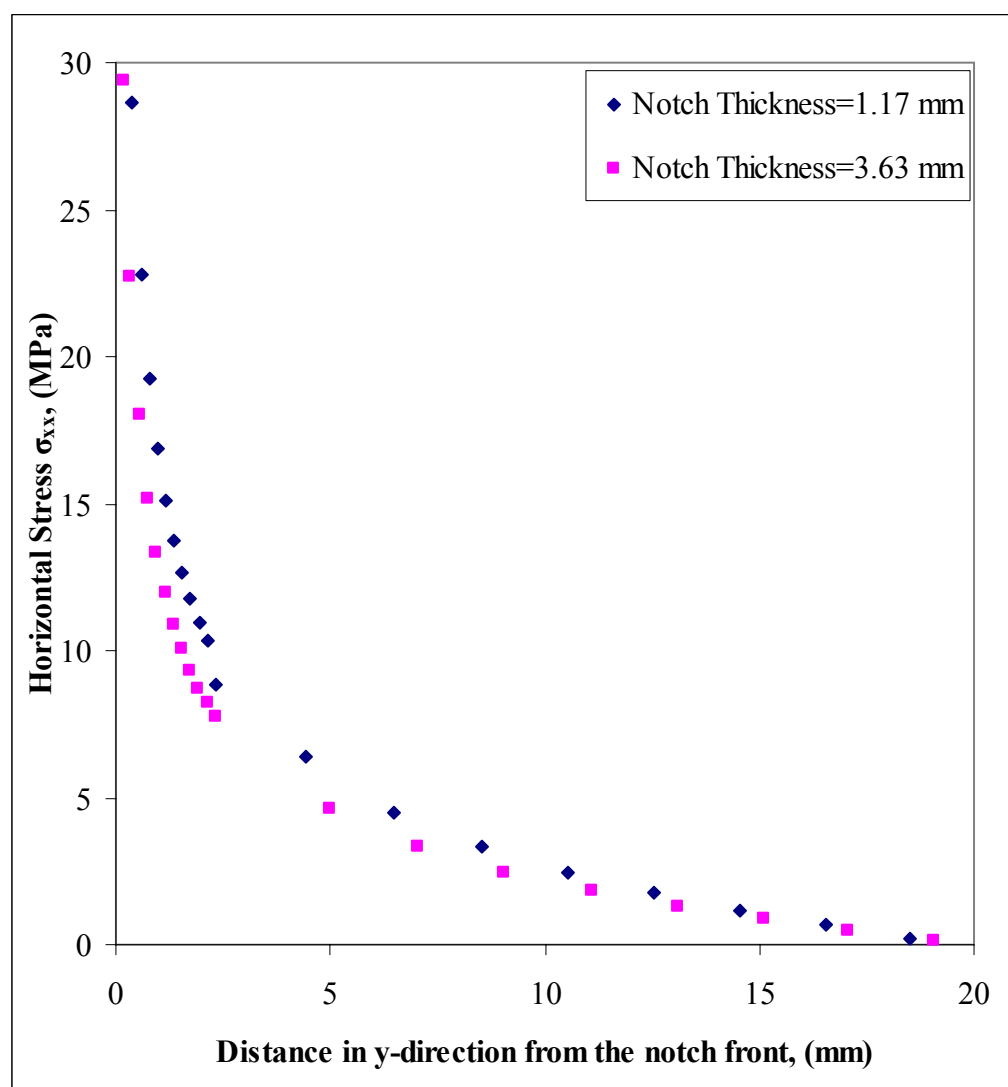


**Figure 6.8** Horizontal stress versus distance in y-direction from the notch front

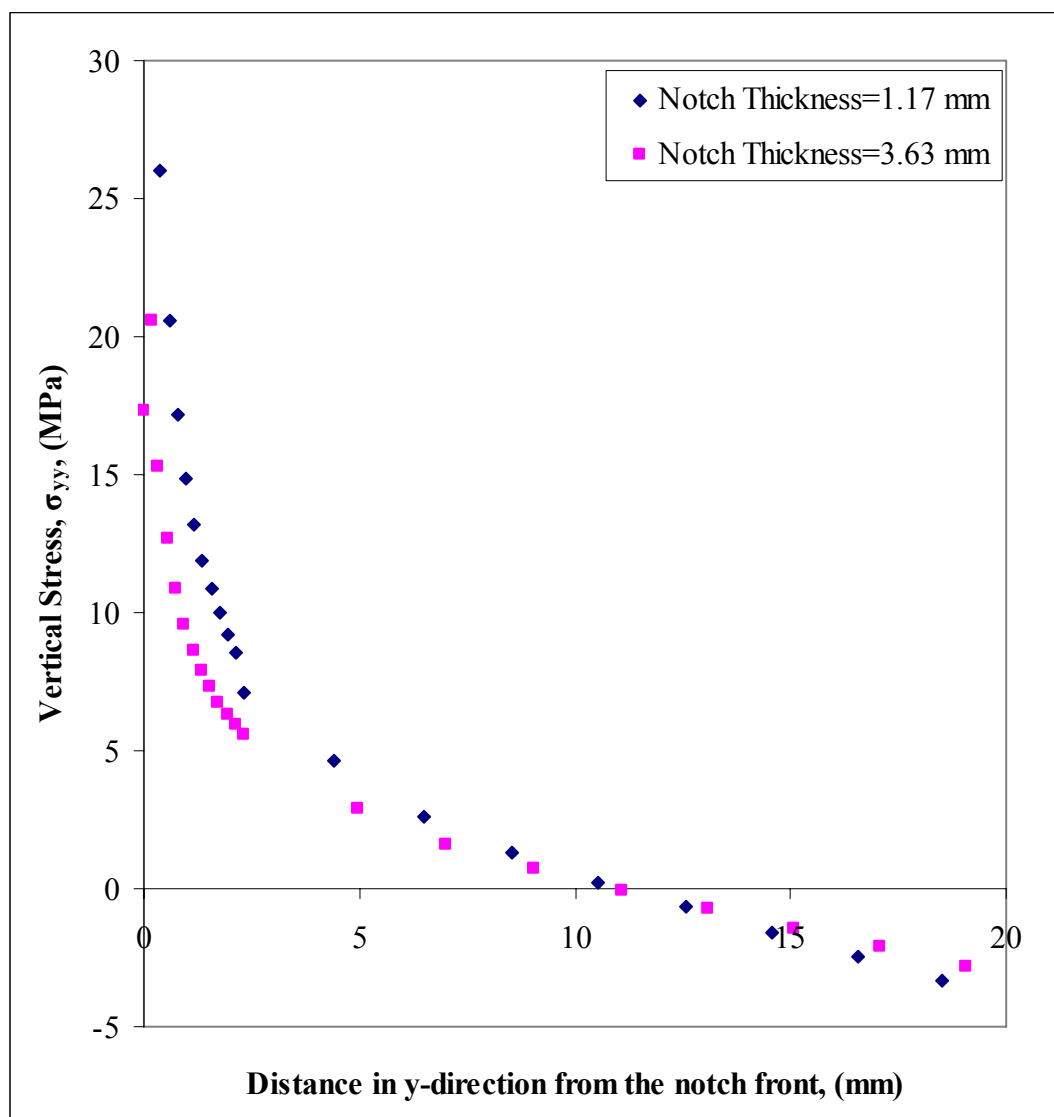


**Figure 6.9** Vertical stress versus distance in y-direction from the notch front

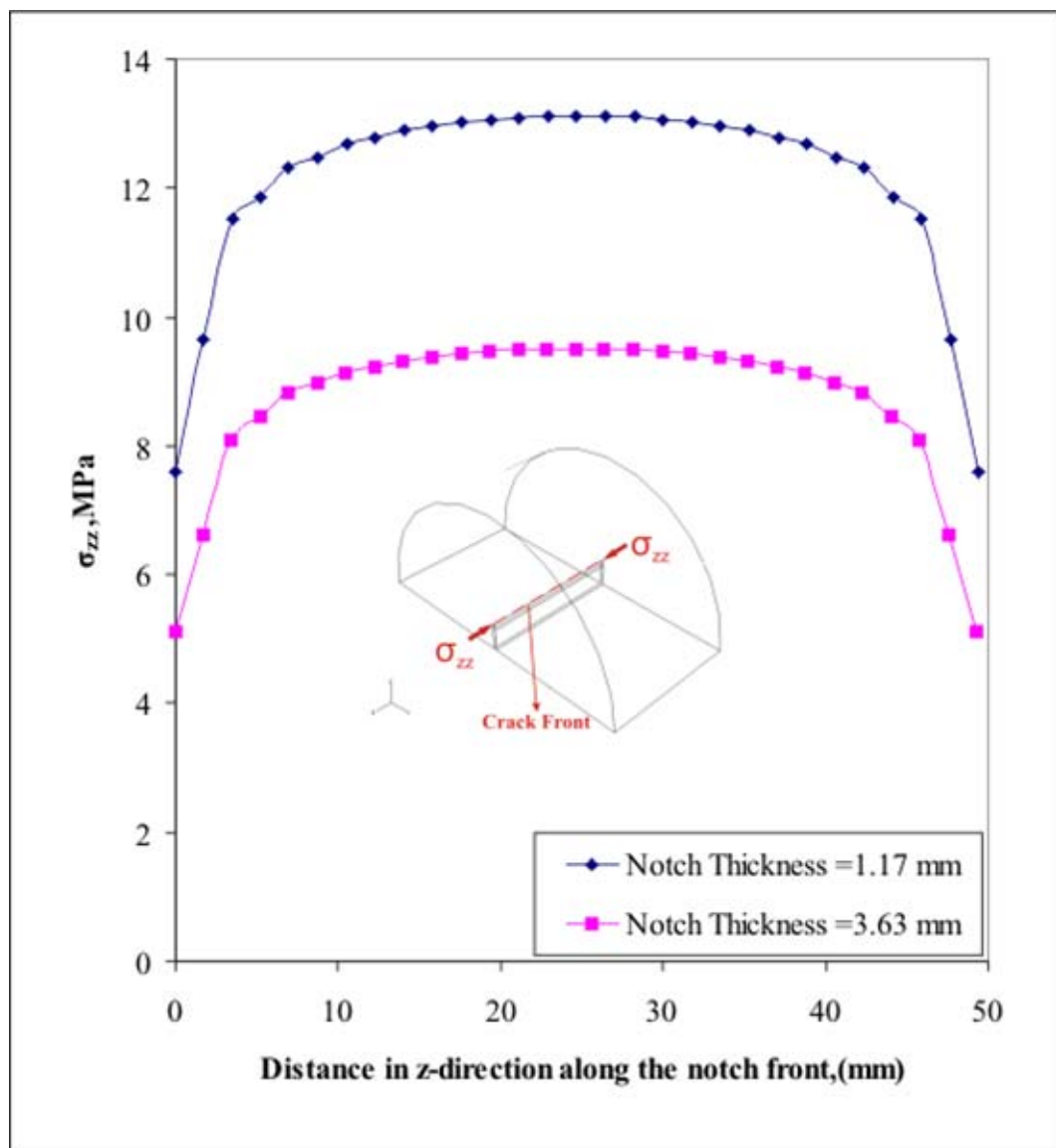


**Figure 6.10**  $\sigma_{zz}$  stresses of two different notch thickness values versus distance in z-direction along the notch front

### 6.3 Results for Changing Loading Span of the Beam

For SCB specimens under three point bending load at the bottom is applied by two rollers separated by a span S. In the changing span analysis, effect of S/R on the SIF and fracture toughness values were investigated. Seven different S/R ratios were employed in the experiments. All specimens were prepared with a/R=0.2 and nearly the same notch thickness. Results are presented in Table 6.5 through 6.11 for S/R=0.3, 0.4, 0.5, 0.6, 0.7, 0.8 and 0.9. The labels used in tables are:

$P_{max}$ : Failure load, (kN),

U: Vertical displacement, (mm),

CMOD: Crack mouth opening displacement, (mm),

$K_I$ : Stress intensity factor for Mode I calculated with ABAQUS, ( $Pa\sqrt{m}$ ),

$K_{II}$ : Stress intensity factor for Mode II calculated with ABAQUS, ( $Pa\sqrt{m}$ ),

$Y_I$ : Normalized stress intensity factor,

$K_{IC}$ : Fracture toughness, ( $MPa\sqrt{m}$ )

k: Stiffness (kN/mm)

**Table 6.5** Results of a/R=0.2, S/R=0.3 SCB specimens

Specimen Code	$P_{max}$ , kN	U mm	CMOD mm	$K_I$ $Pa\sqrt{m}$	$K_{II}$ $Pa\sqrt{m}$	$Y_I$	$K_{IC}$ $MPa\sqrt{m}$	k kN/mm
1	33.80	0.426	-	36.588	-0.000187	1.056	1.237	80.63
2	39.20	0.421	-	35.693	-0.000270	1.047	1.399	97.18
3	38.90	0.441	-	35.610	-0.000252	1.020	1.385	90.59
Average	37.30	0.429	-	35.964	-0.000236	1.041	1.340	89.47
$\pm$	$\pm$	$\pm$	$\pm$	$\pm$	$\pm$	$\pm$	$\pm$	$\pm$
STD	3.03	0.011	-	0.542	0.000043	0.019	0.090	8.33

**Table 6.6** Results of a/R=0.2, S/R=0.4 SCB specimens

Specimen Code	P <sub>max.</sub> kN	U mm	CMOD mm	K <sub>I</sub> Pa $\sqrt{m}$	K <sub>II</sub> Pa $\sqrt{m}$	Y <sub>I</sub>	K <sub>IC</sub> MPa $\sqrt{m}$	k kN/mm
1	26.10	0.433	0.054	64.951	0.000320	1.853	1.695	59.48
2	22.50	0.301	0.029	66.534	0.000259	1.870	1.497	73.64
3	29.90	0.304	0.040	64.011	0.000322	1.811	1.914	99.93
Average	26.17	0.346	0.041	65.165	0.000300	1.845	1.702	77.68
±	±	±	±	±	±	±	±	±
STD	3.70	0.075	0.013	1.275	0.000036	0.030	0.208	20.53

**Table 6.7** Results of a/R=0.2, S/R=0.5 SCB specimens

Specimen Code	P <sub>max.</sub> kN	U mm	CMOD mm	K <sub>I</sub> Pa $\sqrt{m}$	K <sub>II</sub> Pa $\sqrt{m}$	Y <sub>I</sub>	K <sub>IC</sub> MPa $\sqrt{m}$	k kN/mm
1	14.70	0.216	-	94.544	0.000197	2.622	1.390	65.19
2	15.50	0.232	0.037	95.541	0.000167	2.641	1.481	67.28
3	14.60	0.267	0.029	92.261	0.000534	2.613	1.347	54.02
Average	14.93	0.238	0.033	94.116	0.000299	2.625	1.406	62.16
±	±	±	±	±	±	±	±	±
STD	0.49	0.026	0.006	1.681	0.000204	0.014	0.068	7.13

**Table 6.8** Results of a/R=0.2, S/R=0.6 SCB specimens

Specimen Code	P <sub>max.</sub> kN	U mm	CMOD mm	K <sub>I</sub> Pa $\sqrt{m}$	K <sub>II</sub> Pa $\sqrt{m}$	Y <sub>I</sub>	K <sub>IC</sub> MPa $\sqrt{m}$	k kN/mm
1	14.00	0.344	-	121.882	0.002378	3.352	1.706	39.41
2	10.20	0.149	0.017	123.491	0.002408	3.354	1.260	69.45
3	9.00	0.268	0.027	119.521	0.001028	3.282	1.076	33.80
4*	9.92	0.235	-	119.391	0.002168	3.385	1.184	39.79
Average	11.07	0.253	0.022	121.631	0.001938	3.330	1.347	47.56
±	±	±	±	±	±	±	±	±
STD	2.61	0.098	0.008	1.997	0.000788	0.041	0.324	19.17

\*=Specimen has a joint inside (These specimens dimensions and results are not considered when calculating the averages and standart deviations)

**Table 6.9** Results of a/R=0.2, S/R=0.7 SCB specimens

Specimen Code	P <sub>max.</sub> kN	U mm	CMOD mm	K <sub>I</sub> Pa $\sqrt{m}$	K <sub>II</sub> Pa $\sqrt{m}$	Y <sub>I</sub>	K <sub>IC</sub> MPa $\sqrt{m}$	k kN/mm
1	9.06	0.199	0.029	143.450	0.001500	4.032	1.300	44.19
2	9.54	0.146	0.025	153.770	0.000231	4.051	1.467	61.89
3	10.20	0.280	-	138.113	0.000004	3.892	1.409	36.90
Average	9.60	0.209	0.027	145.111	0.000578	3.992	1.392	47.66
±	±	±	±	±	±	±	±	±
STD	0.57	0.067	0.002	7.960	0.000806	0.087	0.085	12.85

**Table 6.10** Results of a/R=0.2, S/R=0.8 SCB specimens

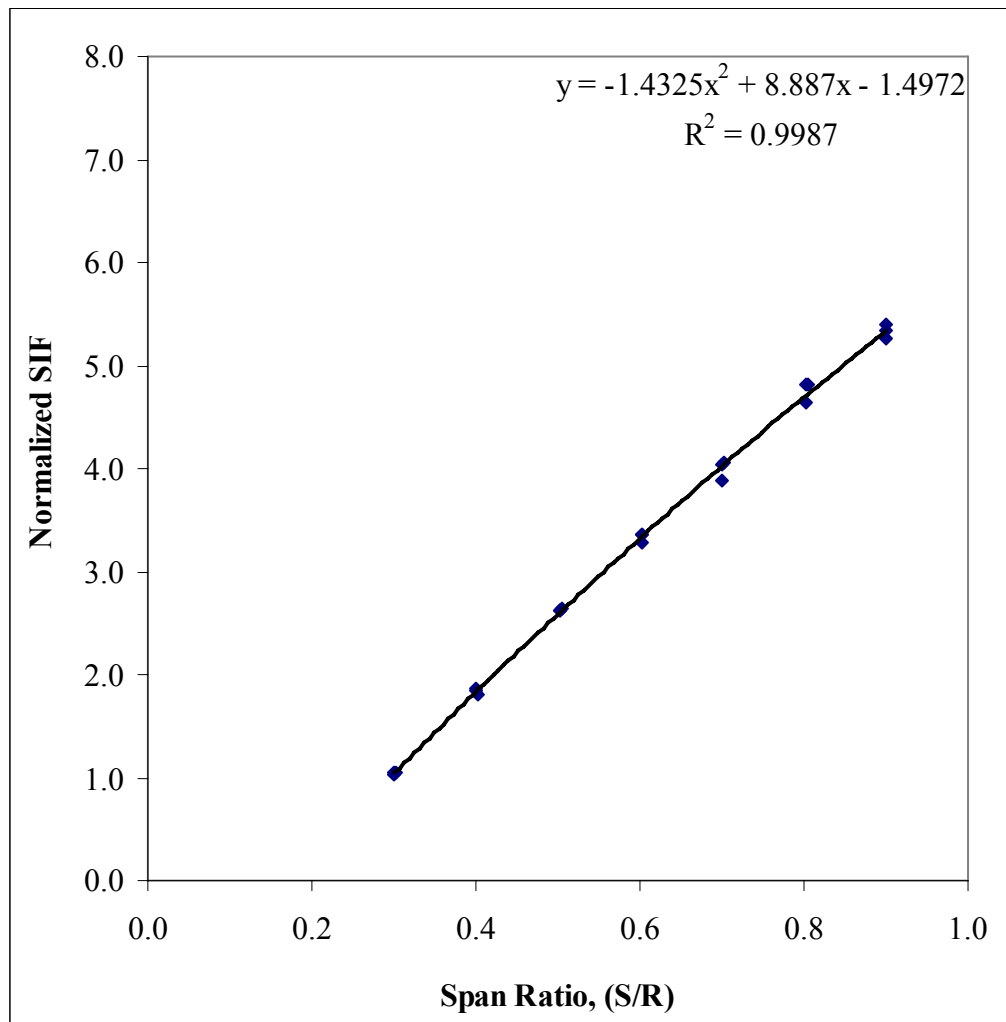
Specimen Code	P <sub>max.</sub> kN	U mm	CMOD mm	K <sub>I</sub> Pa $\sqrt{m}$	K <sub>II</sub> Pa $\sqrt{m}$	Y <sub>I</sub>	K <sub>IC</sub> MPa $\sqrt{m}$	k kN/mm
1	7.90	0.213	0.013	162.688	-0.000398	4.632	1.285	36.16
2	7.17	0.128	0.024	177.608	-0.000822	4.811	1.273	56.59
3	7.37	0.216	0.033	179.389	-0.000378	4.808	1.322	34.39
Average	7.48	0.186	0.023	173.228	-0.000533	4.750	1.294	42.38
±	±	±	±	±	±	±	±	±
STD	0.38	0.050	0.010	9.172	0.000251	0.103	0.025	12.34

**Table 6.11** Results of a/R=0.2, S/R=0.9 SCB specimens

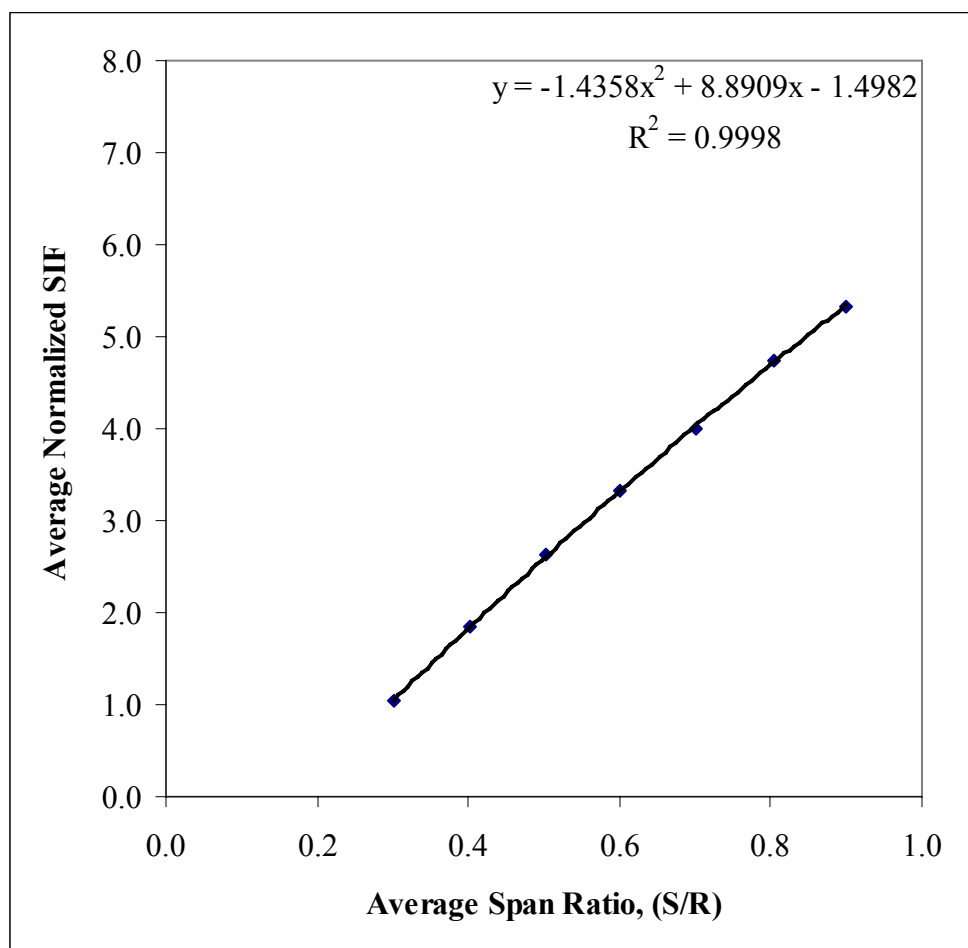
Specimen Code	P <sub>max.</sub> kN	U mm	CMOD mm	K <sub>I</sub> Pa $\sqrt{m}$	K <sub>II</sub> Pa $\sqrt{m}$	Y <sub>I</sub>	K <sub>IC</sub> MPa $\sqrt{m}$	k kN/mm
1	7.16	0.170	0.020	192.083	-0.001009	5.395	1.375	40.90
2	6.64	0.213	-	185.429	-0.000268	5.343	1.231	29.39
3	7.80	0.156	0.012	191.590	-0.000166	5.269	1.494	49.63
Average	7.20	0.180	0.016	189.701	-0.000481	5.336	1.367	39.97
±	±	±	±	±	±	±	±	±
STD	0.58	0.030	0.006	3.708	0.000460	0.063	0.132	10.15

By using above tables, Figure 6.11 shows the normalized SIF values versus span ratios (S/R) for all specimens in different S/R groups. In Figure 6.12, specimens are grouped and categorized in their particular S/R ratio group, averages are taken for each group, and then the results are plotted based on the average values of each group. Figure 6.12 shows the average normalized SIF values versus average span

ratios. It is seen from the figures that, normalized SIF values increase with increasing span length.

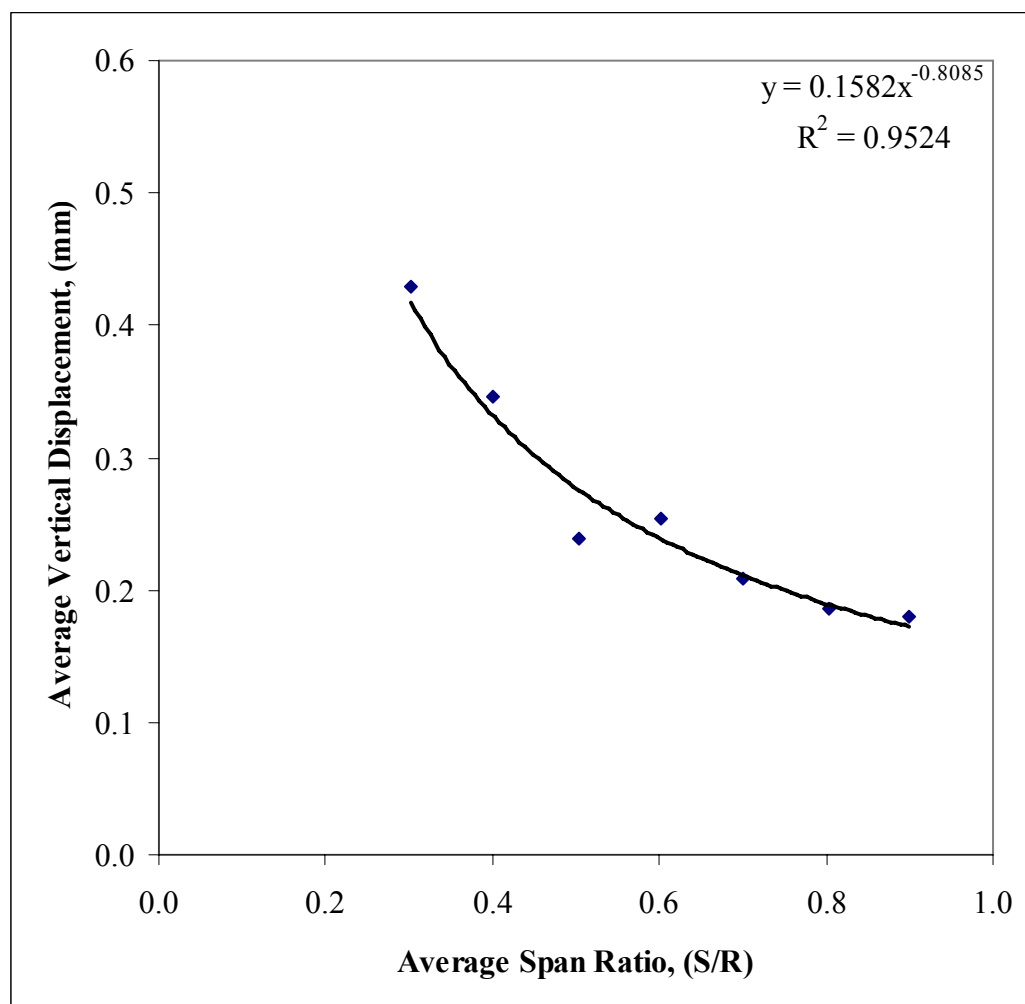


**Figure 6.11** Normalized SIF  $\left[ Y_I = \frac{K_I}{\sigma_0 \sqrt{\pi a}} \right]$  versus span ratio (S/R)



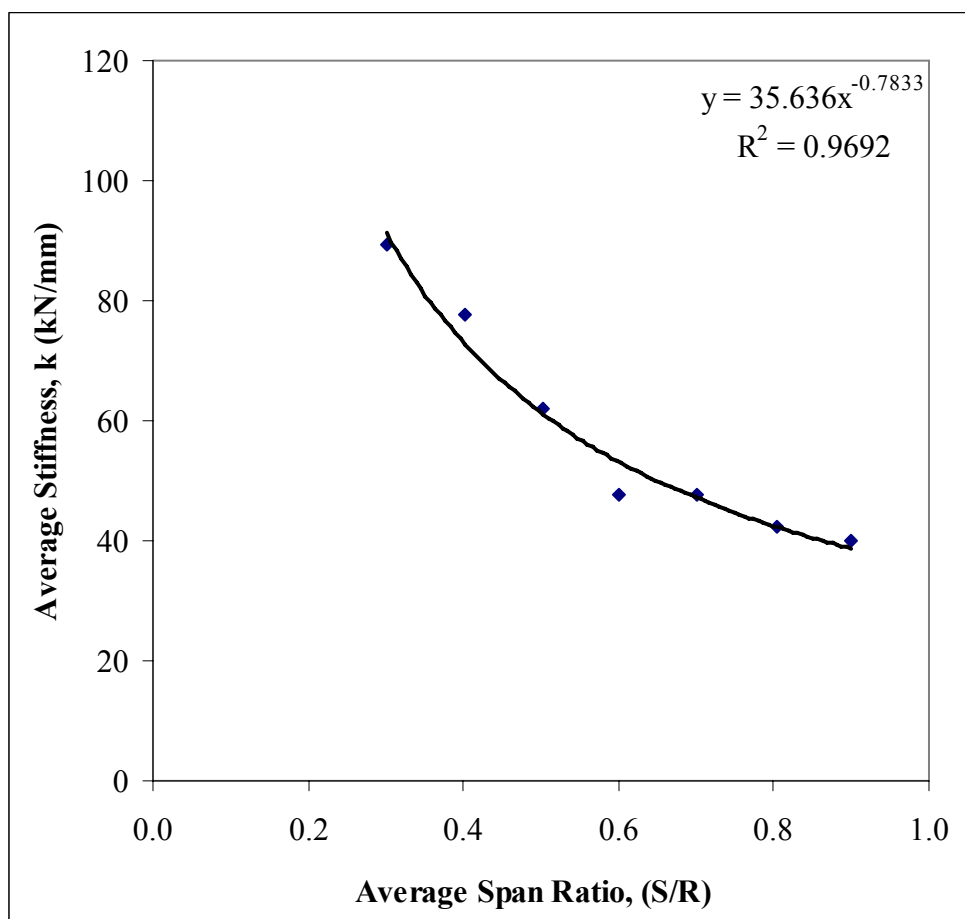
**Figure 6.12** Average normalized SIF  $\left[ Y_I = \frac{K_I}{\sigma_0 \sqrt{\pi a}} \right]$  versus average span ratio (S/R)

In Figure 6.13, it is seen that vertical displacement decreases with increasing span ratio (S/R).



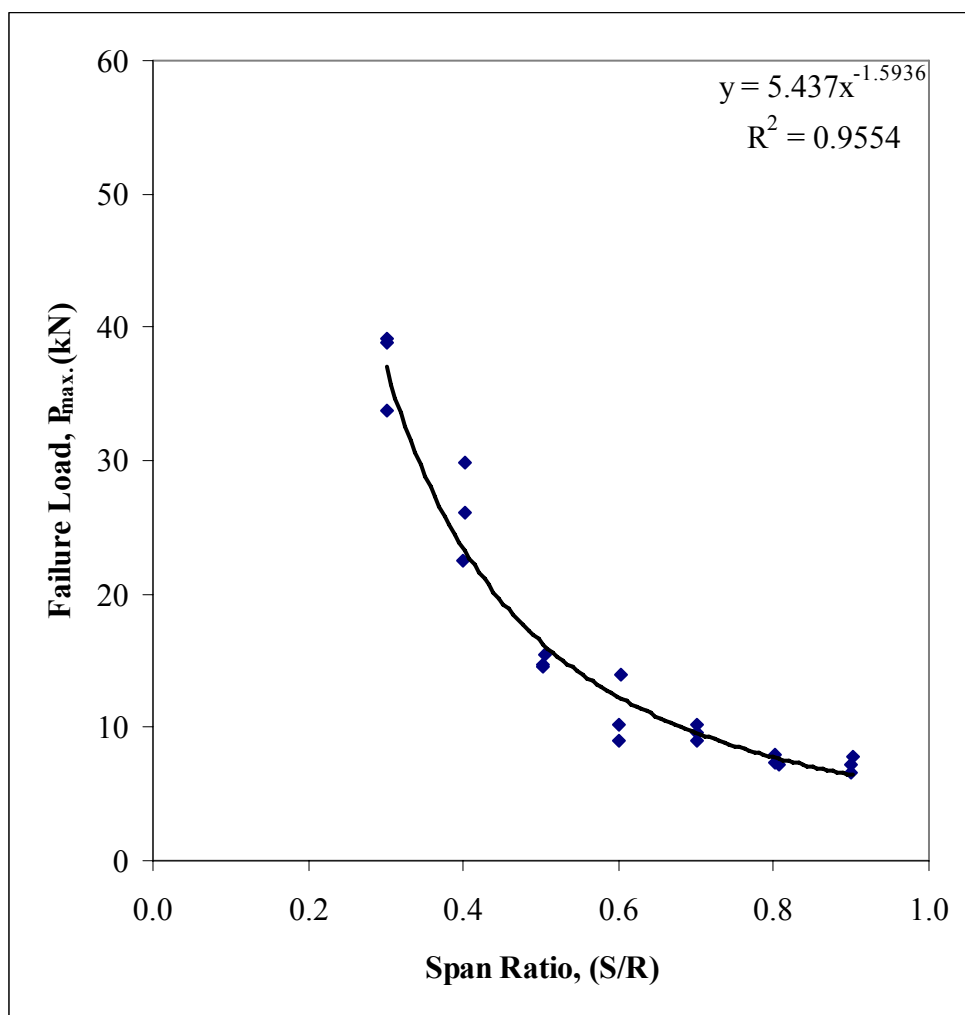
**Figure 6.13** Average vertical displacement versus average span ratio (S/R)

Figure 6.14 shows the decrease in stiffness of the specimens with increasing S/R.



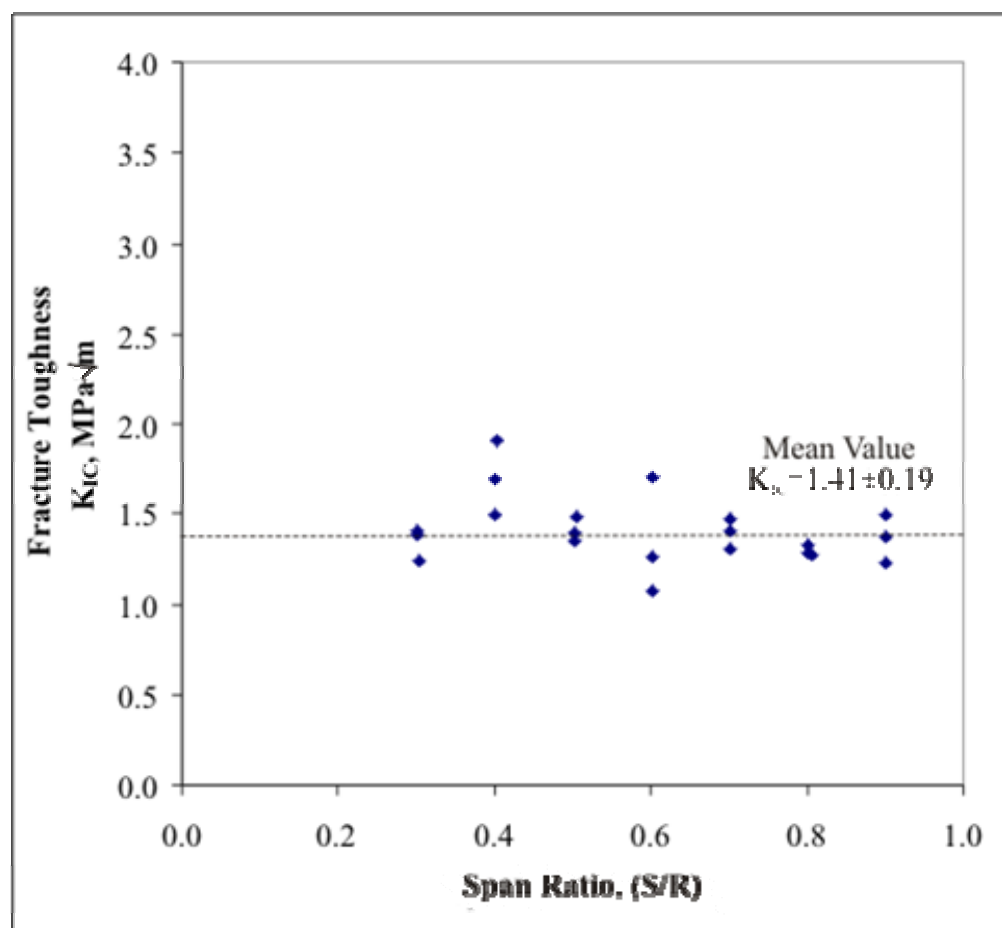
**Figure 6.14** Average stiffness versus average span ratio (S/R)

Figure 6.15 shows the load values obtained in all experiments for the S/R investigation.



**Figure 6.15** Failure load versus span ratio (S/R)

In Figure 6.16 it is seen that fracture toughness of andesite does not show any clear change with increasing S/R ratios. Therefore we can say that change in span ratio does not effect the fracture toughness of the andesite. Fracture toughness value of the Ankara andesite is found as  $1.41 \pm 0.19$  MPa $\sqrt{m}$  considering all experiments, here in this S/R investigations.



**Figure 6.16** Fracture toughness versus span ratio (S/R)

On the other hand grouping and finding average of each group and then as in Figure 6.17 plotting and checking the average, fracture toughness is equal to the  $1.41 \pm 0.19$  as seen in Figure 6.16.

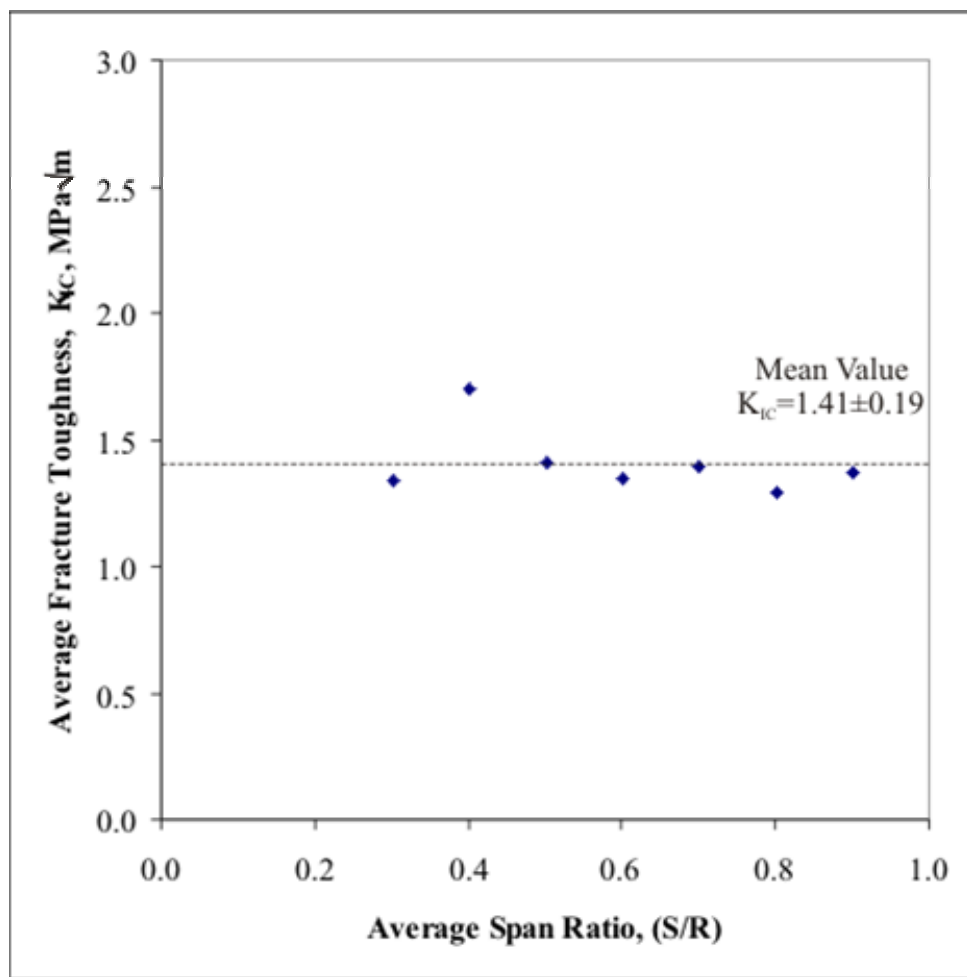


**Figure 6.17** Average fracture toughness versus average span ratio (S/R)

#### **6.4 Flattened Loading Surface Results**

In flattened loading surface analysis, effect of flattened face on the normalized SIF and fracture toughness values were investigated. Four different flat end (f) dimensions were tried in the experiments. All of the specimens were prepared with  $a/R=0.2$ ,  $S/R=0.7$  and nearly the same notch thickness of around 1 mm. Three dimensional ABAQUS analyses results, experimental results and graphical analysis of these results are shown below in Tables 6.12, 6.13, 6.14 and 6.15 for  $f \leq 15$  mm, 20 mm, 22.5 mm, 25 mm, respectively. The labels used in tables are:

$P_{max}$ : Failure load, (kN),

$U$ : Vertical displacement, (mm),

CMOD: Crack mouth opening displacement, (mm),

$K_I$ : Stress intensity factor calculated with ABAQUS, ( $Pa\sqrt{m}$ ),

$K_{II}$ : Stress intensity factor calculated with ABAQUS, ( $Pa\sqrt{m}$ ),

$Y_I$ : Normalized stress intensity factor,

$K_{IC}$ : Fracture toughness, ( $MPa\sqrt{m}$ )

$k$ : Stiffness(kN/mm)

**Table 6.12** Results of f $\cong$  15mm SCB specimens

Specimen Code	P <sub>max.</sub> kN	U mm	CMOD mm	K <sub>I</sub> $Pa\sqrt{m}$	K <sub>II</sub> $Pa\sqrt{m}$	Y <sub>I</sub>	K <sub>IC</sub> $MPa\sqrt{m}$	k kN/mm
1	7.81	0.242	0.042	138.634	0.021330	3.988	1.083	31.72
2	7.39	0.198	0.022	138.030	-0.012020	3.987	1.020	36.39
3	7.48	0.244	0.023	140.544	-0.012840	3.929	1.051	27.11
4	8.05	0.236	0.033	138.079	-0.011550	3.913	1.112	28.17
5	8.20	0.213	0.035	141.722	-0.012708	4.014	1.162	39.02
Average	7.79	0.227	0.031	139.402	-0.005558	3.966	1.086	32.48
$\pm$	$\pm$	$\pm$	$\pm$	$\pm$	$\pm$	$\pm$	$\pm$	$\pm$
STD	0.35	0.02	0.009	1.651	0.015040	0.043	0.055	5.15

**Table 6.13** Results of f $\cong$  20mm SCB specimens

Specimen Code	P <sub>max.</sub> kN	U mm	CMOD mm	K <sub>I</sub> $Pa\sqrt{m}$	K <sub>II</sub> $Pa\sqrt{m}$	Y <sub>I</sub>	K <sub>IC</sub> $MPa\sqrt{m}$	k kN/mm
1	8.58	0.188	0.047	141.517	-0.011280	4.069	1.214	42.29
2	8.29	0.183	0.023	146.473	-0.011910	3.992	1.214	46.40
3	8.86	0.165	0.026	138.063	-0.011320	4.019	1.223	46.49
4	8.23	0.228	0.012	136.575	-0.000090	3.940	1.124	35.27
Average	8.49	0.191	0.027	140.657	-0.008650	4.005	1.194	42.61
$\pm$	$\pm$	$\pm$	$\pm$	$\pm$	$\pm$	$\pm$	$\pm$	$\pm$
STD	0.29	0.027	0.015	4.395	0.005714	0.054	0.047	5.27

**Table 6.14** Results of  $f \geq 22.5\text{mm}$  SCB specimens

Specimen Code	$P_{\max.}$ kN	U mm	CMOD mm	$K_I$ $\text{Pa}\sqrt{\text{m}}$	$K_{II}$ $\text{Pa}\sqrt{\text{m}}$	$Y_I$	$K_{IC}$ $\text{MPa}\sqrt{\text{m}}$	k kN/mm
1	9.24	0.297	0.029	127.278	-0.010610	3.849	1.176	29.33
2	8.52	0.187	0.014	136.524	-0.011032	3.935	1.163	42.65
3*	6.43	0.215	0.019	142.403	-0.011470	3.989	0.916	29.20
Average	8.88	0.242	0.021	131.901	-0.010821	3.892	1.170	35.99
$\pm$	$\pm$	$\pm$	$\pm$	$\pm$	$\pm$	$\pm$	$\pm$	$\pm$
STD	0.51	0.077	0.010	6.538	0.000298	0.061	0.009	9.42

\*=Specimen has a joint inside (These specimens dimensions and results are not considered when calculating the averages and standart deviations)

**Table 6.15** Results of  $f \geq 25\text{mm}$  SCB specimens

Specimen Code	$P_{\max.}$ kN	U mm	CMOD mm	$K_I$ $\text{Pa}\sqrt{\text{m}}$	$K_{II}$ $\text{Pa}\sqrt{\text{m}}$	$Y_I$	$K_{IC}$ $\text{MPa}\sqrt{\text{m}}$	k kN/mm
1	8.93	0.292	0.036	137.553	-0.011150	3.892	1.228	25.71
2	7.74	0.134	0.032	140.774	0.012900	4.000	1.090	54.23
3	6.44	0.162	0.028	142.010	0.000289	3.983	0.914	42.90
4*	6.59	0.188	-	141.966	-0.000267	3.906	0.935	37.29
Average	7.70	0.196	0.032	140.112	0.000680	3.958	1.077	40.95
$\pm$	$\pm$	$\pm$	$\pm$	$\pm$	$\pm$	$\pm$	$\pm$	$\pm$
STD	1.25	0.084	0.004	2.301	0.012030	0.058	0.157	14.36

\*=Specimen has a joint inside (These specimens dimensions and results are not considered when calculating the averages and standart deviations)

In the modeling work, upper surface load P value was taken as 1N as before, however this time the load P was divided by the area of flat end, and a pressure type boundary condition was applied to the upper surface of the SCB specimen models.

In Figure 6.18, stress intensity factors for all specimens are given and stress intensity factor for the case with no flat loading end is also included as the case with  $f=0$ , that is, zero flat end case.

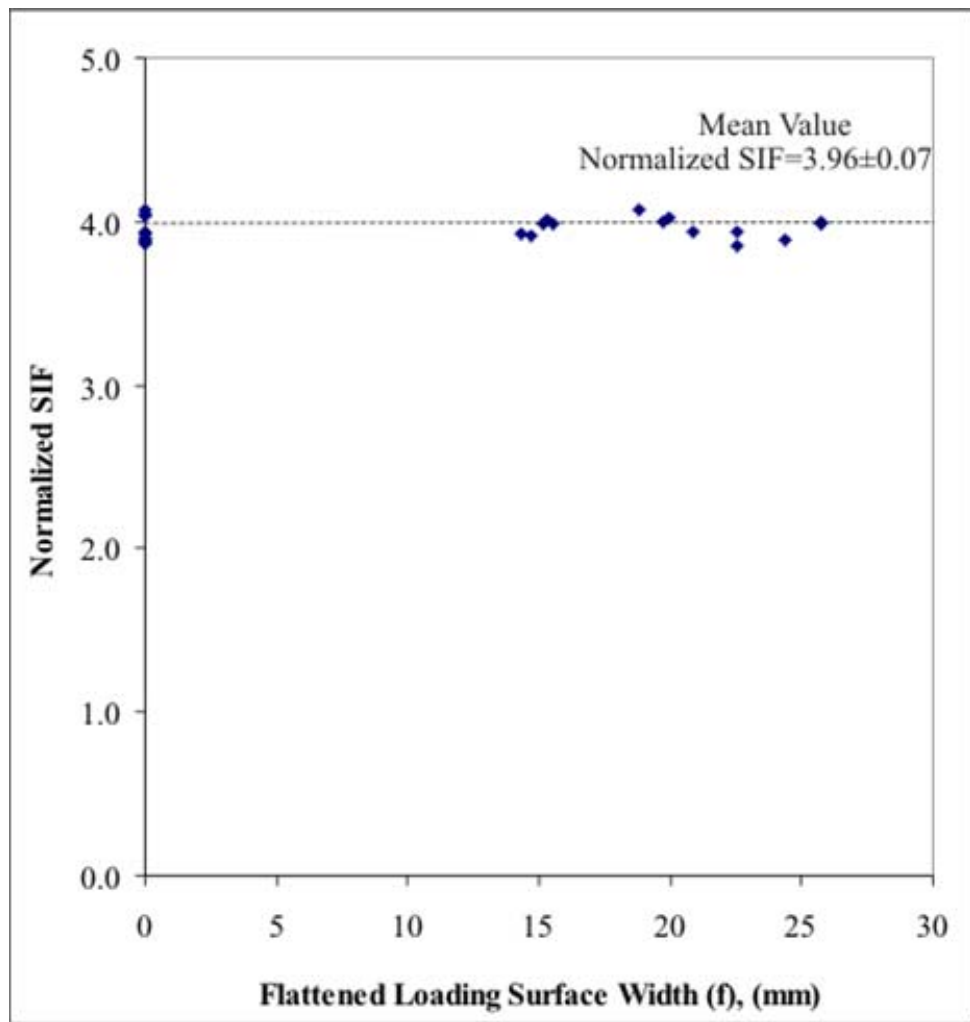


**Figure 6.18** Normalized SIF  $\left[ Y_I = \frac{K_I}{\sigma_0 \sqrt{\pi a}} \right]$  versus flattened loading surface width

In Figure 6.19, results are shown for grouping, averaging individually for each group, and then plotting the fit to the averages.

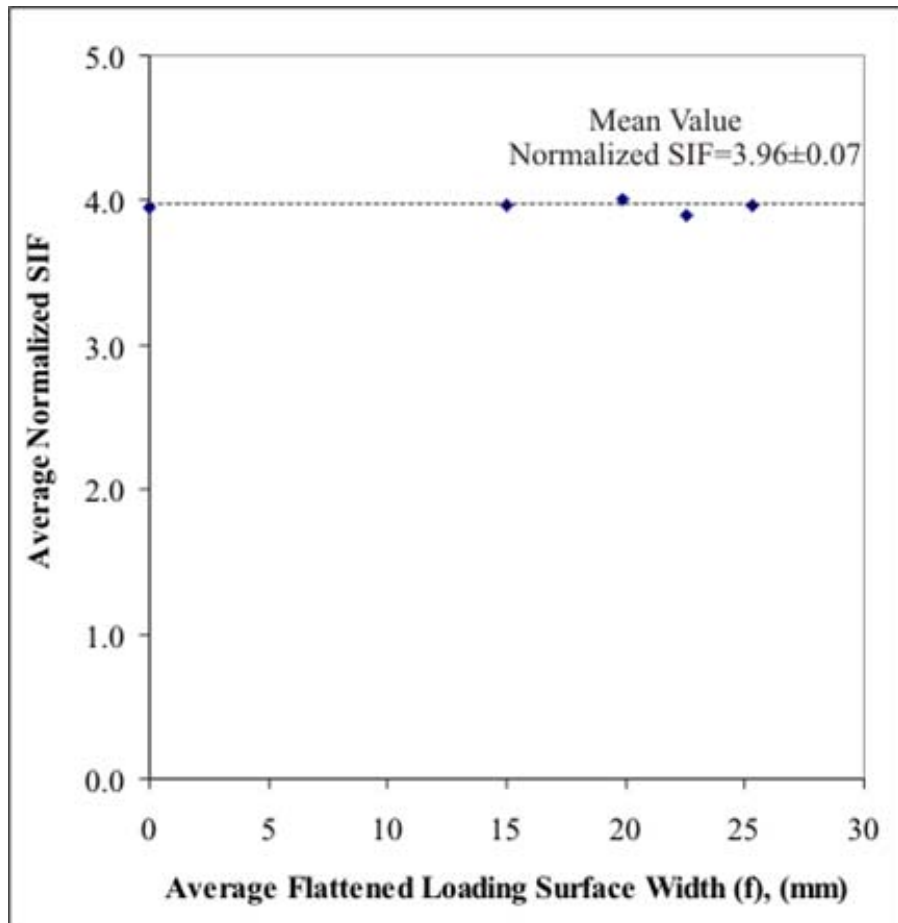


**Figure 6.19** Average normalized SIF  $\left[ Y_I = \frac{K_I}{\sigma_0 \sqrt{\pi a}} \right]$  versus average flattened loading surface width

It is seen from Figure 6.18 and Figure 6.19 that flattening of the specimen's loading surfaces have no effect on the normalized stress intensity factor.

In Figure 6.20 nine fracture toughness values for non-flattened specimens are also included. Six of these non-flattened specimens were taken from the  $1 \text{ mm} < t_n < 2 \text{ mm}$  notch thickness experiments. The remaining three were taken from the  $S/R=0.7$  span ratio analysis. All of the nine specimens have approximately equal  $a/R=0.2$  and  $S/R=0.7$  values.

It is seen from the Figure 6.20 and 6.21 average fracture toughness values of the flattened surface specimens do not change with increasing width of the flat loading end. However, as seen especially in Figure 6.21, a decrease in fracture toughness is possible, although the quality of correlation is low. In fact, if flat ended results are grouped and averaged in their own the fracture toughness value is  $1.13 \pm 0.06$ , which is about 20% lower than the result found with regular SCB specimens having no flat ends.

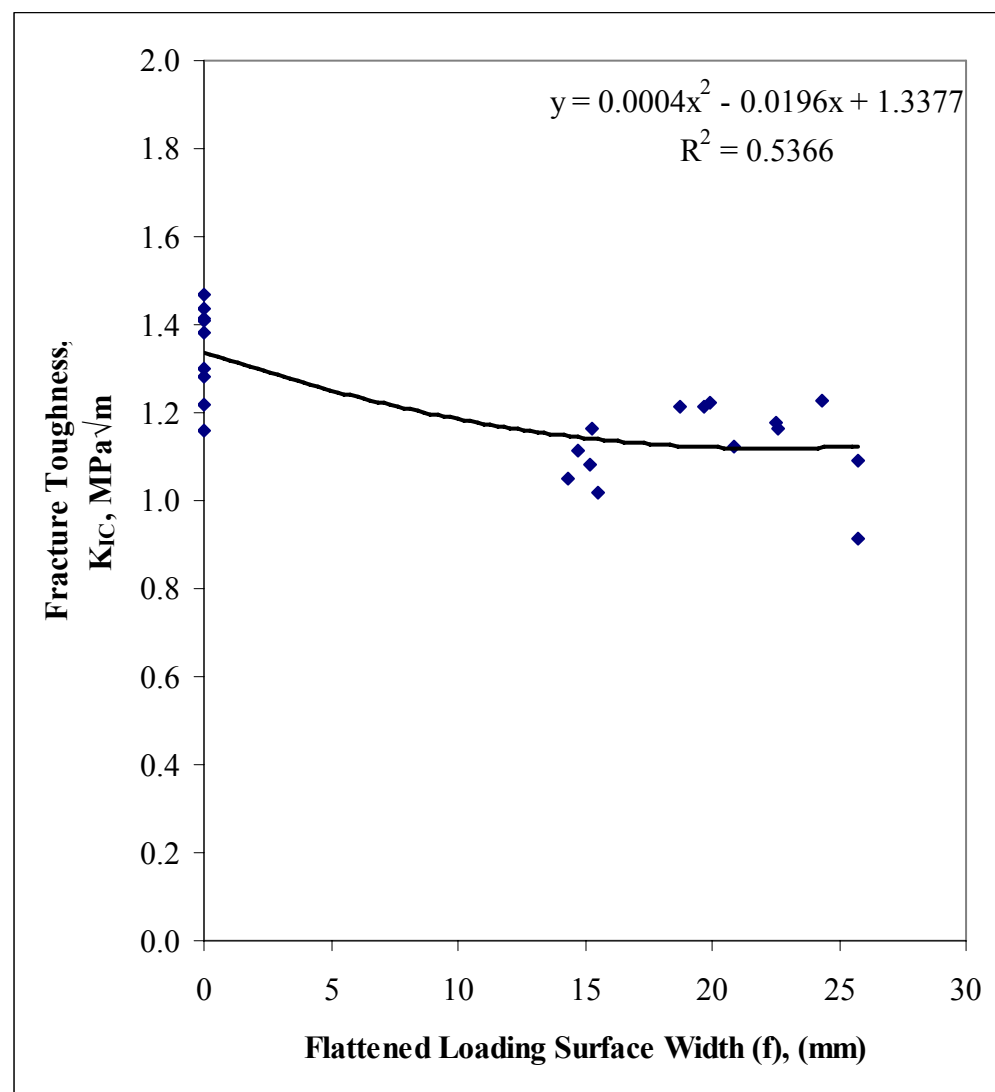


**Figure 6.20** Fracture toughness versus flattened loading surface width

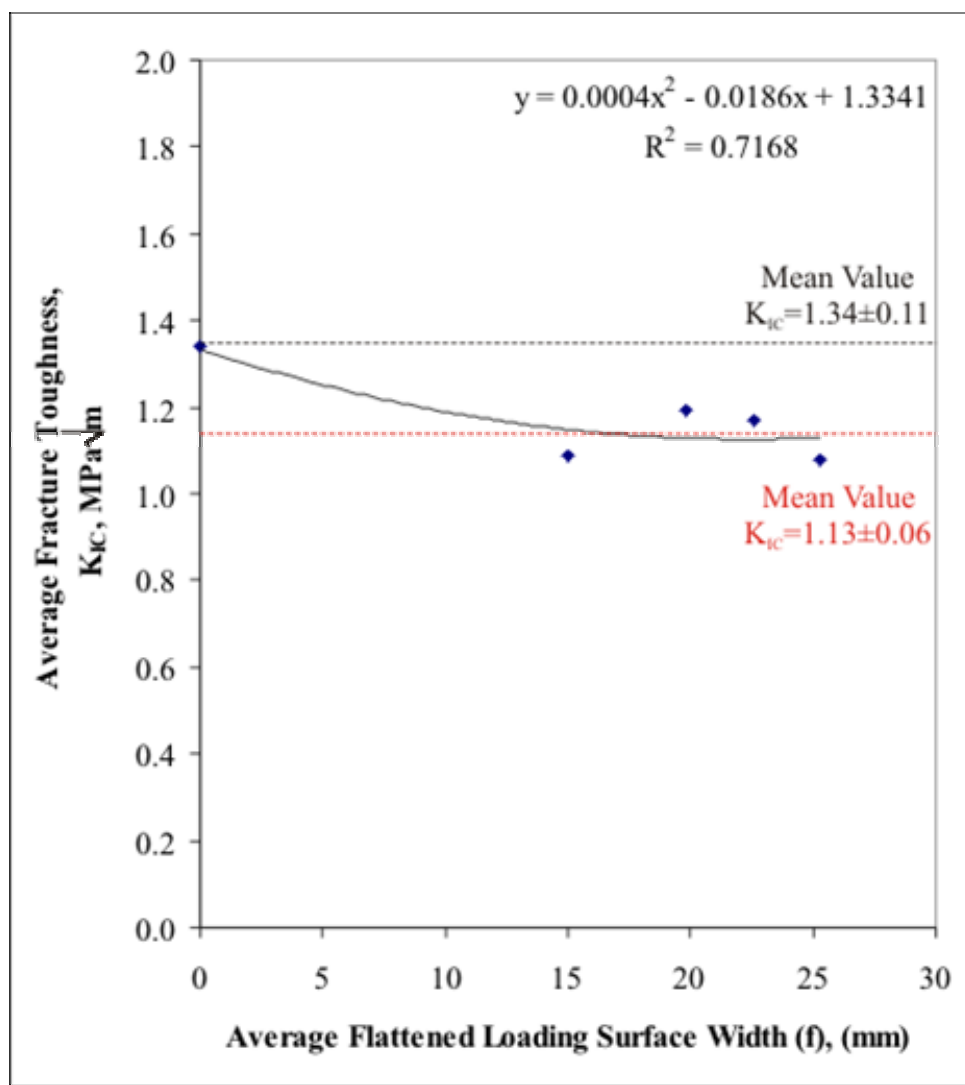


**Figure 6.21** Average fracture toughness versus average flattened loading surface width

In Figure 6.22 and 6.23 notch tip stresses  $\sigma_{xx}$  and  $\sigma_{yy}$  are plotted against the distance  $y$  parallel to the notch plane. As seen from the figures tensile crack tip stresses around the notch tip turn to compression as the upper loading surface is approached. For specimens with no flat ends ( $f=0$ ), higher tensile stresses are observed around the notch front.  $\sigma_{xx}$  stress is 0-30% higher in tension compared to the stresses for flattened specimens. Similarly,  $\sigma_{yy}$  stress shows a 10-15% higher tensions around the notch front.

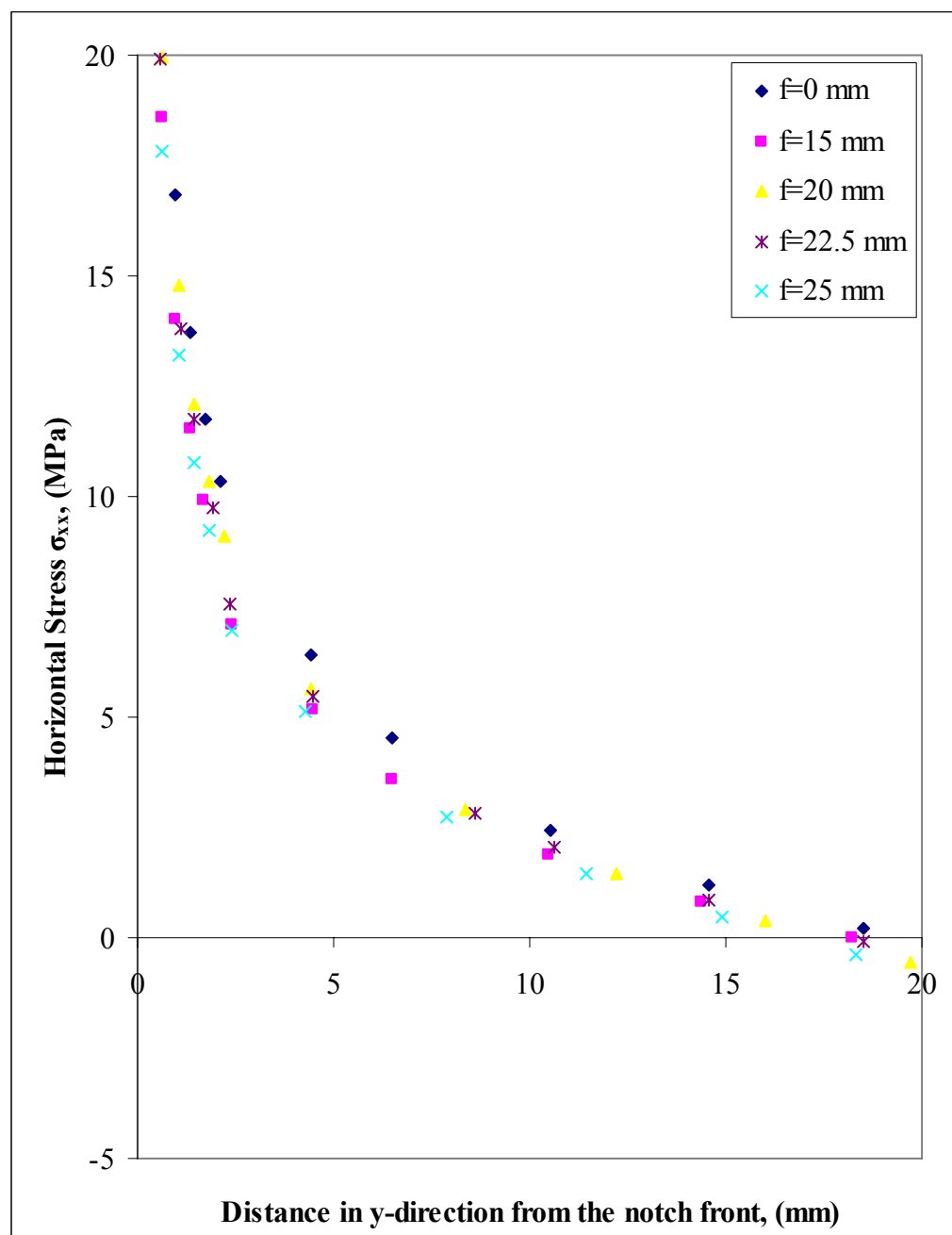


**Figure 6.22** Horizontal stress distributions of flattened and non-flattened specimens

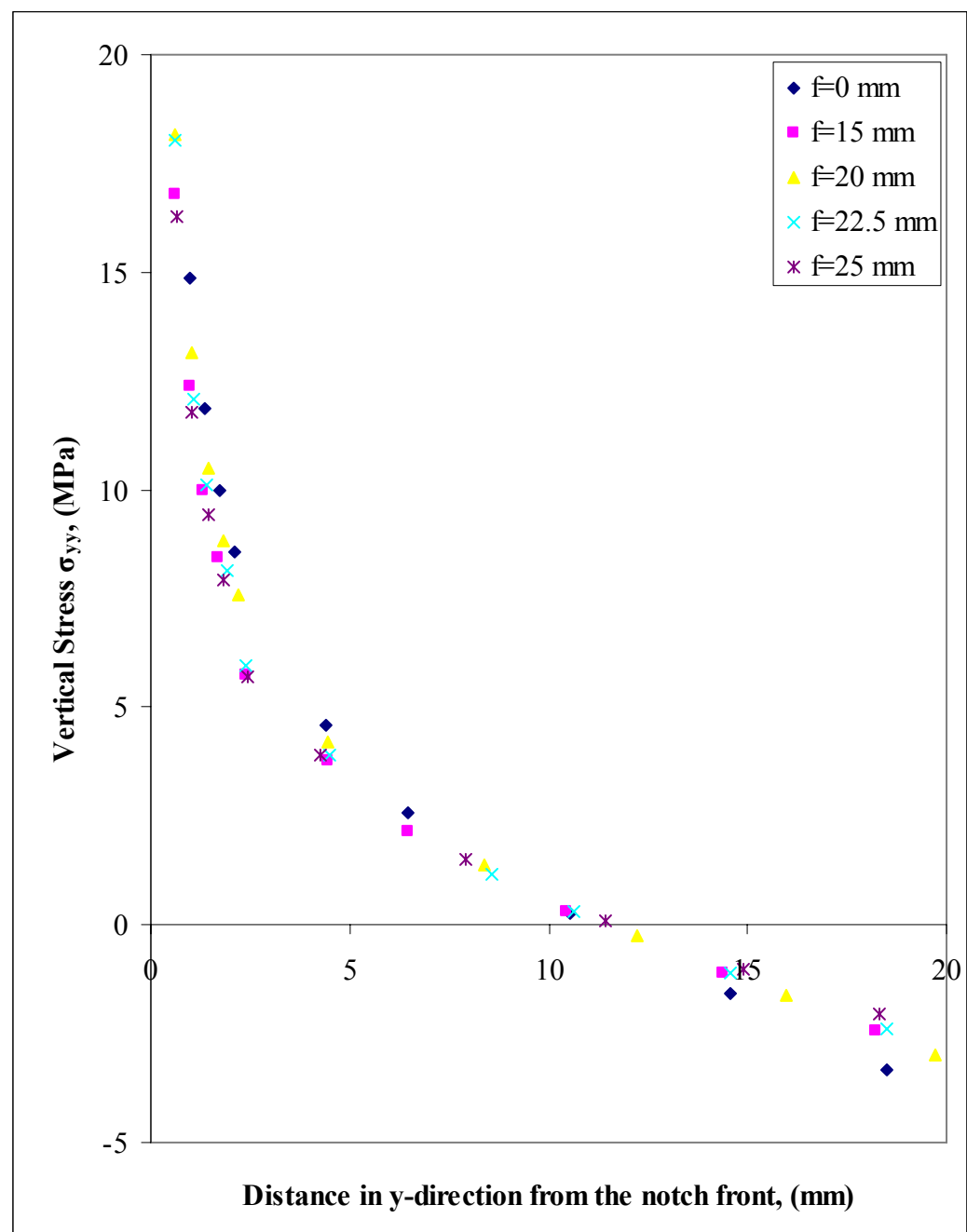


**Figure 6.23** Vertical stress distribution of flattened and non-flattened specimens

Figure 6.24 shows out of plane stress  $\sigma_{zz}$  distribution at the crack front along the thickness B. Again, like the other two stress components, this stress is about 15-20% higher in tension at the notch front for  $f=0$  specimens.

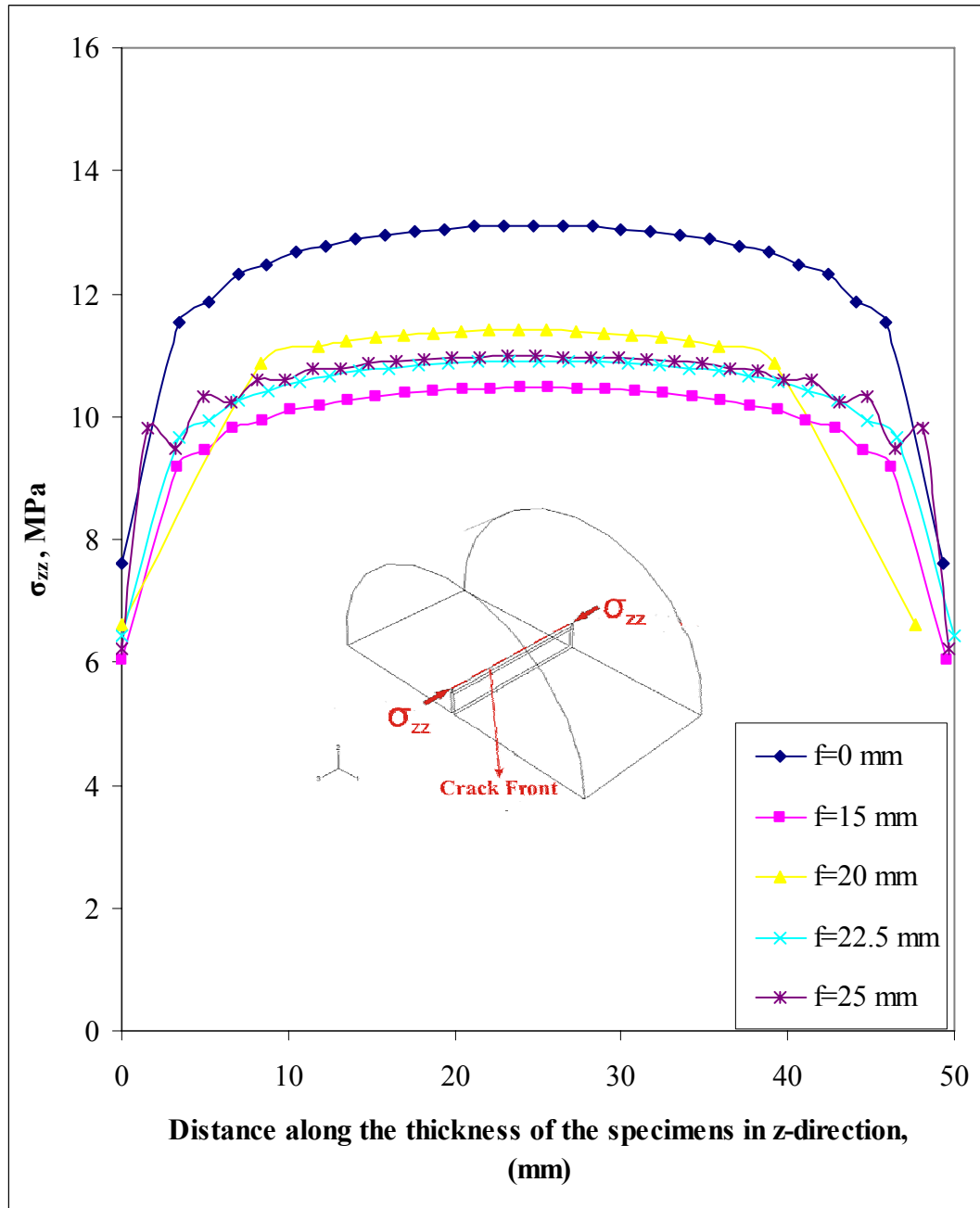


**Figure 6.24** Variation of the  $\sigma_{zz}$  at the notch front along the thickness (in z-direction)

As a result is seen that crack front for regular SCB specimens is under the influence of about 20% higher tensile stress fields. This might be the explanation of obtaining a fracture toughness value of about 20% higher than flattened specimens. Having a flat end reduces the complex tensile stresses around the notch tip and provides an easy path for crack find its way towards the maximum principal stress.  $\sigma_1 = \sigma_{yy}$  applied at the upper end of the specimen. It might be concluded that tensile stress field gradients around the crack front effect the fracture toughness values and this point must be taken into account in selecting a certain specimen type for  $K_{IC}$  testing. Further investigations are needed to clarify this problem.

## **6.5 Effect of Geometrical Variations in Dimensions When Preparing the SCB Specimens**

$P_{max}$ : Failure Load, (kN),

$U$ : Vertical Displacement, (mm),

CMOD: Crack Mouth Opening Displacement, (mm),

$K_I$ : Stress Intensity Factor Calculated With Abaqus, ( $Pa\sqrt{m}$ ),

$K_{II}$ : Stress Intensity Factor Calculated with Abaqus, ( $Pa\sqrt{m}$ ),

$Y_I$ : Normalized Stress Intensity Factor,

$K_{IC}$ : Fracture Toughness, ( $MPa\sqrt{m}$ ),

$k$ : Stiffness(kN/mm).

**Table 6.16** Results of dimension changes SCB specimens

Specimen Code	P <sub>max.</sub> kN	U mm	CMOD mm	K <sub>I</sub> Pa $\sqrt{m}$	K <sub>II</sub> Pa $\sqrt{m}$	Y <sub>I</sub>	K <sub>IC</sub> MPa $\sqrt{m}$	k kN/mm
1*	8.64	0.174	-	142.288	0.001451	4.058	1.229	51.62
2*	8.70	0.172	0.022	126.198	0.001256	3.599	1.097	48.41
3*	9.29	0.157	-	130.894	0.001298	3.776	1.215	57.28
4**	9.06	0.199	0.029	143.450	0.001500	4.033	1.300	44.19
5**	9.54	0.146	0.025	153.770	0.000231	4.051	1.467	61.89
6**	10.20	0.280	-	138.113	0.000004	3.892	1.409	36.90
7***	10.70	0.239	-	134.446	0.003336	3.862	1.438	43.43
8***	10.10	0.172	0.027	136.962	0.000862	3.927	1.383	56.08
9***	7.77	0.180	0.032	149.179	0.001655	3.932	1.159	41.95
10***	9.17	0.145	-	139.769	-0.000017	3.880	1.281	63.09
11***	10.30	0.160	0.039	137.364	0.000027	3.901	1.414	64.34
Average	9.41	0.184	0.029	139.312	-0.005558	3.901	1.308	51.74
±	±	±	±	±	±	±	±	±
STD	0.87	0.041	0.006	7.809	0.001002	0.132	0.123	9.45

\*: Additional specimens , \*\*: Span ratio analysis specimens (S/R=0.7),

\*\*\*: Notch thickness analysis specimens (1 mm< t<sub>n</sub><2 mm)

It is seen from Figure 6.25 that with increasing height of the specimen normalized stress intensity factor shows a decreasing trend. By taking the first SIF value (4.051) and the last SIF value (3.599) in the Figure 6.25. 0.452 change in SIF value is calculated, and this change is approximately equivalent to the 11%.

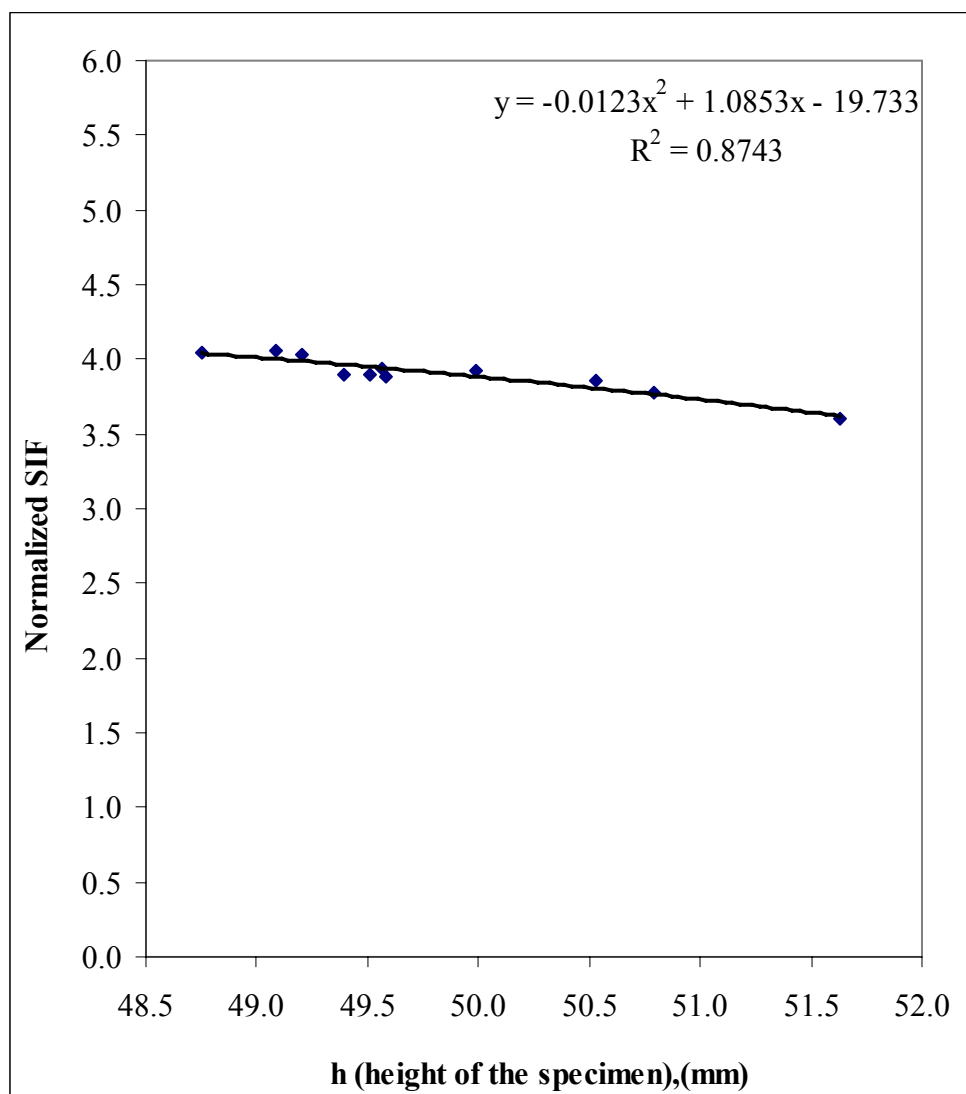


**Figure 6.25** Normalized SIF  $\left[ Y_I = \frac{K_I}{\sigma_0 \sqrt{\pi a}} \right]$  versus h

Similarly It is seen from Figure 6.26 that with increasing height of the specimen normalized stress intensity factor is decreased 0.459 by taking the first SIF value (4.058) and the last SIF value (3.599). This change is approximately equivalent to the 11%.

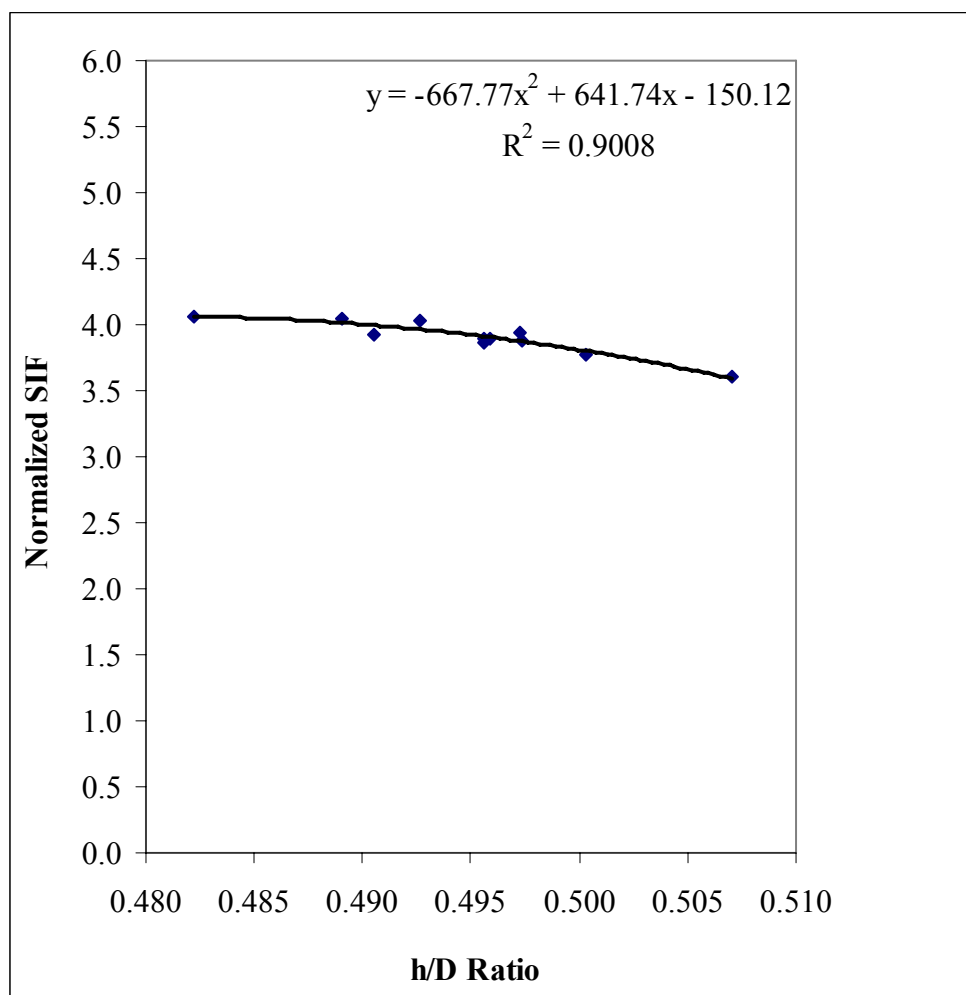


**Figure 6.26** Normalized SIF  $\left[ Y_I = \frac{K_I}{\sigma_0 \sqrt{\pi a}} \right]$  versus h/D Ratio

Considering the low quality of correlation factors, it is seen from Figures 6.27, 6.28 and 6.29 that fracture toughness is not effected by little dimensional variations due to specimen preparation processes.

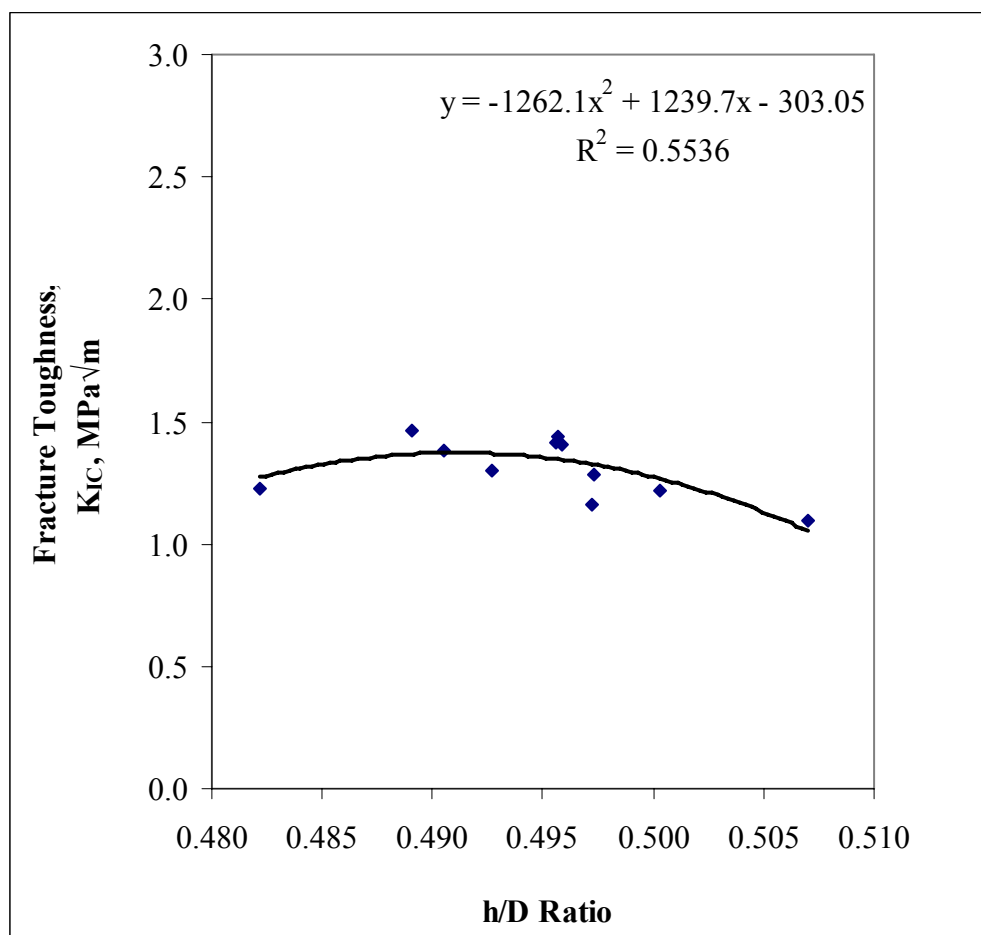


**Figure 6.27** Fracture toughness versus h/D Ratio

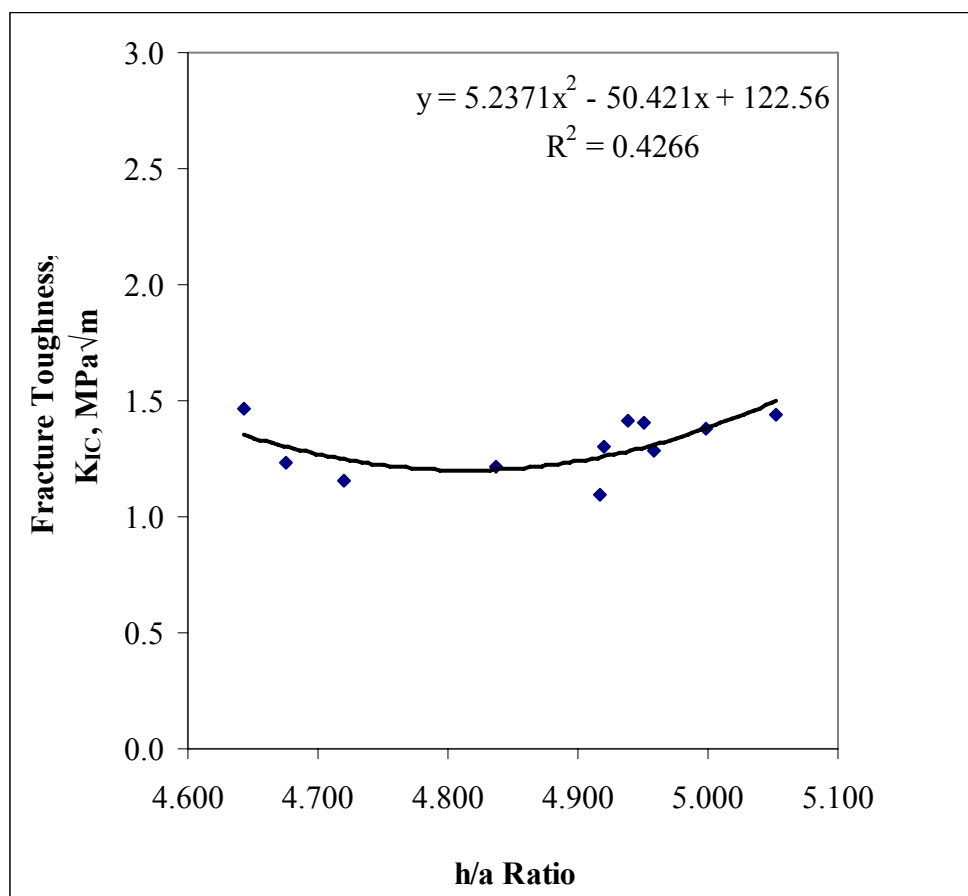


**Figure 6.28** Fracture toughness versus h/a ratio

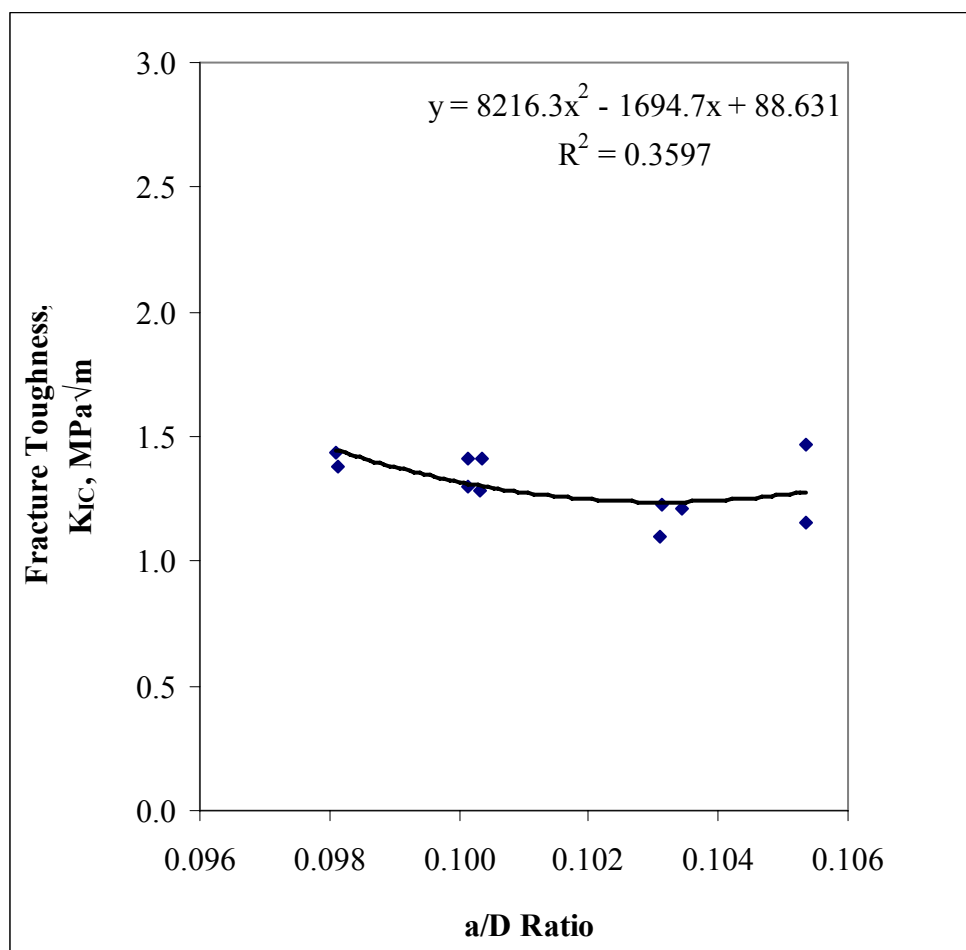


**Figure 6.29** Fracture toughness versus a/D Ratio

## **CHAPTER 7**

### **CONCLUSION**

In this study, including the effects of initial notch thickness, different loading span ratios (S/R), flattened loading end and the effect of geometrical variations in dimensions when preparing the specimens were carried out.

According to the results of notch thickness analysis, it was found that up to 2 mm fracture toughness was not affected by variations in the thickness of preliminary notches. However, for 2.5 mm and over notch thicknesses a decreasing trend is observed. It can be concluded that fracture toughness experiments with preliminary saw cut notches can safely be conducted with saws of diameters up to 2 mm.

For span ratio (S/R) analysis, it was found that fracture toughness of andesite did not show any clear change with increasing S/R ratio. Therefore it can be concluded that span ratio does not affect the fracture toughness of the andesite.

For specimens with flat loading ends, it was found that fracture toughness was lower than the value found from regular SCB type specimens loaded at a point at the top by a steel roller.

The final analysis is the effect of geometrical variations in dimensions when preparing the SCB specimens. It is found that, height of the specimen was affected normalized stress intensity factor and a decreasing trend was observed with increasing height of the specimen. On the other hand differences in the height has no effect on the fracture toughness.

## **7.1 Recommendations**

For later studies notch thickness can be tried different rock types by using five or more different saw thickness for verification of the notch thickness effect on the fracture toughness.

On the other hand effect of notch angle can be investigated of SCB by using same a/R, S/R, notch thickness and rock type.

Besides, crack initiation can be investigated by opening double notches and notches can be angled to extend the investigation by taking same a/R, S/R, notch thickness and rock type.

## REFERENCES

- ABAQUS Analysis User's Manual, Version 6.5 Documentation.
- ABAQUS/CAE User's Manual, Version 6.5 Documentation.
- ABAQUS, Inc., "Modeling Fracture and Failure with ABAQUS", 2006.
- Abrahamsson, S., Niklasson, B., and Ouchterlony, F., "Fragmentation monitoring of production blasts at Mrica" SveDeFo Report DS 1987: 6, Swedish Detonic Research Foundation, Stockholm, 1987.
- Alkılıçgil, Ç., "Development of New Method for Mode I Fracture", M.S. Thesis, METU, Ankara, 145 p., 2006.
- Almeida, L.C.R., et al., "Mechanical characterization of rock splitting planes in granitic rocks", Int. J. of Rock Mech. Min. Sci., Technical Note, Article in Press, 2006.
- Altındağ R., "The relationships between fracture toughness and other mechanical properties of rocks", DEÜ Mühendislik Fakültesi Fen ve Mühendislik Dergisi, Vol. 2, pp. 39-47, May 2000.
- Anderson, T.L., "Fracture mechanics: Fundamentals and Applications", CRC Press, Inc., Florida, 1991.
- Atkinson, B.K., "Subcritical crack growth in geological materials". J. Geophys. Res.; 89: 4077-4114, 1984.
- Atkinson, B.K., "Fracture Mechanics of Rock", Academic Press, London, 1987.
- Backers, T., et al, "Effect of loading rate on Mode I fracture toughness, roughness and micromechanics of sandstone", Int. J. of Rock Mech. Min. Sci., Technical Note, Vol. 40, pp. 425–433, 2003.
- Backers T., "Fracture Toughness Determination and Micromechanics of Rock Under Mode I and Mode II Loading", PhD. Doctoral Thesis, University of Potsdam, Germany, 95 p., 2004.
- Barenblatt, G.I., "Advances in Applied Mechanics", Vol. 7(H.L. Dryden and T. von Karman editors) Academiz Press, pp. 55-129, 1962.
- Barker, L.M. "A simplified method for measuring plane strain fracture toughness", Eng. Fract. Mech.; 9: 361-369, 1977.

Barton M. and Rajan S.D., "Finite Element Primer for Engineers", Term Paper Presentation, The Graduate Engineering Course CEE598 Finite Elements for Engineers, Arizona State University, USA, 2000.

Bearman, R.A., "The use of the point load test for the rapid estimation of Mode I fracture toughness", Int. J. Rock Mech. Min. Sci., Vol. 36, pp. 257-263, 1999.

Begley, J.A. and Landes, J.D., "The J-integral as a Fracture Criterion", ASTM STP 514, American Society for Testing and Materials, Philadelphia, pp. 1-20, 1972.

Chang, S. H., Chung-In Lee, Jeon, S., "Measurement of rock fracture toughness under modes I and II and mixed-mode conditions by using disc-type specimens", Engineering Geology, Vol. 66, pp. 79–97, 2002.

Chong, K.P. & Kuruppu, M.D. "New specimen for fracture toughness determination of rock and other materials", Int. J. Fract.; 26: 59-62, 1984.

Chong, K.P. and Kuruppu, M.D., "New specimens for mixed mode fracture investigations of geomaterials", Engineering Fracture Mechanics, Vol. 30, no. 5, p. 701-712, 1988.

DaqView and DaqViewXL Documents.

DBK Option Cards & Modules User's Manual, 2003."

Dolan T.J., "Preclude Failure: A Philosophy for Material Selection and Simulated Service Testing.", SESA J. Exp. Mech., Jan. 1970.

Dugdale, D.S., "Yielding in Steel Sheets Containing Slits", Journal of the Mechanics and Physics of Solids, Vol 8, pp. 100-104, 1960.

EFunda Engineers, Fracture Mechanics. EFunda Engineering Fundamentals. [http://www.efunda.com/formulae/solid\\_mechanics/fracture\\_mechanics/fm\\_intro.cfm](http://www.efunda.com/formulae/solid_mechanics/fracture_mechanics/fm_intro.cfm)

Eshelby, J.D., "The continuum Theory of Lattice Defects." Solid State Physics, Vol.3, 1956

Evans, A.G. "A method for evaluating the time dependent failure characteristics of brittle materials and its application to polycrystalline alumina", J. Mater. Sci.; 7: 1137-1146, 1972.

Fowell, R. J. and Chen, J. F., "The third chevron-notch rock fracture specimen-the cracked chevron-notched Brazilian disk", Proc. 31st U.S. Symp. on Rock Mechanics, pp. 295-302, 1990.

Fowell, R.J. "Suggested methods for determining Mode I fracture toughness using cracked chevron notched Brazilian disc specimens" Int. J. Rock Mech. Min. Sci. & Geomech. Abstr.; 32: 57-64, 1995.

## Getting Started with ABAQUS, Version 6.5 Documentation.

Griffith, A.A. "The Pheonomena of Rupture and Flow in Solids." Philosophical Transactions, Series A, Vol. 221, pp. 163-198, 1920.

Gunsallus, K.L. and Kulhawy, F.H., "A comparative evaluation of rock strength measures", Int. J. Rock Mech. Min. Sci. Geomech. Abstr., 21(5); pp. 233-48, 1984.

Guo, H., Aziz, N.I. & Schmidt, L.C. "Rock fracture toughness determination by the Brazilian test", Eng. Geol.; 33: 177-188, 1993.

Haberfield, C.M. and Johnston 1.W., "Determination of the fracture toughness of a saturated soft rock", Can. Geotech. J., Vol. 27, pp. 276-284, 1990.

Inglis, C.E., "Stress in a Plate Due to the Presence of Cracks and Sharp Corners." Transactions of the Institute of Naval Architects, Vol. 55, pp. 219 -241, 1913.

Ingraffea, A.R. and Schmidt, R.A., "Experimental verification of a fracture mechanics model for tensile strength prediction of Indiana limestone." Proc. 19th U.S. Symp. On Rock Mechanics, pp. 247-253, 1979.

Irwin, G.R., "Fracture. In: Handbuch der Physik.", Springer Verlag, Berlin, Vol. 6, 1958.

Irwin, G.R., "Fracture Dynamics." Fracturing of Metals, American Society for metals, Cleveland, pp. 147-166, 1948.

Irwin, G.R., "Onset of Fast Crack Propagation in High Strength Steel and Aluminum Alloys." Sagamore Research Conference Proceedings, Vol.2, pp.289-305, 1956.

Irwin, G.R., "Plastic Zone Near a Crack and Fracture Toughness." Sagamore Research Conference Proceedings, Vol. 4, 1961.

ISRM Commission on Standardization of Laboratory and Field Tests, "Suggested Methods for Determining Tensile Strength of Rock Materials", Int. J. Rock Mech. Min. Sci. & Geomech. Abstr., Vol. 15, pp. 99-103, 1978.

ISRM Commission on Standardization of Laboratory and Field Tests, "Suggested Methods for Determining the Uniaxial Compressive Strength and Deformability of Rock Materials", Int. J. Rock Mech. Min. Sci. & Geomech. Abstr., Vol. 16, pp. 135-140, 1979.

ISRM Commission on Testing Methods, "Suggested Method for Determining Fracture Toughness of Rocks", Int. J. Rock Mech. Min. Sci. & Geomech. Abstr., Vol. 25, pp. 71-96, 1988.

ISRM Commission on Testing Methods, "Suggested Method for Determining Mode I Fracture Toughness Using Cracked Chevron Notched Brazilian Disc

(CCNBD) Specimens”, Int. J. Rock Mech. Min. Sci. & Geomech. Abstr., Vol. 32, pp. 57-64, 1995.

Khan, K. and Al-Shayea, N. A., “Effect of Specimen Geometry and Testing Method on Mixed Mode I-II Fracture Toughness of a Limestone Rock from Saudi Arabia”, Rock Mech. Rock Engng., Vol. 33, pp. 179-206, 2000.

Kuruppu, M.D. “Fracture toughness measurement using chevron notched semi-circular bend specimen.” Int. J. Fract.; 86: L33-L38, 1997.

Banks L., “Finite Elements and Fracture Mechanics Presentation”, The Dreszer Fracture Mechanics Laboratory Department of Solid Mechanics, Materials and Systems Tel Aviv University, Tel Aviv, 2003.

Lim, I.L., Johnston, I.W., Choi, S.K. and Boland, J.N., “Fracture Testing of a Soft Rock with Semi-circular Specimens Under Three-point Bending. Part I-Mode I”, Int. J. Rock Mech. Min. Sci. & Geomech. Abstr., Vol. 31, No. 3, pp. 185-197, 1994.

Lim, I.L., Johnston, I.W., Choi, S.K. and Boland, J.N., “Fracture Testing of a Soft Rock with Semi-circular Specimens Under Three-point Bending. Part II- Mixed Mode”, Int. J. Rock Mech. Min. Sci. & Geomech. Abstr., Vol. 31, No. 3, pp. 199-212, 1994.

Lim, I.L., et.al, “Stress intensity factors for semi-circular specimens under three-point bending”, Engineering Fracture Mechanics, Vol. 44, No. 3, pp. 363-382, 1993.

Matsuki, K., Nozuyama, Y. and Takahashi, H., “Size effect in the fracture toughness testing of rocks using a boring core”, Proc. Spring Meeting Min. Metall. Inst, Japan, pp. 193-194, 1987.

Meredith, P.G.A., “Fracture mechanics study of experimentally deformed crustal rocks”, Unpublished Ph. D. Thesis, University of London, 1983.

Mott, N.F., “Fracture of Metals: Theoretical Considerations.” Engineering, Vol. 165, pp.16-18, 1948.

Müller, W., and Rummel, F., Bruchzahigkeitsmessungen an Gesteinen. Bericht zu den BMFT-FE-Vorhaben 03e-3068-B. Ruhr University, Bochum, F. R. G., 1984.

MTS System Catalog, 1992.

Nordlund, E., Li, C., Carlsson, B., “Mechanical properties of the diorite in the prototype repository at Äspö HRL—laboratory tests”, International Progress Report, IPR-99-25, SKB, June 1999.

Orowan, E., “Fracture and Strength of Solids.” Reports on Progress in Physics, Vol.XII, p.185, 1948.

Ouchterlony, F., "Suggested methods for determining the fracture toughness of rock." Int. J. Rock Mech. Min. Sci. & Geomech. Abstr.; 25: 71-96, 1988.

Ouchterlony, F., "A presentation of the ISRM Suggested Methods for determining fracture toughness of rock material", Proc. 6th Int. Congr. Rock Mechanics, Balkema, Rotterdam, Vol. 2, pp. 1181-1186, 1987.

Ouchterlony, F., "Unreported data", Swedish Detonic Research Foundation, Stockholm, Sweden, 1987.

Rice, J.R., "A Path Independent Integral and the Approximate Analysis os Strain Concentration by Notches and Cracks." Journal of Applied Mechanics, Vol. 35, pp.379-386, 1968.

Santay, A.Ö., "Critical Analysis of Short Rod Fracture Toughness Testing Method", M.S. Thesis, METU, Ankara, 83 p., 1990.

Schmidt, R.A. and Lutz, T.J., " $K_{IC}$  and  $J_{IC}$  of Westerly granite effects of thickness and in-plane dimensions", ASTM STP 678, pp.166-182, 1979.

Shetty, D.K., Rosenfield, A., and Duckworth, W.H., "Fracture toughness of ceramics measured by Chevron-notch diametral compression test", Journal of American Ceramic Society, Vol. 68, no. 12, p. C325-C327, 1985.

Shih, C.F. "Relationship between the J-integral and the Crack Opening Displacement for Stationary and Extending Cracks." Journal of the Mechanics and Physics of Solids, Vol 29, pp.305-326, 1981.

Shih, C.F. and Hutchinson, J.W., "Fully Plastic Solutions and Large-Scale Yielding Estimates for Plane Stress Crack Problems." Journal of Engineering Materials and Technology, Vol.98, pp. 289-295, 1976.

Shiryaev, A. & Kotkis, A.M., "Methods for determining fracture toughness of brittle porous materials." Industrial Laboratory; 48: 917-918, 1982.

Singh R.N. and Sun G.X., "An investigation into factors affecting fracture toughness of coal measures sandstone", J. Mines, Metals & Fuels, pp. 11I-118, 1990.

Sousa, J.L.A.O. and Bittencourt, T.N., "Experimental Analysis of Fracture Processes in Concrete", Journal of the Brazilian Society of Mechanical Sciences, Vol. 23, No. 4, 2001.

Staub, I., Janson, T. & Fredriksson, A. "Äspö Pillar Stability Experiment -Geology and properties of the rock mass around the experiment volume." Äspö Hard Rock Laboratory – International Progress Report (IPR-99-25), 2003.

Sun, Z. and Ouchterlony, F., "Fracture toughness of Stripa granite cores", Int. J. Rock Mech. Min. Sci. & Geomech. Abstr., Vol. 23, pp. 399-409, 1986.

Şener, S., "Fracture Toughness Tests on Brazilian Discs of Ankara Andesite", M.S. Thesis, METU, Ankara, 122 p., 2002.

Takahashi, H., Hashida, T., and Fukazawa, T., "Fracture toughness tests by use of core based specimens", GEEE Research Report, No. T-002-86, Faculty of Engineering, Tohoku University, Sendai, Japan, 1986.

Thiercelin, M. & Roegiers, J.M., "Fracture toughness with the modified ring test." In: Proc. 27th US Symp. Rock Mech., Alabama: 284-290, 1986.

Wang, C.H., "Introduction to Fracture Mechanics, Lecture Notes.", Public Release Melbourne, 1996.

Wells, A.A., "Unstable Crack Propagation in Metals: Cleavage and Fast Fracture .", Proceedings of the Crack Propagation Symposium, Vol 1, Paper 84, Cranfield, UK, 1961

Westergaard, H.M., Bearing Pressure and Cracks, J.Appl. Mech., Trans., ASME, pp. A-49, A-53, June 1939.

Whittaker, B.N., Singh, R.N., Sun, G., "Rock Fracture Mechanics-Principles, Design and Applications", Elsevier, Amsterdam, 1992.

Williams, M.L., "On the Stres Distribution at the Base of a Stationary Crack.", J.Appl. Mech., Vol. 24, Trans.,ASME, Vol. 79, pp. 109-114, 1957

Willis, J.R., J.Mech. Physics of Solids, Vol. 15, pp. 151-162, 1967

Yi, X., "Fracture toughness and crack growth in short rod specimens of rock", Licentiate Thesis, Lulea Univ. Techn., Lulea, Sweden, 1987.

Yoon, J. and Jeon, S., "Experimental verification of a PTS mode II test for rock", Int. J. of Rock Mech. Min. Sci., Vol. 41, Paper 1A 02, 2004.

Yu Y., "Measuring properties of rock from the site of permanent shiplock in three Gorges project", Test Report, Yangtze River Scientific Research Institute, June 2001.

Zhang, Z.X., "An empirical relation between mode I fracture toughness and the tensile strength of rock", Int. J. of Rock Mech. Min. Sci., Technical Note, Vol. 39, pp. 401-406, 2002.

Zhao X. L., Roegiers J.-C., and Guo M., "The determination of fracture toughness of rocks by chevron-notched brazilian disk specimens", School of Petroleum & Geological Engineering Conference Paper, No: 9014, The University of Oklahoma, Oklahoma, USA, 1990.

# APPENDIX A

## SPECIMEN DIMENSIONS TABLES

### A.1 Specimen Dimensions of Notch Thickness Analysis

**Table A.1** Dimensions of  $t_n < 1$  mm,  $a/R=0.2$ ,  $S/R=0.7$  SCB specimens

Specimen Code	h mm	D mm	B mm	a mm	R mm	a/R	$t_n$ mm	$t_n/a$	S/R
1	50.71	102.01	50.25	10.00	51.01	0.196	0.80	0.080	0.686
2	48.89	99.21	50.62	10.00	49.61	0.202	0.84	0.084	0.706
3	49.14	99.82	50.51	10.00	49.92	0.200	0.82	0.082	0.701
4	49.95	99.94	50.52	10.00	49.97	0.200	0.91	0.091	0.700
5	49.20	99.88	50.47	10.50	49.95	0.210	0.85	0.081	0.701
6*	48.59	99.15	50.23	10.50	49.58	0.212	1.00	0.095	0.706
Average	49,58	100,17	50,47	10,10	50,09	0,202	0,84	0,084	0,699
$\pm$	$\pm$	$\pm$	$\pm$	$\pm$	$\pm$	$\pm$	$\pm$	$\pm$	$\pm$
STD	0.75	1.07	0.14	0.22	0.53	0.005	0.04	0.004	0.007

\*=Specimen has a joint inside (These specimens dimensions and results are not considered when calculating the averages and standart deviations)

**Table A.2** Dimensions of  $1 \text{ mm} < t_n < 2 \text{ mm}$ ,  $a/R=0.2$ ,  $S/R=0.7$  SCB specimens

Specimen Code	h mm	D mm	B mm	a mm	R mm	a/R	t <sub>n</sub> mm	t <sub>n</sub> /a	S/R
1	50.53	101.95	49.94	10.00	50.98	0.196	1.17	0.117	0.687
2	49.99	101.92	49.86	10.00	50.97	0.196	1.17	0.117	0.687
3	48.83	99.28	50.70	10.00	49.65	0.201	1.06	0.106	0.705
4	49.56	99.67	48.03	10.50	49.84	0.211	1.18	0.112	0.702
5	49.58	99.69	49.36	10.00	49.85	0.201	1.31	0.131	0.702
6	49.39	99.66	50.51	10.00	49.83	0.201	1.28	0.128	0.702
Average	49.65	100.36	49.73	10.08	50.18	0.201	1.20	0.119	0.698
±	±	±	±	±	±	±	±	±	±
STD	0.57	1.23	0.96	0.20	0.62	0.005	0.09	0.009	0.008

**Table A.3** Dimensions of  $2 \text{ mm} < t_n < 3 \text{ mm}$ ,  $a/R=0.2$ ,  $S/R=0.7$  SCB specimens

Specimen Code	h mm	D mm	B mm	a mm	R mm	a/R	t <sub>n</sub> mm	t <sub>n</sub> /a	S/R
1	50.09	101.86	51.84	10.00	50.94	0.196	2.20	0.220	0.687
2	50.36	101.85	51.65	10.00	50.93	0.196	2.14	0.214	0.687
3	49.00	99.17	50.42	10.50	49.59	0.212	2.13	0.203	0.706
4	49.63	99.28	49.56	10.00	49.64	0.201	2.27	0.227	0.705
5	49.68	99.71	48.28	10.50	49.86	0.211	2.29	0.218	0.702
6	49.31	99.35	50.44	10.50	49.68	0.211	2.26	0.215	0.705
Average	49.68	100.20	50.37	10.25	50.10	0.205	2.22	0.216	0.699
±	±	±	±	±	±	±	±	±	±
STD	0.50	1.29	1.33	0.27	0.65	0.007	0.07	0.008	0.009

**Table A.4** Dimensions of  $3 \text{ mm} < t_n < 4 \text{ mm}$ ,  $a/R=0.2$ ,  $S/R=0.7$  SCB specimens

Specimen Code	h mm	D mm	B mm	a mm	R mm	a/R	$t_n$ mm	$t_n/a$	S/R
1	49.58	99.92	50.24	10.00	49.96	0.200	3.55	0.355	0.701
2	49.65	99.80	49.79	9.00	49.90	0.180	3.63	0.403	0.701
3	49.27	99.61	50.48	9.50	49.81	0.191	3.48	0.366	0.703
4	49.31	99.68	50.20	11.00	49.84	0.221	3.96	0.360	0.702
5*	49.47	99.80	49.81	9.50	49.90	0.190	3.48	0.366	0.701
Average	49.45	99.75	50.18	9.88	49.88	0.198	3.66	0.371	0.702
$\pm$	$\pm$	$\pm$	$\pm$	$\pm$	$\pm$	$\pm$	$\pm$	$\pm$	$\pm$
STD	0.19	0.14	0.29	0.85	0.07	0.017	0.21	0.022	0.001

\*=Specimen has a joint inside (These specimens dimensions and results are not considered when calculating the averages and standart deviations)

## A.2 Specimen Dimensions of Span Ratio (S/R) Analysis

**Table A.5** Dimensions of  $a/R=0.2$ ,  $S/R=0.3$  SCB specimens

Specimen Code	h mm	D mm	B mm	a mm	R mm	a/R	$t_n$ mm	$t_n/a$	S/R
1	49.17	99.18	50.27	9.50	49.59	0.192	1.00	0.105	0.302
2	49.40	99.69	50.85	9.50	49.85	0.191	0.98	0.103	0.301
3	49.52	99.90	50.84	10.00	49.95	0.200	1.07	0.107	0.300
Average	49.36	99.59	50.65	9.67	49.80	0.194	1.02	0.105	0.301
$\pm$	$\pm$	$\pm$	$\pm$	$\pm$	$\pm$	$\pm$	$\pm$	$\pm$	$\pm$
STD	0.18	0.37	0.33	0.29	0.19	0.005	0.05	0.002	0.001

**Table A.6** Dimensions of a/R=0.2, S/R=0.4 SCB specimens

Specimen Code	h mm	D mm	B mm	a mm	R mm	a/R	t <sub>n</sub> mm	t <sub>n</sub> /a	S/R
1	49.26	99.80	50.67	10.00	49.90	0.200	1.25	0.125	0.401
2	48.99	99.99	51.03	10.50	50.03	0.210	1.26	0.120	0.400
3	49.55	99.31	50.50	10.00	49.65	0.201	1.35	0.135	0.403
Average	49.26	99.70	50.73	10.17	49.86	0.204	1.29	0.127	0.401
±	±	±	±	±	±	±	±	±	±
STD	0.28	0.35	0.27	0.29	0.19	0.005	0.06	0.008	0.002

**Table A.7** Dimensions of a/R=0.2, S/R=0.5 SCB specimens

Specimen Code	h mm	D mm	B mm	a mm	R mm	a/R	t <sub>n</sub> mm	t <sub>n</sub> /a	S/R
1	48.72	99.54	50.60	10.50	49.78	0.211	1.22	0.116	0.502
2	48.47	99.20	50.60	10.50	49.61	0.212	1.26	0.120	0.504
3	48.47	99.20	50.60	10.50	49.61	0.212	1.26	0.120	0.504
Average	48.55	99.31	50.60	10.50	49.67	0.211	1.25	0.119	0.503
±	±	±	±	±	±	±	±	±	±
STD	0.14	0.20	0.00	0.00	0.10	0.000	0.02	0.002	0.001

**Table A.8** Dimensions of a/R=0.2, S/R=0.6 SCB specimens

Specimen Code	h mm	D mm	B mm	a mm	R mm	a/R	t <sub>n</sub> mm	t <sub>n</sub> /a	S/R
1	48.89	99.66	48.91	10.00	49.84	0.201	1.12	0.112	0.602
2	48.88	99.71	48.28	10.00	49.86	0.201	1.14	0.114	0.602
3	49.32	99.71	50.03	10.50	49.86	0.211	1.06	0.101	0.602
4*	48.54	99.32	50.58	10.00	49.67	0.201	1.21	0.121	0.604
Average	49.03	99.69	49.07	10.17	49.85	0.204	1.11	0.109	0.602
±	±	±	±	±	±	±	±	±	±
STD	0.25	0.03	0.89	0.29	0.01	0.006	0.04	0.007	0.000

\*=Specimen has a joint inside (These specimens dimensions and results are not considered when calculating the averages and standart deviations)

**Table A.9** Dimensions of a/R=0.2, S/R=0.7 SCB specimens

Specimen Code	h mm	D mm	B mm	a mm	R mm	a/R	t <sub>n</sub> mm	t <sub>n</sub> /a	S/R
1	49.20	99.86	49.89	10.00	49.94	0.200	1.30	0.130	0.701
2	48.75	99.68	47.99	10.50	49.85	0.211	1.24	0.118	0.702
3	49.51	99.85	50.03	10.00	49.93	0.200	1.35	0.135	0.701
Average	49.15	99.80	49.30	10.17	49.90	0.204	1.30	0.128	0.701
±	±	±	±	±	±	±	±	±	±
STD	0.38	0.10	1.14	0.29	0.05	0.006	0.06	0.009	0.001

**Table A.10** Dimensions of a/R=0.2, S/R=0.8 SCB specimens

Specimen Code	h mm	D mm	B mm	a mm	R mm	a/R	t <sub>n</sub> mm	t <sub>n</sub> /a	S/R
1	49.32	99.75	50.59	10.00	49.88	0.200	1.38	0.138	0.802
2	48.25	99.22	49.56	10.50	49.63	0.212	1.51	0.144	0.806
3	48.61	99.79	49.91	11.00	49.91	0.220	1.38	0.125	0.801
Average	48.73	99.59	50.02	10.50	49.81	0.211	1.42	0.136	0.803
±	±	±	±	±	±	±	±	±	±
STD	0.55	0.32	0.52	0.50	0.15	0.010	0.08	0.009	0.002

**Table A.11** Dimensions of a/R=0.2, S/R=0.9 SCB specimens

Specimen Code	h mm	D mm	B mm	a mm	R mm	a/R	t <sub>n</sub> mm	t <sub>n</sub> /a	S/R
1	49.45	99.92	49.82	10.00	49.97	0.200	1.05	0.105	0.901
2	49.67	100.03	51.06	10.00	50.02	0.200	1.18	0.118	0.900
3	49.99	99.90	50.00	10.50	49.95	0.210	1.16	0.110	0.901
Average	49.70	99.95	50.29	10.17	49.98	0.203	1.13	0.111	0.900
±	±	±	±	±	±	±	±	±	±
STD	0.27	0.07	0.67	0.29	0.04	0.006	0.07	0.007	0.001

### A.3 Specimen Dimensions of Flattened SCB Analysis

**Table A.12** Dimensions of  $f \approx 15\text{mm}$   $a/R=0.2$ ,  $S/R=0.7$  SCB specimens

Specimen Code	h mm	D mm	B mm	a mm	R mm	a/R	t <sub>n</sub> mm	t <sub>n</sub> /a	S/R	f mm	A mm <sup>2</sup>
1	48.47	99.32	50.04	9.50	49.66	0.191	1.04	0.109	0.705	15.18	759.6
2	48.45	99.98	51.20	10.00	49.99	0.200	1.08	0.108	0.700	15.54	795.4
3	48.92	99.92	48.33	9.50	49.96	0.190	0.98	0.103	0.701	14.32	692.1
4	48.96	99.92	50.27	10.00	49.96	0.200	1.06	0.106	0.701	14.71	739.2
5	48.37	99.94	50.22	10.00	49.98	0.200	0.98	0.098	0.700	15.31	768.9
Average	48.63	99.81	50.01	9.80	49.91	0.196	1.03	0.105	0.701	15.01	751.0
±	±	±	±	±	±	±	±	±	±	±	±
STD	0.28	0.28	1.04	0.27	0.14	0.005	0.05	0.005	0.002	0.49	38.6

**Table A.13** Dimensions of  $f \approx 20\text{mm}$   $a/R=0.2$ ,  $S/R=0.7$  SCB specimens

Specimen Code	h mm	D mm	B mm	a mm	R mm	a/R	t <sub>n</sub> mm	t <sub>n</sub> /a	S/R	f mm	(A) mm <sup>2</sup>
1	47.85	100.06	50.92	10.00	50.05	0.200	0.96	0.096	0.699	18.77	955.7
2	48.05	99.92	48.34	10.00	49.97	0.200	1.00	0.100	0.700	19.72	953.3
3	47.78	100.11	51.53	10.00	50.07	0.200	1.18	0.118	0.699	19.95	1028.0
4	48.21	100.09	51.09	10.00	50.05	0.200	0.95	0.095	0.699	20.87	1066.1
Average	47.97	100.04	50.47	10.00	50.03	0.200	1.02	0.102	0.700	19.83	1000.8
±	±	±	±	±	±	±	±	±	±	±	±
STD	0.19	0.09	1.44	0.00	0.05	0.000	0.11	0.011	0.001	0.86	55.7

**Table A.14** Dimensions of  $f \approx 22.5\text{mm}$   $a/R=0.2$ ,  $S/R=0.7$  SCB specimens

Specimen Code	$h$ mm	D mm	B mm	a mm	R mm	$a/R$	$t_n$ mm	$t_n/a$	S/R	f mm	(A) $\text{mm}^2$
1	48.67	100.07	50.82	9.00	50.03	0.180	0.91	0.101	0.700	22.53	1144.7
2	48.13	100.10	51.04	10.00	50.05	0.200	1.01	0.101	0.699	22.56	1151.5
3*	47.63	99.36	49.98	10.00	49.68	0.201	0.95	0.095	0.704	23.69	1183.7
Average	48.40	100.08	50.93	9.50	50.04	0.190	0.96	0.101	0.699	22.54	1148.1
±	±	±	±	±	±	±	±	±	±	±	±
STD	0.38	0.02	0.16	0.71	0.01	0.014	0.07	0.000	0.000	0.02	4.8

\*=Specimen has a joint inside (These specimens dimensions and results are not considered when calculating the averages and standart deviations)

**Table A.15** Dimensions of  $f \approx 25\text{mm}$   $a/R=0.2$ ,  $S/R=0.7$  SCB specimens

Specimen Code	$h$ mm	D mm	B mm	a mm	R mm	$a/R$	$t_n$ mm	$t_n/a$	S/R	f mm	(A) $\text{mm}^2$
1	48.23	99.91	50.20	10.00	49.96	0.200	1.00	0.100	0.701	24.36	1222.5
2	47.20	99.94	50.38	10.00	49.98	0.200	1.04	0.104	0.700	25.74	1296.8
3	47.21	99.81	48.55	9.50	49.91	0.190	1.08	0.114	0.701	25.74	1249.3
4*	47.67	99.88	48.83	10.00	49.94	0.200	1.05	0.105	0.701	26.05	1271.9
Average	47.55	99.88	49.71	9.83	49.95	0.197	1.04	0.106	0.701	25.28	1256.2
±	±	±	±	±	±	±	±	±	±	±	±
STD	0.59	0.07	1.01	0.29	0.03	0.006	0.04	0.007	0.000	0.80	37.6

\*=Specimen has a joint inside (These specimens dimensions and results are not considered when calculating the averages and standart deviations)

## APPENDIX B

### SPECIMEN PHOTOS AFTER EXPERIMENTS

#### B.1 Notch Thickness Specimen Photos After Experiments



**Figure B.1** Notch thickness specimens after experiments

## B.2 Span Ratio (S/R) Analysis Specimens After Experiments



**Figure B.2** Span ratio (S/R) analysis specimens after experiments

### B.3 Flattened Loading Face Specimens After Experiments

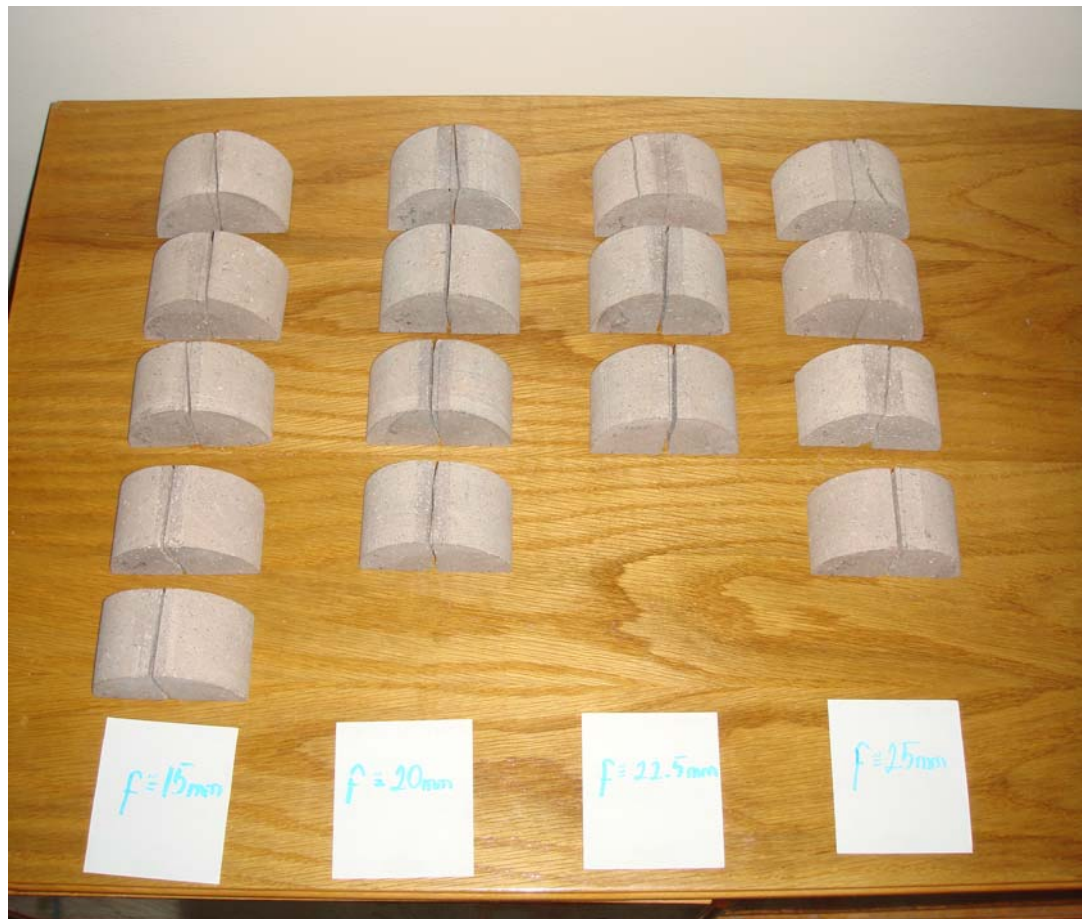


**Figure B.3** Flattened loading face specimens after experiments